UNIVERSIDADE FEDERAL DE PERNAMBUCO
CENTRO DE TECNOLOGIA E GEOCIÊNCIAS
DEPARTAMENTO DE OCEANOGRAFIA
PROGRAMA DE PÓS-GRADUAÇÃO EM OCEANOGRAFIA

LUCAS MEDEIROS GUIMARÃES

VARIABILIDADE INTERANUAL DA pCO_2 NA INTERFACE OCEANO-ATMOSFERA DO ATLÂNTICO TROPICAL ENTRE AS LATITUDES 3ºS E 14ºS

Recife
2024

LUCAS MEDEIROS GUIMARÃES

VARIABILIDADE INTERANUAL DA pCO_2 NA INTERFACE OCEANO-ATMOSFERA DO ATLÂNTICO TROPICAL ENTRE AS LATITUDES 3ºS E 14ºS

Tese apresentada ao Programa de Pós-Graduação em Oceanografia da Universidade Federal de Pernambuco, como requisito parcial para a obtenção do título de Doutor em Oceanografia.

Área de concentração: Oceanografia Abiótica.

Orientador: Profº. Drº Manuel de Jesus Flores Montes
Coorientadora: Dra. Nathalie Lefèvre

Recife
2024

.Catalogação de Publicação na Fonte. UFPE - Biblioteca Central

Guimarães, Lucas Medeiros.
Variabilidade interanual da pCO2 na interface oceano-atmosfera do Atlântico tropical entre as latitudes 3°S e 14°S / Lucas Medeiros Guimarães. - Recife, 2024.
93f.: il.

Tese (Doutorado) - Universidade Federal de Pernambuco, Centro de Tecnologia e Geociências, Programa de Pós-Graduação em Oceanografia, 2024.
Orientação: Manuel de Jesus Flores Montes.
Coorientação: Nathalie Lefèvre.

1. Fugacidade do CO2; 2. Temperatura da superfície do mar; 3. Nordeste do Brasil; 4. Corrente Sul Equatorial; 5. Zona de convergência intertropical; 6. Fluxo do CO2. I. Montes, Manuel de Jesus Flores. II. Lefèvre, Nathalie. III. Título.

UFPE-Biblioteca Central

LUCAS MEDEIROS GUIMARÃES

VARIABILIDADE INTERANUAL DA pCO_2 NA INTERFACE OCEANO-ATMOSFERA DO ATLÂNTICO TROPICAL ENTRE AS LATITUDES 3ºS E 14ºS

Tese apresentada ao Programa de Pós-Graduação em Oceanografia da Universidade Federal de Pernambuco, Cento de Tecnologia e Geociências, como requisito parcial para a obtenção do título de Doutor em Oceanografia.

Aprovado em 31 de julho de 2024.

Banca Examinadora

_____

Prof. Dr. Manuel de Jesus Flores-Montes (Orientador)
Universidade Federal de Pernambuco

_____

Profa. Dra. Doris Regina Aires Veleda (Examinadora Interna)
Universidade Federal de Pernambuco

_____

Prof. Dr. Fernando Antônio do Nascimento Feitosa (Examinador Interno)
Universidade Federal de Pernambuco

_____

Profa. Dra. Elisabete de Santis Braga (Examinadora Externa)
Universidade de São Paulo

_____

Dr. Carlos Esteban Delgado Noriega (Examinador Externo)
Universidade Federal de Pernambuco

AGRADECIMENTOS

Primeiramente quero agradecer aos professores Manoel de Jesus Flores Montes e Nathalie Lefèvre pela orientação.

Aos meus familiares, que sempre apoiam as decisões que tomo em minha vida profissional, me dando suporte para que eu possa seguir em frente e crescer na vida.

Aos meus *roommates* que convivi diariamente aqui em Recife desde minha chegada em 2019: Marcão, Deco, Ramilla, Isaías, Keynes, Amanda e Emmanuel obrigado por terem dividido apartamento comigo e terem suportado meus momentos.

Em especial, quero agradecer à Amanda Gabriella, minha amiga-irmã, que conheci em 2012, mas nesses anos em Recife, nossa amizade ficou cada dia mais forte e hoje em dia ela é MINHA PESSOA.

Ao meu psicólogo André, que me ouviu e buscou sempre me acolher de forma humana e profissional, me fazendo refletir sobre todos os acontecimentos de minha vida.

Aos meus amigos que deixei na Bahia, obrigado pelo acolhimento nas minhas idas e voltas da nossa terrinha linda.

Aos meus amigos que fiz em Pernambuco, obrigado também por terem me acolhido e mostrado as melhores coisas da cidade do Recife e o melhor cantinho da cidade, a Várzea.

Às minhas lendas, Laís, Luana, Renato, Thiago e, em especial, Viniciui. Vocês foram meu alívio em 2022, com um *plot twist* de minha vida que eu nunca imaginei que aconteceria.

Aos meus amigos que fiz na Fusion Box. Sempre foi terapêutico treinar, encontrar vocês e desestressar do mundo lá fora um pouco.

À banca examinadora, professoras Doris Regina Aires Veleda e Elisabete de Santis Braga, ao professor Fernando Antônio do Nascimento Feitosa e ao pesquisador Carlos Esteban Delgado Noriega, pelos conselhos ditos para reforçar meu conhecimento.

Aos professores do curso da Pós-Graduação em Oceanografia – UFPE.

O presente trabalho foi realizado com o apoio da Conselho Nacional de Desenvolvimento Científico e Tecnológico (CNPq) – através de bolsa de pesquisa 140555/2019-6

Por último, mas não menos importante, eu quero agradecer a mim mesmo por não ter desistido. Somente eu sei o quanto foi árduo o desenvolvimento desta tese. Lucas, te amo! Siga firme.

RESUMO

O Atlântico Tropical é o segundo oceano mais importante em termos de fonte de CO_2 para a atmosfera, depois do Pacífico tropical. Poucos estudos em relação ao fluxo ar-mar do CO_2 foram realizados próximo à costa da região Nordeste do Brasil. O presente trabalho teve como objetivo principal: determinar os fluxos de CO_2 na região Nordeste do Brasil para compreender os fatores que influenciam sobre as variações temporais e espaciais da pCO_2 na borda oeste do Atlântico tropical. Foram analisadas as tendências de 2008 a 2020 da fugacidade de CO_2 em águas superficiais do mar (fCO_{2sw}) e do fluxo marítimo de CO_2 entre as latitudes 3° e 14° S. Os dados de pCO_2 foram coletados por navios mercante voluntários equipados com sistema autônomo de navegação. Foi utilizado de base de dados de parâmetros de carbono, temperatura, salinidade, ventos, correntes marítimas e clorofila *a* para identificar quais fatores físicos, químicos e biológicos influenciam na variabilidade pCO_2. Foi possível determinar a variabilidade do fluxo do CO_2 entre o oceano e a atmosfera, como fonte ou sumidouro, através da diferença entre as fugacidades do CO_2 desses compartimentos. Os resultados mostraram que há contraste aparente entre as áreas 3°S – 8°S e 8°S – 14°S com maior fCO_{2sw} e fluxo de CO_2 observado acima de 8ºS do que abaixo de 8ºS. As concentrações de clorofila *a* são muito baixas em cada região e não podem explicar a diferença norte-sul de fCO_{2sw}. Essa diferença é causada principalmente por parâmetros físicos, como Temperatura da Superfície do Mar, Salinidade da Superfície do Mar, Vento, Precipitação e correntes superficiais, que são distintos em cada região. No geral, toda região é fonte de CO_2 para a atmosfera. A área sul é geralmente uma fonte durante todo o ano, exceto de julho a setembro, quando atua como um fraco sumidouro de CO_2, com valores negativos do fluxo. Foi possível perceber que há anos de anomalias na distribuição de CO_2 devido aos eventos do fenômeno *El Niño* que influenciam a posição da Zona de Convergência Intertropical (ITCZ). Essa mudança na ITCZ, altera a temperatura e a salinidade da região do Atlântico Tropical, principalmente na área norte deste estudo. A falta de dados em alguns meses não coletados levanta dúvidas sobre a distribuição do CO_2, mas estas informações trazem importantes elucidações da variabilidade sazonal e espacial da pCO_2 para a região da borda oeste do Atlântico Tropical Sul adjacente à região Nordeste brasileira. Porém, mostra também, a importância da continuação para aprimoramento dos estudos do ciclo do carbono e a monitoramento contínuo do CO_2, não só nesta área, mas nas zonas costeiras, para ajudar a documentar e investigar a variabilidade do fluxo de CO_2.

Palavras-chave: CSE. Fugacidade do CO_2. TSM. Nordeste do Brasil. SSM.

ABSTRACT

The Tropical Atlantic is the second most important ocean in terms of source of CO_2 to the atmosphere, after the tropical Pacific. Few studies regarding the air-sea flux of CO_2 have been carried out near the coast of the Northeast region of Brazil. The main objective of this work was to determine CO_2 fluxes in the Northeast region of Brazil to understand the factors that influence the temporal and spatial variations of pCO_2 on the western border of the tropical Atlantic. Trends from 2008 to 2020 in CO_2 fugacity in sea surface waters (fCO_{2sw}) and maritime CO_2 flux between latitudes 3° and 14° S were analyzed. pCO_2 data were collected by volunteer merchant ships equipped with an autonomous system navigation. A database of carbon parameters, temperature, salinity, winds, maritime currents and chlorophyll *a* were used to identify which physical, chemical and biological factors influence pCO_2 variability. It was possible to determine the variability of the CO_2 flux between the ocean and the atmosphere, as a source or sink, through the difference between the CO_2 fugacity of these compartments. The results showed that there is an apparent contrast between the areas 3°S – 8°S and 8°S – 14°S with greater fCO_{2sw} and CO_2 flux observed north of 8°S than south of 8°S. Chlorophyll *a* concentrations are very low in each region and cannot explain the north-south difference in fCO_{2sw}. This difference is mainly caused by physical parameters, such as Sea Surface Temperature, Sea Surface Salinity, Wind, Precipitation and surface marine currents, which are different in each region. In general, every region is a source of CO_2 to the atmosphere. The southern area is generally a year-round source, except from July to September, when it acts as a weak CO_2 sink, with negative flux values. It was possible to notice that there have been years of anomalies in the distribution of CO_2 due to the El Niño phenomenon events that influence the position of the Intertropical Convergence Zone (ITCZ). This change in the ITCZ alters the temperature and salinity of the Tropical Atlantic region, mainly in the northern area of this study. The lack of data in some uncollected months raises doubts about the distribution of CO_2, but this information brings important elucidations of the seasonal and spatial variability of pCO_2 for the region on the western border of the South Tropical Atlantic adjacent to the Brazilian Northeast region. However, it also shows the importance of continuing to improve studies of the carbon cycle and continuous monitoring of CO_2, not only in this area, but in coastal areas, to help document and investigate the variability of CO_2 flux.

Keywords: SST. Northeastern of Brazil. SSS. CO_2 Fugacity. SEC

LISTA DE FIGURAS

REVISÃO BIBLIOGRÁFICA

Figura 1 - Emissões globais de dióxido de carbono (CO_2) provenientes da combustão de energias e de processos industriais entre 1900 e 2022 16
Figura 2 – Medições da pressão parcial do CO_2 registrado pela versão 2023 do SOCAT 21
Figura 3 - A - Sistema underway para CO_2 instalado no Navio Mercante Cap. San Lorenzo; B – Compartimento seco, com computador e o detector infravermelho de CO_2 da Licor 7000; e o C – compartimento molhado, com os equilibradores, que têm a função de equilibrar a pCO_2 da água que flui pelo sistema 22
Figura 4 – Esquema do sistema underway para CO_2 23
Figura 5 – Posição média sazonal da Zona de Convergência Intertropical 25
Figura 6 - Concentração média global do CO_2 atmosférico em partes por milhão (ppm). Desde 1980, o NOAA/GML produzem dados mensais baseados em uma média das medições diretas de múltiplas estações. 27

ARTIGO 1 - REGIONAL DIFFERENCES OF THE AIR-SEA CO_2 FLUX BETWEEN 3ºS AND 14ºS IN THE SOUTHWESTERN TROPICAL ATLANTIC

Fig. 1 – Map of the Southwestern Tropical Atlantic with all cruises tracks with underway CO_2 measurements. 36
Fig. 2 – a) Schematic representation of surface (solid line) and subsurface (dashed line) currents along the Tropical Atlantic between 30°N – 30°S and 60°W – 15°E, with the box showing for the study area (adapted from Stramma; Schott, 1999); b) Schematic representation of mean currents and edgy generation between 3º S – 14º S and 40º W – 30 º W (Northeast Brazilian coast). Surface currents in solid line and subsurface currents in dashed line (Adapted from Dossa et al., 2021) 38
Fig. 3 - Data collected from 2008 to 2020 by 4 merchant ships: Monte Olivia, Rio Blanco, Santa Cruz and Cap San Lorenzo along the France-Brazil line 38
Fig. 4– Climatological (2008-2020) maps of surface marine currents data for a) austral Summer (December-January-February), b) Autumn (March-April-May), c) Winter (June-July-August), and d) Spring (September-October-November), near to Brazilian coast between la latitudes 3º S and 14º S 40

Fig. 5 – Quarterly climatology of Chlorophyll-a from 2008 to 2020.....42
Fig. 6 – Monthly distribution of fCO_2 from 3ºS to 14ºS in the Southwestern Tropical Atlantic, from 2008 to 2020 43
Fig. 7 – Monthly Variability of a) SST, b) Sea Surface Salinity, c) Fugacity of CO_2 in seawater and d) CO_2 Flux in the northern region (blue line) and the southern region (red line), averaged over 2008 – 2020 45

ARTIGO 2 - CO_2 FLUX ALONG THE SOUTHWEST TROPICAL ATLANTIC OCEAN ADJACENT TO THE NORTHEAST OF BRAZIL (3ºS TO 14ºS) FROM 2008 TO 2020

Figure 1 - Map of the Southwestern Tropical Atlantic with all cruise tracks with underway CO_2 measurements and schematic representation of mean currents and edgy generation between 3° S – 14° S and 40° W – 30° W (Northeast Brazilian coast). Surface currents in in solid line and subsurface currents in dashed line (Adapted from Guimarães et al., 2024).....58
Figure 2 - The time evolution of seawater fCO_2 (a) and atmosphere fCO_2 (b) measured by merchant ships at 3°S-14°S from 2008 to 2020. 61
Figure 3 - Monthly Distribution of fCO_{2sw} for each year, from 2008 to 2020, divided into northern sub-region (3ºS – 8ºS) and southern sub-region (8ºS – 14ºS). The monthly average was calculated for each day collected in the month of the year and each dotted line color represents a collected year. Red line represents the monthly variability.....62
Figure 4 - Monthly Mean of Sea Surface Temperature (SST) measured by volunteer ships from 2008 to 2020 divided in northern sub-region (3ºS – 8ºS) and southern sub-region (8ºS – 14ºS). The monthly average was calculated for each day collected in the month of the year and each dotted line color represents a collected year.....63
Figure 5 - Distribution of the fCO_{2sw} as a function of latitude along the March of each year with data. 2009, 2010, 2011, 2015 and 2017.....65
Figure 6 - Combination of SST data measured in situ by ships (blue points) and satellite images of SST (red line), from 2008 to 2020 divided in northern sub-region (3ºS – 8ºS) and southern sub-region (8ºS – 14ºS) 67
Figure 7 - SST anomaly by satellite image data from 2008 to 2020.....67
Figure 8 - The daily wind speed at 10 m by WindSAT from 2008 to 2020 at North subregion (3°S – 8°S) and South subregion (8°S – 14°S).....68

Figure 9 - Monthly Mean of Sea Surface Salinity (SSS) measured by volunteer ships from 2008 to 2020 divided into northern sub-region (3ºS – 8ºS) and southern sub-region (8ºS – 14ºS) ..72
Figure 10 - The precipitation anomaly and daily precipitation by GPCP from 2008 to 2020 at North subregion (3°S – 8°S) and South subregion (8°S – 14°S).....73

SM 1 - Distribution of the fCO_{2sw} as a function of latitude along the different months of the years 2008, 2009 (red), 2010 (blue), 2011, 2012, 2013, 2014, 2015 (cyan), 2016 (magenta), 2017 (green), 2018 (yellow), 2019 (black) and 2020 for months from January to December.75
SM 2 - Distribution of the Sea Surface Temperature as a function of latitude along the different months of the years 2008, 2009 (red), 2010 (blue), 2011, 2012, 2013, 2014, 2015 (cyan), 2016 (magenta), 2017 (green), 2018 (yellow), 2019 (black) and 2020 for months from January to December.....77
SM 3 - Distribution of the Sea Surface Salinity as a function of latitude along the different months of the years 2008, 2009 (red), 2010 (blue), 2011, 2012, 2013, 2014, 2015 (cyan), 2016 (magenta), 2017 (green), 2018 (yellow), 2019 (black) and 2020 for months from January to December.....79

LISTA DE TABELAS

REVISÃO BIBLIOGRÁFICA

Tabela 1 -Estudos de Temperatura da Superfície do Mar (SST), pressão parcial do CO2 (pCO_2) e fluxo de CO_2 na região do oceano Atlântico tropical 30

ARTIGO 1 - REGIONAL DIFFERENCES OF THE AIR-SEA CO_2 FLUX BETWEEN 3ºS AND 14ºS IN THE SOUTHWESTERN TROPICAL ATLANTIC

Table 1 - Summary of Data Collected on Cruises in the Southwestern Tropical Atlantic. The merchant ship is identified for each voyage: MO – Monte Olivia Ship; RB – Rio Blanco Ship; SC – Santa Cruz Ship; and SL – Cap San Lorenzo. 39

ARTIGO 2 - CO_2 FLUX ALONG THE SOUTHWEST TROPICAL ATLANTIC OCEAN ADJACENT TO THE NORTHEAST OF BRAZIL (3ºS TO 14ºS) FROM 2008 TO 2020

Table 1 - Summary of Data Collected on Cruises in the Southwestern Tropical Atlantic. The merchant ship is identified for each voyage: MO – Monte Olivia Ship; RB – Rio Blanco Ship; SC – Santa Cruz Ship; and SL – Cap San Lorenzo. 39
Table 2 - Mean CO_2 Flux ($mmol^{-2}$ d^{-1}) between Northern Subregion (3°S – 8°S) and Southern Subregion (8°S – 14°S) from 2008 to 2020.....70

SUMÁRIO

1 INTRODUÇÃO 14

1.1. OBJETIVOS 15

1.1.1. Objetivo Geral 15

1.1.2. Objetivos Específicos 15

2. REVISÃO BIBLIOGRÁFICA 16

2.1. DINÂMICA DO DIÓXIDO DE CARBONO (CO_2) 16

2.2. COMPORTAMENTO DO CO_2 NA ÁGUA DO MAR 18

2.3. SISTEMA DE MEDIÇÃO AUTOMATIZADA DA pCO_2 20

2.4. FUGACIDADE DO CO_2 MARINHO NA REGIÃO TROPICAL 23

2.5. fCO_2 NO OCEANO ATLÂNTICO ADJACENTE AO NORDESTE DO BRASIL 27

3. MATERIAIS E MÉTODOS 32

4. **RESULTADOS** 33

4.1. ARTIGO 1 - REGIONAL DIFFERENCES OF THE AIR-SEA CO_2 FLUX BETWEEN 3 AND 14ºS IN THE SOUTH-WESTERN TROPICAL ATLANTIC 33

4.1.1. Introduction 33

4.1.2. Materials and Methods 35

4.1.3. Results and Discussion 39

4.1.4. Conclusion 47

4.1.5. References 48

4.2. ARTIGO 2 – CO_2 FLUX THROUGHOUT 2008 AND 2020 IN THE SOUTHWEST TROPICAL ATLANTIC OCEAN ADJACENT TO THE NORTHEAST OF BRAZIL (3ºS TO 14ºS) 55

4.2.1. Introduction 55

4.2.2. Methods and Data 58

4.2.3. Results and Discussion 60

4.2.4. Conclusion 74

4.2.5. Supplementary Material 75

4.2.6. References 81

5. CONSIDERAÇÕES FINAIS 86

REFERÊNCIAS 88

APÊNDICE 93

1 INTRODUÇÃO

Este documento de Tese de Doutorado está organizado em formato de revisão bibliográfica e artigos científicos, abordando discussões sobre o fluxo do CO_2 e sua variabilidade na interface oceano-atmosfera no oceano Atlântico tropical Sudoeste adjacente à região Nordeste brasileira, entre as coordenadas 3ºS e 30°O, 14ºS e 37°O.

Até o presente momento, este é o primeiro trabalho utilizando dados coletados da pressão parcial do CO_2 (pCO_2) nessa região do oceano Atlântico Tropical Sudoeste, adjacente ao Nordestes brasileiro, trazendo uma análise da variabilidade em 12 anos de coleta de dados, de 2008 a 2020. Podendo assim, trazer dados observacionais de como a fugacidade do CO_2 na água do mar (fCO_2) está variando ao longo dos anos.

Esta Tese apresenta-se em 3 capítulos:

- O capítulo 1 é a revisão bibliográfica sobre o dióxido de carbono (CO_2) na água do mar, seu comportamento e a variabilidade da pCO_2 e da fCO_2 na água do mar, além da análise da fugacidade do CO_2 marinho.
- O capítulo 2 é representado pelo artigo intitulado **"***Regional Differences Of The Air-Sea* Co_2 *Flux Between 3ºs And 14ºs In The Southwestern Tropical Atlantic*", publicado na *Marine and Freshwater Research*, que determina a variabilidade espacial da fugacidade do CO_2 da água do mar entre as latitudes 3º S e 14º S coletados por navios voluntários.
- O capítulo 3 é representado pelo artigo previamente intitulado "Air-sea CO_2 *Flux Throughout 2008 and 2020 in the Southwest Tropical Atlantic Ocean Adjacent to the Northeast of Brazil (3ºs to 14ºs)",* que aborda a variabilidade interanual do CO_2 na mesma região, observando algumas anomalias encontradas nos valores do fCO_{2sw} com as anomalias da temperatura da superfície do mar.

O presente trabalho foi realizado com o apoio do Conselho Nacional de Desenvolvimento Científico e Tecnológico (CNPq - 140555/2019-6), do Laboratório de Oceanografia Química da Universidade Federal de Pernambuco (LOQuim/UFPE) com o *Laboratoire d'Oceanographie et du Climat: Expérimentations et Approches Numériques* – LOCEAN/IPSL – *Institut de Recherche pour le Dévelopment* (IRD), na França.

1.1. OBJETIVOS

1.1.1. Objetivo Geral

Estimar a pressão parcial do dióxido de carbono (pCO_2) na interface ar-mar do oceano adjacente à região Nordeste do Brasil para compreender os fatores que influenciam sobre as suas variações temporais e espaciais na borda oeste do Atlântico tropical.

1.1.2. Objetivos Específicos

- Correlacionar eventos atmosféricos e climatológicos com os dados medidos da pCO_2 entre as latitudes 3ºS e 14ºS no período de 2008 a 2020;

- Analisar a base de dados dos parâmetros do carbono, temperatura, salinidade, ventos, correntes marítimas e clorofila *a* para o período do estudo, para identificar as correlações entre os fatores físicos e biológicos, e influência na variabilidade da fCO_2 nessa região.

- Determinar a taxa de variação ao logo do tempo do fluxo de CO_2 entre o oceano e a atmosfera (fonte/sumidouro) através da diferença entre as fugacidades do CO_2 (fCO_2) desses compartimentos.

2. REVISÃO BIBLIOGRÁFICA

2.1. DINÂMICA DO DIÓXIDO DE CARBONO (CO_2)

O efeito estufa constitui-se como um fenômeno natural que resulta no aumento da temperatura da superfície do planeta Terra. Este processo é causado pela absorção de energia solar por determinados compostos presentes na atmosfera terrestre, os quais são conhecidos como gases estufa. Dentre os principais gases responsáveis por esse efeito, destacam-se o vapor d'água (H_2O), dióxido de carbono (CO_2), óxido nitroso (N_2O), ozônio (O_3) e metano (CH_4) (IPCC, 2014; HOUGHTON, 2015).

Estudos científicos mostram o impacto que as ações antrópicas exercem na modificação deste fenômeno natural (FRIEDLINGSTEIN et al., 2020, 2022; LE QUÉRÉ et al., 2014; QUÉRÉ et al., 2018). Friedlingstein et al. (2022) revelaram que as emissões cumulativas de CO_2 provenientes de fontes fósseis, no período de 1850 à 2021, atingiram aproximadamente 465 ± 25 GtC. Durante a década de 2012 a 2021, o crescimento de CO_2 atmosférico foi de 5,2 GtC ano^{-1} (FRIEDLINGSTEIN et al., 2022). A Fig. 1 mostra as tendências nas emissões globais de CO_2 provenientes de combustão de energia e processos industriais de 1900 até 2022. Pode ser notado que no ano de 2020, houve uma diminuição de mais de 5% das emissões devido à pandemia de COVID-19. Porém, em 2021, as emissões recuperaram os níveis anteriores à pandemia, crescendo mais de 6% (IEA, 2022).

Figura 1 - Emissões globais de dióxido de carbono (CO_2) provenientes da combustão de energias e de processos industriais entre 1900 e 2022

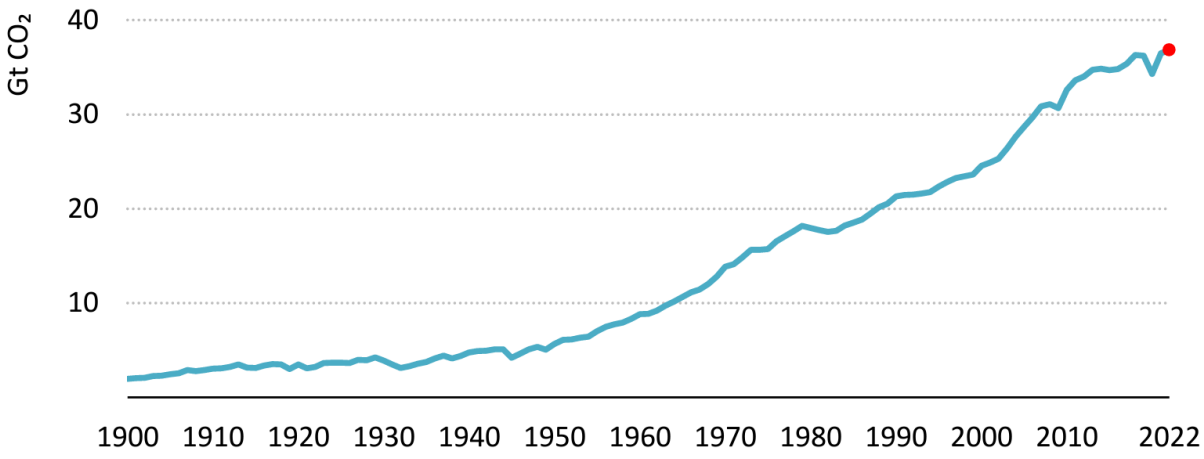

Fonte: IEA, 2022.

O estudo de Friedlingstein et al. (2022) ainda detalha a contribuição de cada combustível fóssil para esse panorama, com o carvão, o petróleo e o gás natural respondendo por cerca de

46%, 35% e 15% das emissões, respectivamente. Além disso, 3% das emissões são atribuídas à oxidação de processos energéticos e industriais, abrangendo atividades como a produção de cimento e carbonatação. Outro fator revelado por essa pesquisa é a contribuição do desmatamento através de queimadas, responsável por 1% das emissões totais de CO_2 (FRIEDLINGSTEIN et al., 2022). Incêndios florestais, são agentes agravantes desse cenário, pois promovem a degradação ambiental, devido à supressão vegetação (BONAN, 2008).

A dinâmica do CO_2 desempenha um papel crítico na regulação do equilíbrio climático e ambiental da Terra. O aumento das concentrações deste gás estufa na atmosfera está associado ao aquecimento global e às mudanças climáticas. Essas mudanças térmicas repercutem substancialmente nos padrões climáticos, nos regimes de chuvas, nas ocorrências de eventos extremos, no derretimento das calotas polares e na consequente elevação do nível do mar, nas alterações dos padrões de circulação atmosférica e oceânica, além da acidificação dos oceanos, impactando ecossistemas marinhos sensíveis, como os recifes de coral e em diversas outras variáveis climáticas (FINDLAY; TURLEY, 2021; SENEVIRATNE et al., 2012).

Dentro do contexto do ciclo do carbono, o CO_2 é um composto essencial, desempenhando um papel crítico nas interações entre os principais compartimentos: atmosfera e oceano (SABINE et al., 2004). O oceano assume um papel de destaque como um reservatório no ciclo de carbono, atuando como um mitigador dos impactos climáticos decorrentes do aumento de CO_2 atmosférico. O sistema oceânico atua na absorção de uma parcela substancial das emissões anuais de CO_2. Estimativas apontam que aproximadamente 25% das emissões anuais de CO_2 são absorvidas através da superfície oceânica, tornando o oceano como um potencial sumidouro de CO_2 atmosférico (FRIEDLINGSTEIN et al., 2022; QUÉRÉ et al., 2018; SABINE et al., 2004). Esta capacidade de absorção de CO_2 atmosférico deverá diminuir ao longo dos próximos anos, em consequência do aumento das emissões antrópicas de CO_2 – principalmente pela queima dos combustíveis fósseis supracitados, o desmatamento, os incêndios florestais (ANDRES et al., 2012; QUÉRÉ et al., 2018) – e da saturação das águas oceânicas (IPCC, 2014). Essa absorção oceânica de CO_2 atmosférico revela uma complexidade marcante em sua distribuição global.

A pressão parcial do gás de CO_2 sobre a superfície oceânica varia espacial e temporalmente. De acordo com as diferenças entre as pressões parciais do CO_2 da atmosfera e da superfície oceânica, uma massa d'água supersaturada funciona como fonte de CO_2 para a atmosfera, e uma insaturada funciona como sumidouro de CO_2 atmosférico. Enquanto os oceanos de altas latitudes, como o oceano Atlântico Norte, desempenham o papel de

sumidouros significativos de CO_2 atmosférico (BRONSELAER et al., 2016), os oceanos tropicais – i.e. oceano Pacífico Tropical – são considerados fontes líquidas de CO_2 para a atmosfera (TAKAHASHI et al., 2009).

A complexidade desse cenário de distribuição global do CO_2 é ainda mais acentuada em regiões equatoriais e tropicais, onde há uma grande variabilidade de fatores climáticos e biogeoquímicos nos oceanos convergindo na caracterização destas regiões como os principais contribuintes da variabilidade interanual das trocas oceano-atmosfera de CO_2 em escala global (WANG et al., 2015; WANNINKHOF et al., 2013). O oceano Atlântico tropical, mais especificamente, é reconhecido não apenas pela sua importância na absorção e liberação de CO_2, mas também é considerado a segunda maior fonte oceânica de CO_2 para a atmosfera, depois do Oceano Pacífico tropical (LEFÉVRE; DIVERRÉS; GALLOIS, 2010; TAKAHASHI et al., 2009).

Destaca-se então a importância dos estudos, avaliações e monitoramento da dinâmica das trocas na interface oceano-atmosfera do CO_2, enfatizando uma compreensão mais aprofundada dos processos que ocorrem com esse composto no ciclo do carbono.

2.2. COMPORTAMENTO DO CO_2 NA ÁGUA DO MAR

O CO_2 se encontra na água do mar, tanto na forma de gás dissolvido como na forma de carbonatos e bicarbonatos, apresentando uma importância no controle do mecanismo ácido-base do meio, visto que as três formas estão ligadas por uma estreita relação de equilíbrio (MILLERO, 2007).

Mais de 90% do carbono oceânico é inorgânico. A concentração do carbono inorgânico total dissolvido é dada pela soma das concentrações de três espécies deste composto coexistentes, onde: menos de 1% está sob a forma de CO_2, cerca de 90% estão sob a forma de íons bicarbonato (HCO_3^-) e abaixo de 10% sob a forma de íons carbonato (CO_3^{2-}). Estas diferentes espécies de carbono inorgânico são ligadas entre si pelas suas equações de equilíbrio (DICKSON, 2010; MILLERO, 2007). O CO_2 dissolvido se dissocia formando íons bicarbonato e carbonato com liberação de íons H^+, conforme as reações abaixo:

$$CO_{2\,(aq)} + H_2O \rightarrow H_2CO_3 \text{ (ácido carbônico)} \quad (1)$$

O H_2CO_3 e o CO_2 são espécies eletronicamente neutras. Como o H_2CO_3 ocorre apenas em pequenas quantidades, suas espécies não são dissociáveis e o CO_2 é expresso como $[CO_2] = [H_2CO_3] + [CO_{2aq}]$. As duas equações de equilíbrio químico para o HCO_3^- e CO_3^{2-} são expressas abaixo:

$$CO_2 + H_2O \leftrightarrow HCO_3^- + H^+ \text{ com um } K_1 = \frac{[HCO_3^-][H^+]}{CO_2} \quad (2)$$

$$HCO_3^- \leftrightarrow CO_3^{2-} + H^+ \text{ com um } K_2 = \frac{[CO_3^{2-}] + [H^+]}{HCO_3^-} \quad (3)$$

As constantes de dissociação K_1 e K_2 dependem da temperatura e salinidade da água do mar, além da pressão.

O carbono inorgânico dissolvido (DIC) pode ser definido como a soma das formas inorgânicas do carbono e pode ser expresso em µmol kg^{-1}.

$$DIC = [HCO_3^-] + [CO_3^{2-}] + [CO_2] \quad (4)$$

A capacidade do sistema carbonato oceânico para neutralizar tais mudanças na concentração de CO_2 atmosférico é foco de vários estudos. Esta capacidade depende dos aportes de cátions do lixiviamento das rochas e da dissolução dos carbonatos de origem química e biogênica, segundo a reação a seguir (MILLERO, 2007):

$$CO_2 + CaCO_3 + H_2O \leftrightarrow 2HCO_3 + Ca^{2+} \quad (5)$$

Essa capacidade de neutralizar a entrada de prótons na água do mar é a alcalinidade.

Uma definição mais completa de alcalinidade total (TA) pode ser descrita como: o número de moles de íons H^+ equivalentes ao excesso de receptores de prótons (bases formadas a partir dos ácidos fracos com uma constante de dissociação $K \leq 10^{-4.5}$ a 25° C) sobre os doadores (ácidos cuja constante de dissociação $K > 10^{-4.5}$) em uma parcela de 1kg de água do mar (MILLERO, 2007).

$$TA = [HCO_3^-] + 2[CO_3^{2-}] + [B(OH)_4^-] + [OH^-] + [HPO_4^{2-}] + 2[PO_4^{3-}] + [H_3SiO_4^-] + [NH_3] + [HS^-] - [H^+] - [HSO_4^-] - [HF] - [H_3PO_4] \quad (6)$$

As variações nas concentrações de CO_2 (pCO_2) na água do mar estão intrinsecamente relacionadas a diferentes processos complexos de trocas gasosas com a atmosfera. Dentre esses processos, destacam-se a solubilidade dos gases na água, a bomba biológica, a reatividade com a água do mar e a circulação de massas d'água. A bomba biológica exerce um papel

determinante na transferência do carbono inorgânico da atmosfera para as regiões profundas dos oceanos. Esse mecanismo se dá através da síntese de matéria orgânica pelos produtores primários (fitoplâncton). Este processo consiste na absorção do CO_2 atmosférico pelo fitoplâncton, resultando na diminuição da pressão parcial do CO_2 na água. Por sua vez, cria-se um gradiente favorável à absorção de CO_2 atmosférico pela água do mar, impulsionando a troca gasosa por diferença de pressão (LIBES, 2009).

Outro mecanismo importante nas trocas oceano-atmosfera é a chamada bomba de solubilidade, cuja dinâmica está relacionada ao efeito da temperatura da água do mar sobre a solubilidade do CO_2. De acordo com a relação termodinâmica expressa pela derivada parcial $\frac{\partial fCO_2}{\partial SST}/fCO_2$ estabelecida por Takahashi et al. (1993), a pCO_2 na água varia aproximadamente 4,23% $°C^{-1}$ em resposta a mudanças de temperatura. Desta maneira, tal aumento da solubilidade do CO_2 na água do mar ocorre principalmente em altas latitudes, mais especificamente nas zonas de formação de águas profundas. Nestas áreas, as águas frias e densas apresentam uma maior capacidade de absorver o CO_2 atmosférico por conta da elevada solubilidade. Esse processo resulta na transferência do CO_2 para as regiões mais profundas dos oceanos. Uma vez incorporado às águas profundas e inserido na circulação oceânica termohalina, o CO_2 percorre uma trajetória que culmina no seu retorno à atmosfera em regiões de ressurgência, como a ressurgência equatorial (MARINOV; SARMIENTO, 2004; TAKAHASHI et al., 1993).

As interações gasosas do CO_2 na interface oceano-atmosfera são comumente quantificadas pela diferença na pressão desse gás na água do mar e o ar acima dela. Entretanto, é crucial observar que o CO_2 não segue um comportamento típico de um gás ideal (WEISS, 1974). Considerando essa não-idealidade do CO_2, mesmo em pressões mais baixas, utiliza-se da *fugacidade* como propriedade termodinâmica para expressar a pressão de um gás corrigida para a não idealidade do comportamento de um gás real. Em uma faixa de temperatura de 0° a 30°C, a diferença entre a pressão parcial do CO_2 e a sua fugacidade está entre 1 e 1.5 µatm (MURPHY et al., 1994).

2.3. SISTEMA DE MEDIÇÃO AUTOMATIZADA DA *p*CO_2

Ao longo das últimas décadas, as medições da pressão parcial do CO_2 marinho têm desempenhado um papel crucial na determinação dos fluxos globais e regionais desse gás na interface oceano-atmosfera. Em 2007, a comunidade internacional de pesquisa de carbono marinho criou o *Surface Oceano CO_2 Atlas* (SOCAT), um marco na pesquisa biogeoquímica e

climática e na informação política no que se diz respeito às análises de dados de carbono marinho. Esta iniciativa colaborativa representa uma atividade de síntese e consolidação para observações relacionadas à pressão parcial do CO_2 na superfície do oceano, envolvendo a colaboração de mais de 100 fornecedores de dados, controladores de qualidade, gestores de dados e programadores que contribuem para o SOCAT.

Os dados do SOCAT estão disponíveis publicamente, podendo ser analisados e citados, permitindo a quantificação do sumidouro e fonte de carbono, além da acidificação dos oceanos, avaliando os modelos biogeoquímicos oceânicos. Estes dados do SOCAT são lançados em versões. A última versão lançada em 2023 tem cerca de 35,6 milhões de observações de 1957 a 2022 para o oceano aberto e mares costeiros (Fig. 2; BAKKER et al., 2023).

Figura 2 – Medições da pressão parcial do CO_2 registrado pela versão 2023 do SOCAT

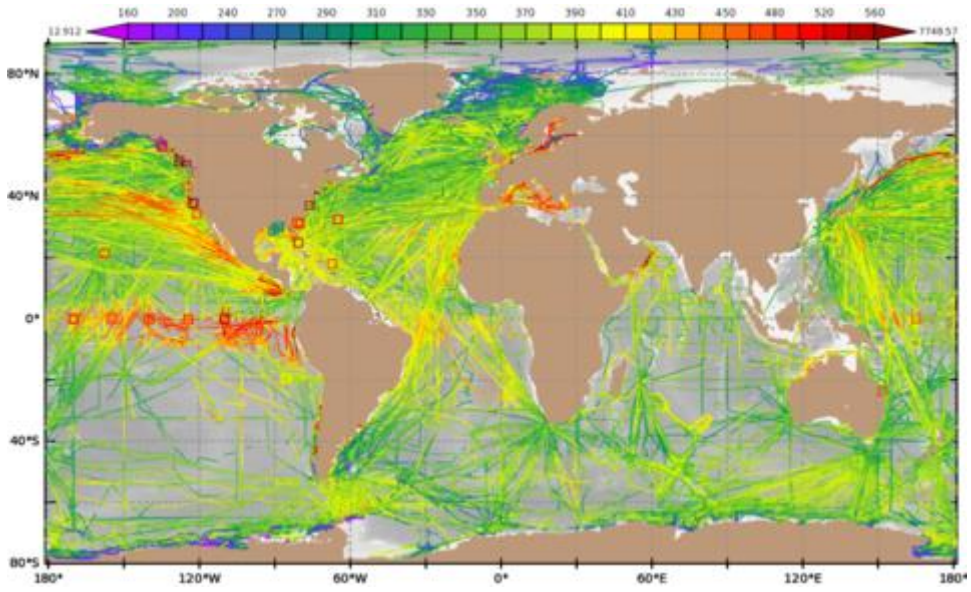

Fonte: Bakker et al., 2023.

Com o intuito de viabilizar uma coleta de dados homogênea e de alta qualidade de dados da pCO_2, a comunidade científica desenvolveu um instrumento analítico dedicado a essa pressão. Assim, houve um maior controle e aprimoramento da qualidade dos dados, podendo ser facilmente acessados (PIERROT; STEINHOFF, 2019).

O sistema de medição automatizada da pCO_2 foi projetado para alcançar uma precisão de 0,1 µatm para medições atmosféricas da pCO_2 e 2 µatm da pCO_2 para a água do mar (PIERROT et al., 2009; PIERROT; STEINHOFF, 2019). Este sistema é amplamente utilizado pela comunidade científica e está diminuindo significativamente as incertezas nas estimativas do fluxo do CO_2 do oceano global (Fig. 3). O sistema de medição automatizada da pCO_2 é descrito

por Pierrot et al. (2009) e detalhado por Pierrot & Steinhoff (2019). O equipamento mede a pCO_2 da água do mar e da atmosfera usando um analisador de detecção infravermelha não-dispersiva com fluxo contínuo a uma taxa de 1,5 – 2,1 litros por minuto. O analisador é calibrado usando gases padrão de CO_2 diferentes de zero em intervalores regulares. As medições atmosféricas são feitas periodicamente através do analisador. O sistema tem uma rotina automática de retrolavagem que reduz o crescimento de organismos e incrustações. Ele pode funcionar sem supervisão por meses, com apenas manutenção periódica mínima e também pode transmitir seus dados diariamente via comunicação por satélite, permitindo assim, análises de dados quase em tempo real e solução de problemas remotos.

Figura 3 - A - Sistema *underway* para CO_2 instalado no Navio Mercante Cap. San Lorenzo; B – Compartimento seco, com computador e o detector infravermelho de CO_2 da Licor 7000; e o C – compartimento molhado, com os equilibradores, que têm a função de equilibrar a pCO_2 da água que flui pelo sistema

Fonte: Autor, 2019.

O arranjo sistemático é composto por três compartimentos distintos com suas diferentes funções (Fig. 4). O compartimento “molhado” é por onde a água circula, tendo como elementos essenciais os balanceadores, o condensador, o medidor de vazão de água e as válvulas que controlam a circulação hídrica. O compartimento “seco”, por sua vez, contém componentes para as medições, como o analisador, a válvula selecionadora de gás, o computador e as fontes de alimentação. Além disso, há o compartimento “deck” incluindo o modem de satélite Iridium,

o receptor GPS e um transdutor de pressão externo, que contribuem para a funcionalidade remota e rastreamento preciso do sistema (PIERROT et al., 2009).

Este sistema de análise automatizada de CO_2 marinho se tornou o padrão a ser utilizado para medições *underway* deste gás devido a sua versatilidade para ser utilizado em qualquer plataforma e requerendo uma manutenção mínima, ótima precisão e qualidade no conjunto de dados.

Figura 4 – Esquema do sistema *underway* para CO_2

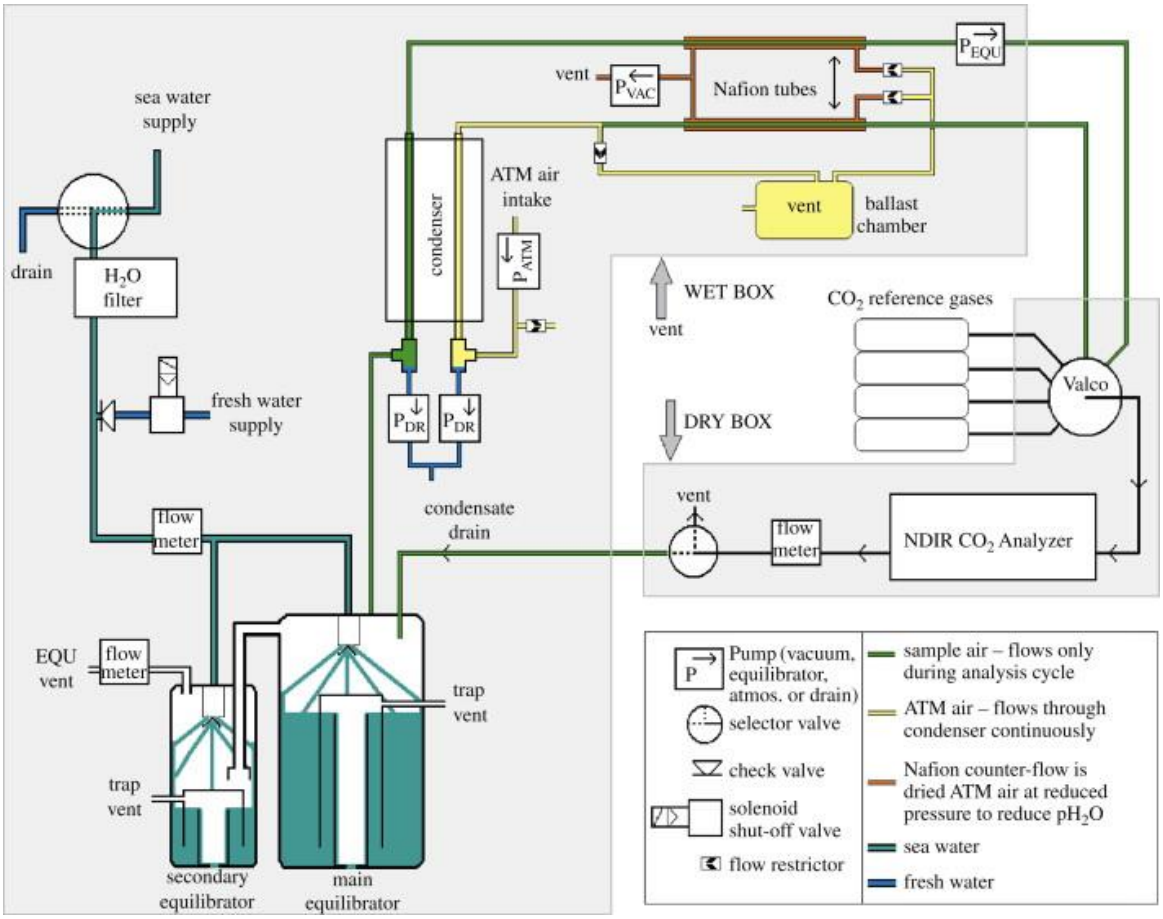

Fonte: Pierrot et al., 2009.

2.4. FUGACIDADE DO CO_2 MARINHO NA REGIÃO TROPICAL

A pressão parcial ou fugacidade do CO_2 (fCO_2) na região tropical é influenciado por fatores físico-químicos como temperatura e salinidade, fatores biológicos (clorofila, nutrientes e fotossíntese) e fatores climáticos , como o *El Niño* e a Zona de Convergência Intertropical (SABINE et al., 2004; TAKAHASHI et al., 1993, 2002, 2009). Todos estes atuando de forma conjunta e simultânea trazendo uma complexidade na distribuição do CO_2 na região.

A temperatura da água do mar influencia diretamente na solubilidade do CO_2. As oscilações térmicas desempenham um papel determinante na capacidade de dissolução desse gás, apresentando uma relação inversa à sua solubilidade. Temperaturas mais baixas favorecem a dissolução de CO_2, possibilitando que águas mais frias retirem maior quantidade desse gás da atmosfera (CARROLL; SLUPSKY; MATHER, 1991).

Takahashi et al. (1993) estimaram que a pCO_2 da superfície marinha tem uma dependência de temperatura de 4,23% ± 0,02 $^oC^{-1}$ para uma salinidade na faixa de 34 e 36 e uma temperatura de 20 a 28º C. Esta estimativa é baseada em um estudo de laboratório utilizando uma alíquota de água superficial do Atlântico Norte (TAKAHASHI et al., 1993). Já Wanninkhof et al. (2022) realizaram uma abordagem mais abrangente da dependência da temperatura em relação à pCO_2 ao longo de 3 décadas de estudo nas principais bacias oceânicas. Os resultados obtidos por Wanninkhof et al. (2022) corroboraram com a estimativa empírica por Takahashi et al. (1993). A pesquisa obteve uma dependência de temperatura de 4,13 ± 0,01 $^oC^{-1}$ (WANNINKHOF et al., 2022).

A salinidade, por sua vez, associada à quantidade de sais dissolvidos na água, também exercerá influência nas propriedades de dissolução do CO_2 (CARROLL; SLUPSKY; MATHER, 1991). Estudos sobre a pCO_2 da superfície marinha evidenciaram uma forte correlação entre esse parâmetro e a salinidade da superfície do mar (BONOU et al., 2016; IBÁNHEZ; ARAUJO; LEFÈVRE, 2016; LEFÉVRE; DIVERRÉS; GALLOIS, 2010), cujo o baixo valor da pCO_2 da superfície marinha está associado à baixa salinidade local.

No contexto dos fatores biológicos, a presença de clorofila, a disponibilidade de nutrientes e os processos fotossintéticos desempenham um papel determinante nessa absorção do CO_2 dissolvido na água do mar. A atividade fotossintética, por exemplo, pode atuar na remoção desse composto na água do mar, enquanto a presença de nutrientes pode influenciar diretamente na produtividade biológica, impactando as trocas de carbono (LIBES, 2009).

Como fator climático, a Zona de Convergência Intertropical (ITCZ – *Intertropical Convergence Zone*) é um dos principais eventos da variação da fugacidade do CO_2 da superfície da água do marinha na região tropical (LEFÈVRE et al., 2020). A ITCZ associa-se às altas Temperaturas da Superfície do Mar (TSM) na região tropical do oceano Atlântico, contribuindo para a baixa salinidade, devido às fortes chuvas, e as baixas concentrações de fCO_2 (LEFÈVRE et al., 2014; LEFÉVRE; DIVERRÉS; GALLOIS, 2010).

A ITCZ se deve à encontro de ventos alísios do nordeste do hemisfério norte com os ventos alísios do sudeste do hemisfério sul em baixos níveis da atmosfera. Essa convergência de ventos na região equatorial do globo é controlada pelo aquecimento da superfície, que por sua vez desenvolvem uma célula vertical na atmosfera intensificando a convergência de calor e umidade para um ramo ascendente formando bandas de nuvens convectivas. Esse sistema forma a ITCZ, que se caracteriza por ser uma zona de forte precipitação (XIE; CARTON, 2004). A alta precipitação devido a ITCZ afeta a salinidade, que influencia no balanço Evaporação-Precipitação da região do Atlântico Tropical. As altas TSM e suas variações sazonais é um dos fatores determinantes no posicionamento e na intensidade da ITCZ.

A ITCZ tem uma migração meridional sazonal. Durante o verão e outono austral, entre os meses de dezembro e março, a TSM está mais quente, os ventos alísios de nordestes se intensificam, os ventos alísios de sudeste enfraquecem (Fig. 5). Portanto, a ITCZ se localiza mais ao sul, podendo chegar a 5º S de latitude do hemisfério sul. Durante esse período, há chuvas intensas próximas do equador, no norte da região Nordeste do Brasil e no leste da Amazônia. Após esse período, entre os meses de junho e setembro, a TSM fica mais fria no Atlântico Sul, há um aumento das forças dos ventos alísios de sudeste, juntamente com o enfraquecimento dos ventos alísios de nordeste, e assim, muda a ITCZ para uma posição mais ao norte da linha do Equador podendo alcançar 10° – 15° N (ESSIEN et al., 2022; XIE; CARTON, 2004).

Figura 5 – Posição média sazonal da Zona de Convergência Intertropical

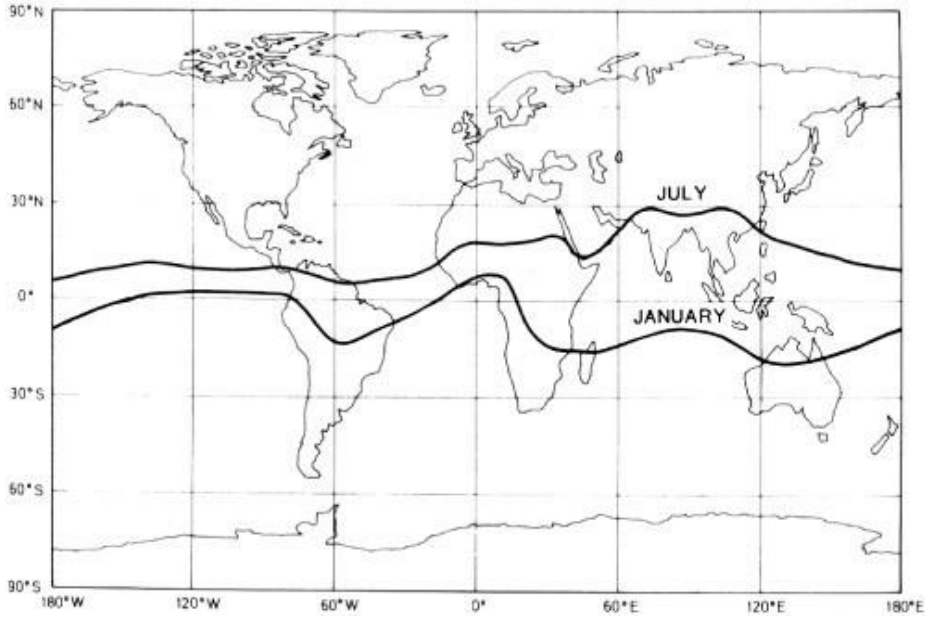

Fonte: (YAN, 2005)

A posição da ITCZ pode ser alterada por alguns fenômenos climáticos que modificam a circulação meridional atmosfera. Um grande exemplo é o chamado de ENSO – *El Niño-Southern Oscillaton* (LEDUC et al., 2009; MÜNNICH; NEELIN, 2005; SCHNEIDER; BISCHOFF; HAUG, 2014). A ENSO é um fenômeno climático de oscilação acima (*El Niño*) ou abaixo (*La Niña*) da média da temperatura da superfície do mar na região do oceano Pacífico tropical, juntamente com a mudança no regime de chuvas e ventos, que influencia amplamente no ciclo global do carbono, afetando a absorção do carbono nos oceanos tropicais (RAYNER; LAW; DARGAVILLE, 1999). A ENSO modula a variabilidade interanual do fluxo do CO_2 nas regiões equatoriais e tropicais dos principais oceanos. No Pacífico tropical, durante os anos de *El Niño*, menos carbono é liberado pelo oceano, enquanto o oposto ocorre nos anos de *La Niña*. No oceano Pacífico equatorial, durante os eventos de *El Niño*, a TSM mais quente reduz a solubilidade do CO_2, aumentando a pCO_2 da água do mar. Paralelo a isso, há uma redução das taxas de ressurgência das águas enriquecidas de carbono inorgânico dissolvido e ricas de nutrientes no oeste do Pacífico ao longo do equador, reduzindo pCO_2 da água do mar da superfície. Estas mudanças influenciam diretamente nas anomalias do fluxo do CO_2 do Pacífico tropical, diminuindo a concentração de carbono inorgânico dissolvido na superfície oceânica. Durante os eventos de *La Niña* acontecem o oposto (AYAR et al., 2022). O Atlântico tropical é o segundo maior oceano que sofre influência do ENSO (HASTENRATH, 2012).

Dessa forma, se pode perceber que há muitos fatores bastante importantes para serem estudados para se fazer a análise da variação da pCO_2 e nos processos dinâmicos das propriedades da água que influenciam a tendência da pCO_2. E perceber que existem anomalias interanuais que irão alterar na distribuição do CO_2.

Dessa forma, a abordagem mais apropriada para expressar a termodinâmica do fluxo do CO_2 é por meio do conceito de fugacidade, que fornece uma representação mais precisa dessas condições não ideais (WANNINKHOF; THONING, 1993; WEISS, 1974). A fCO_2 é um parâmetro chave na determinação da direção e magnitude dos fluxos de CO_2 entre o oceano e atmosfera. Portanto, é ela é utilizada em cálculos relacionados às trocas gasosas. O fluxo ar-mar do CO_2, expresso em mmol m^{-2} d^{-1}, é calculado através da fórmula:

$$FCO_2 = kS\,(fCO_{2sw} - fCO_{2atm}) \tag{7}$$

Onde k é a velocidade de transferência do gás, que tem sido relatado por Sweeney et al. (2007), calculado com base no campo de vento do Centro Europeu de Previsões Meteorológicas de Médio Prazo (ECMWF), S é a solubilidade, medida em função da temperatura e salinidade

(WEISS, 1974) e (fCO_{2sw} - fCO_{2air}) é referido como a ΔfCO_2, como sendo a força termodinâmica do fluxo do gás.

Em 2021, a concentração média global do CO_2 atmosférico atingiu cerca de 414,7 ± 0,1 ppm. Com os dados preliminares de 2022, Friedlingstein et al. (2022) estimaram que a concentração de CO_2 na atmosfera alcançou a marca de 417,2 ppm, um valor discrepante de mais de 50% acima em relação aos níveis pré-industriais (antes de 1750), que foi estimado em torno de 278 ppm (FRIEDLINGSTEIN et al., 2022). De acordo com o monitoramento global da pressão do dióxido de carbono (pCO_2) realizado pela *National Oceanic and Atmospheric Administration* (NOAA), Observatório de Mauna Loa – Hawai, em abril de 2024, média global mensal do CO_2 atingiu 423,5 ppm (Fig. 6).

Figura 6 - Concentração média global do CO_2 atmosférico em partes por milhão (ppm). Desde 1980, o NOAA/GML produzem dados mensais baseados em uma média das medições diretas de múltiplas estações.

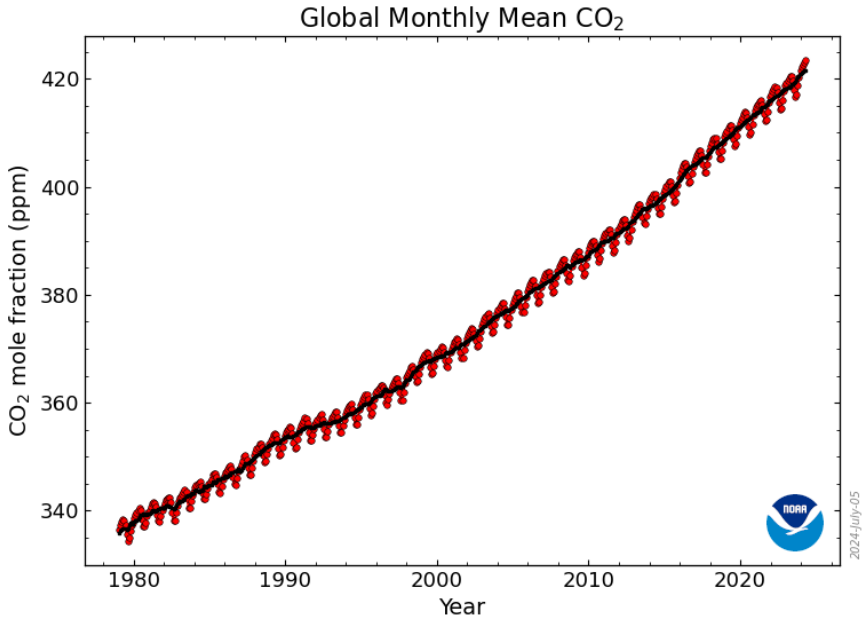

Fonte: NOAA, 2024.

2.5. fCO_2 NO OCEANO ATLÂNTICO ADJACENTE AO NORDESTE DO BRASIL

O Oceano Atlântico Sul é controlado pela Corrente Sul Equatorial que transporta águas oligotróficas e quentes (MEDEIROS et al., 1999), devido a uma baixa concentração de nutrientes na camada superficial e presença de uma termoclina permanente. As massas d'água superficiais (Água Tropical Superficial e Água Central do Atlântico Sul) fluem através do Giro Subtropical passando pela Bacia do Brasil e chegando ao contorno oeste (STRAMMA; SCHOTT, 1999). Na região nordeste do Brasil existe uma escassez de nutrientes nas camadas

superficiais devido ao empilhamento das águas superficiais menos densas e a presença de uma forte estratificação devido a uma termoclina permanente (MEDEIROS et al., 1999).

Para identificar os fatores que controlam a distribuição do CO_2 na superfície oceânica do Atlântico Sul, é importante identificar o efeito das correntes, das variações da temperatura da água, dos processos biológicos e da reatividade química sobre o fluxo de CO_2. Os poucos estudos da variabilidade espacial e temporal dos fluxos de CO_2 nas regiões (ARAUJO et al., 2019; CARVALHO et al., 2017; DE JESUS AFFE et al., 2023; IBÁNHEZ; FLORES; LEFÈVRE, 2017; IBÁNHEZ; FLORES MONTES; LEFÈVRE, 2022; LEFÈVRE et al., 2013; MONTEIRO et al., 2022; VALSALA; MAKSYUTOV, 2010) e as incertezas de caracterização dos fluxos de CO_2 entre a atmosfera e os reservatórios oceânicos e terrestres (FRIEDLINGSTEIN et al., 2020) são fatores que levam a questionar os balanços e estimativas atuais de troca de CO_2 na região do Atlântico tropical.

Outro fator negligenciado na grande maioria dos estudos envolvendo o CO_2 marinho e o ciclo do carbono nos oceanos globais é a complexidade das zonas costeiras. Há lacunas de dados e pesquisas nessas áreas nos oceanos do hemisfério sul do planeta (OLIVEIRA et al., 2023). Esta lacuna é estendida ainda mais quando se trata do Oceano Atlântico Tropical Oeste que banha a região costeira do Nordeste brasileiro. A costa nordestina, entre 3ºS e 14ºS, consiste em aproximadamente 24% do território costeiro do Brasil (KNOPPERS; EKAU; FIGUEIREDO, 1999). Neste contexto, apesar de suas grandes proporções, ainda apresenta inconsistências na temática de concentração e fluxo do CO_2 e no comportamento desse gás como fonte ou sumidouro para a atmosfera local e regional.

Um levantamento bibliográfico realizado por Oliveira et al. (2023) trouxe uma revisão dos estudos do sistema carbonato marinho e do fluxo do CO_2 na interface oceano-atmosfera na costa do Brasil. Dos mais de 100 artigos publicados de 2000 a 2022 que foram revisados por este estudo, cerca de 30 artigos foram voltados aos estudos na região Norte-Nordeste do Brasil. Desses, somente 15 artigos teve uma abordagem voltada à plataforma continental do Nordeste brasileiro (OLIVEIRA et al., 2023).

A pesquisa conduzida por Araújo et al. (2019) avaliou a variabilidade espaço-temporal do CO_2 marinho da região norte e nordeste do Brasil utilizando um conjunto de dados do Programa REVIZEE, abrangendo o período de março de 1995 a setembro de 2001. Os resultados revelaram que a região Nordeste brasileira (entre as latitudes 4º S e 12ºS) era uma fonte de CO_2 para a atmosfera, com uma taxa de 0,3 ± 1,7 mmol m^{-2} d^{-1}. Os processos

termodinâmicos foram os principais contribuintes para variabilidade tanto espacial quanto temporal. A ausência significativa de uma descarga fluvial substancial ao longo da costa oeste brasileira é um fator preponderante que pode influenciar na distribuição do CO_2 no nordeste do Brasil (PASSAIA et al., 2020). Por sua vez, a distribuição do CO_2 na região norte brasileira é influenciada diretamente pela pluma do Rio Amazonas. A pesquisa de Araújo et al. (2019) mostrou que nesta região os fluxos do CO_2 marinho apresentaram variações espaço-temporais com valores negativos, indicando a região como sumidouro deste composto, e a atividade biológica como sendo o principal processo influenciador desta oscilação do fluxo do CO_2. Neste estudo, os valores da pCO_2 observados na região nordeste tiveram uma média de 379 ± 16 µatm, enquanto que na região norte, a média foi de 355 ± 52 µatm. O fluxo do CO_2 para este estudo variou de -0,30 a 4,10 mmol m^2 d^1.

Por meio de cruzeiros oceanográficos, Carvalho et al., 2017 estudaram a pCO_2 da água do mar e da atmosfera da região oceânica adjacente à região Nordeste do Brasil, entre 3º S e 5º S (outubro de 2012) e 1º S e 4ºS (setembro de 2014). No primeiro cruzeiro, a média da fugacidade do CO_2 para água do mar (fCO_{2sw}) atingiu 400,9 ± 7,3 µatm, enquanto a fugacidade do CO_2 atmosférico (fCO_{2atm}) registrou 375,8 ± 2,0 µatm. Já no segundo cruzeiro, a fCO_{2sw} foi de 391,1 ± 6,3 µatm e a fCO_{2atm} foi de 368,9 ± 2,2 µatm. Os dados analisados por esse estudo forneceram indícios de uma supersaturação da água do mar em relação à atmosfera, sinalizando a região estudada como fonte de CO_2 para a atmosfera. Além disso, a pesquisa avaliou a concentração de clorofila a para a região, corroborando novamente a presença de baixas concentrações, sendo a área classificada como oligotrófica (CARVALHO et al., 2017).

Muitos dos estudos da distribuição do CO_2 na região do oceano Atlântico tropical oeste foram voltados pra a área adjacente à pluma do rio Amazonas (COOLEY et al., 2007; IBÁNHEZ et al., 2015; KÖRTZINGER, 2003; LEFÈVRE et al., 2014, 2017, 2020; MONTEIRO et al., 2022; MU et al., 2021; PADÍN et al., 2009). Esta área do Atlântico é afetada pela descarga deste rio e pela migração sazonal da ITCZ, sendo ambas fontes de águas doces para o oceano. Além disso, a região da pluma amazônica tem um complexo sistema de correntes e contracorrentes (SCHOTT; FISCHER; STRAMMA, 1998; STRAMMA, 2008).

Se comparado com os trabalhos desenvolvidos na região amazônica, existem poucos estudos da distribuição do CO_2 voltados ao oceano Atlântico tropical oeste adjacente à região Nordeste brasileira. A maioria dos estudos encontrados são abordados de forma generalizada

(TAKAHASHI et al., 2002, 2009; WANNINKHOF et al., 2013) e com diferentes metodologias utilizadas para análise deste CO_2.

Na tabela 1 abaixo, existe uma comparação de alguns estudos que foram realizados na região do Atlântico tropical sudoeste adjacente ao Nordeste brasileiro. Eles mostram intervalos próximos em relação aos valores de temperatura da superfície do mar, pressão parcial do CO_2 e fluxo do CO_2. Estes estudos utilizaram de metodologias distintas para análise da distribuição do CO_2.

Tabela 1 -Estudos de Temperatura da Superfície do Mar (SST), pressão parcial do CO2 (pCO_2) e fluxo de CO_2 na região do oceano Atlântico tropical

	Latitude	**SST (°C)**	***p*CO₂ (µatm)**	**CO₂ Flux (mmol m² d ⁻¹)**
Andrié et al., 1986	5°N – 5°S	26.5 – 28.8	335.0 – 415.7	0.04 – 4.04
Oudot et al., 1995	5°N – 5°S	26.8 – 28.8	362.5 – 430.5	0.27 – 8.80
Lefèvre et al., 1998	20°N – 20°S	19.7 – 28.8	350.7 – 360.3	-
Lefèvre et al., 2010	3°S – 10°S	26.6 – 28.6	371.1 – 390.7	-0.33 – 2.98
Lefèvre et al., 2014	20°N – 10°S	19.5 – 30.2	180.3 – 437.4	1.20 – 3.62
Carvalho et al. 2017	1ºS – 5ºS	26.5 – 28.0	371.9 – 428.7	0.89 – 14.62
Araújo et al., 2019	3°S – 5°S	25.5 – 29.5	350.0 – 423.0	-0.30 – 4.10
Cotovicz Jr et al 2020	3°32’ – 3°42’S	28.2 – 28.4	458.0 – 475.0	5.0 – 8.4
Guimarães et al, 2024*	3ºS – 14ºS	26.4 – 29.0	360.0 – 450.0	-0.55 – 3.14

* Artigo científico da tese.

Os dados apresentados por Andrié et al (1986) basearam-se um antigo programa francês, no qual foram analisados dados coletados do cruzeiro FOCAL 6, realizado durante janeiro-fevereiro de 1984, ao longo do meridiano de 35° oeste, entre as latitudes 5° N e 5°S. Além disso, Oudot et al. (1995) também utilizaram destes mesmos dados, complementados pelos dados coletados durante o cruzeiro CITHER 1, ocorrido de janeiro a março de 1993. Ambos os estudos revelaram similaridade na distribuição do CO_2 e em seu fluxo, apontando um padrão consistente entre os dois estudos.

Já os resultados apresentados por Araújo et al. (2019) foram obtidos de forma indireta, sendo estimados a partir da coleta de outros parâmetros, que permitiram inferir os dados relativos ao CO_2.

Em relação aos demais estudos mencionados na Tabela 1, todos eles empregaram sistemas de medição contínua de CO_2 *in situ*, que foram instalados em embarcações para a obtenção dos dados. Estudos como os de Lefèvre et al. (1998, 2010, 2014), Carvalho et al. (2017), Cotovicz Jr et al. (2020) e Guimarães et al., (2024) utilizaram do sistema *underway*, previamente descrito na sessão 2.3. Portanto, as diferenças observadas nos resultados relacionados à SST, pCO_2 e fluxo do CO_2 podem ser atribuídas aos diferentes pontos de coletados dados. Porém, apesar dessas variações, há uma proximidade de dados nesses estudos.

3. MATERIAIS E MÉTODOS

Para o seguinte estudo, os dados da pCO_2 foram coletados a partir da infraestrutura de pesquisa francesa ICOS (*Integrated Carbon Observation System*). Como parte do projeto europeu CARBOCHANGE, o grupo francês instalou um sistema de bordo que mede o pCO_2 em um navio de observação voluntário que navegava da França para o Brasil, passando pelo oceano Atlântico adjacente ao Nordeste brasileiro. Este sistema mede fCO_2 na água do mar e na atmosfera por detecção infravermelha não dispersiva usando um analisador Licor 7000 com fluxo contínuo a uma taxa de 1,5–2,1 L min^{-1}. O sistema pCO_2 foi descrito por Pierrot et al. (2009).

As medições começaram em 2008 e foram realizadas tanto nas viagens de ida (França-Brasil), como nas viagens de volta (Brasil-França) do navio. Quando o navio mudou de rota, o sistema de medição pCO_2 foi instalado em um navio diferente para manter a mesma rota de 2008 até 2020. Quatro navios contribuíram para o conjunto de dados de CO_2. O navio também foi equipado com um termossalinógrafo *Seabird* (SBE 21) para medir temperaturas e salinidades durante a navegação. No total, foram realizados 79 cruzeiros ao longo de 12 anos (2008–2020), fornecendo 64.028 medições.

Os dados de pCO_2 estão disponíveis no *Surface Ocean CO_2 Atlas* (SOCAT). Os dados de salinidade da superfície do mar foram validados, arquivados e disponibilizados gratuitamente pelo *French Sea Surface Salinity Observation Service*. Os dados de *Ocean Color* foram coletados através do *Sea-viewing Wide Field-of-view Sensor* (SeaWiFS) desenvolvido e mantido pelo *Goddard Space Flight Center, Ocean Ecology, Laboratory, Oceano Biology Processing Group for Chlorophyll data*. E os dados de correntes de superfície foram coletados pelo *Ocean Surface Current Analysis* (OSCAR) mantidos por *JPL Physical Oceanography DAAC* e desenvolvido por *ESR (Earth and Space Research*). Os dados de velocidade do vento foram obtidos através dos dados do *Windsat* produzidos pelo *Remote Sensing Systems and sponsored* pela *NASA Earth Science MEaSUREs DISCOVER Project and the NASA Earth Science Physical Oceanography Program.* Foram obtidos dados de Temperatura da Superfície do Mar por imagem de satélite através do *MODIS/Aqua Water Reservoir Monthly L3 Global V061*. Para analisar a precipitação, foram usados os conjuntos de dados mensais do *Global Precipitation Climatology Project (GPCP)* de 2008 até 2020..

Para análise dos dados obtidos, foi utilizada linguagem de programação *MatLab* Versão 9.5 (R2018b).

4. RESULTADOS

4.1. ARTIGO 1 - REGIONAL DIFFERENCES OF THE AIR-SEA CO_2 FLUX BETWEEN 3 AND 14ºS IN THE SOUTH-WESTERN TROPICAL ATLANTIC

4.1.1. Introduction

The carbon dioxide (CO_2) distribution in the ocean shows a large spatial and temporal variability. Ocean–atmosphere exchanges are very dynamic and controlled by physical, chemical and biological processes (TAKAHASHI et al., 2002, 2009).

Efforts have been made to determine the temporal evolution of surface seawater CO_2 and sea–air CO_2 fluxes. Recently, more studies have been conducted on the CO_2 distribution in the western tropical Atlantic (ARAUJO et al., 2019; BONOU et al., 2016; CARVALHO et al., 2017; IBÁNHEZ et al., 2015; LEFÈVRE et al., 2014, 2020; LEFÉVRE; DIVERRÉS; GALLOIS, 2010; MONTEIRO et al., 2022; MOUSSA et al., 2016). Nevertheless, few studies exist on the seasonal and spatial variability of CO_2 fluxes south of the equator next to Brazilian coast (CARVALHO et al., 2017; COTOVICZ; CHIELLE; MARINS, 2020; LEFÈVRE et al., 2014; LEFÉVRE; DIVERRÉS; GALLOIS, 2010).

The south-western tropical Atlantic (SWTA) region is oligotrophic (LEFÉVRE; DIVERRÉS; GALLOIS, 2010; SILVA et al., 2019; TAKAHASHI et al., 2009) and characterized by warm surface waters. The coastal ecosystems of north-eastern Brazil have a limited spatial extend to significantly alter the carbon chemistry of the SWTA (CHEN et al., 2013; DE QUEIROZ et al., 2015; NORIEGA et al., 2015; SILVA et al., 2019).

The intertropical convergence zone (ITCZ) is a physical process that influences the balance of evaporation–precipitation in this region (ASSUNÇÃO et al., 2020; PAILLER; BOURLÈS; GOURIOU, 1999; STRAMMA; SCHOTT, 1999). The ITCZ explains the low salinities in the North Equatorial Counter Current (NECC) and affects the fluxes of CO_2 between the ocean and the atmosphere (IBÁNHEZ; FLORES MONTES; LEFÈVRE, 2022).

Previous coastal-budget studies have shown that there are almost no data on the tropical South Atlantic (LARUELLE et al., 2014). There is uncertainty over the CO_2 distribution in these regions, which is attributed to the existence of large areas that remain undersampled (ROOBAERT et al., 2019). This is worse when we approach the Brazilian coast. Most of the studies realized near the Brazilian coast have been located in the northern area (IBÁNHEZ;

ARAUJO; LEFÈVRE, 2016; IBÁNHEZ; FLORES; LEFÈVRE, 2017; LEFÈVRE et al., 2017, 2020; MONTEIRO et al., 2022), focused on the interaction of the CO_2 distribution with the Amazon River plume and the close ocean currents. In this region, there is a complex system of ocean currents, where it is dominated by North Equatorial Current (NEC) and North Equatorial Counter Current (NECC), which is fed by the North Brazil Current (NBC) (RODRIGUES; ROTHSTEIN; WIMBUSH, 2007; STRAMMA; SCHOTT, 1999) and is heavily influenced by freshwater from the Amazon River, with a mean discharge of 209,000 $m^3 s^{-1}$ to the tropical Atlantic ocean, being the largest river by volume of water in the world (DAI; TRENBERTH, 2002; GIFFARD et al., 2019; MOLINIER et al., 1996).

The other studies near to Brazilian coast have been on the south-western part of South Atlantic Ocean (ALBUQUERQUE et al., 2022; KERR et al., 2016; LIUTTI et al., 2021; OLIVEIRA et al., 2019; ORSELLI et al., 2019). There is no considerable important river discharge on the western coast of Brazil (ANA, 2024; PASSAIA et al., 2020) which could have a much greater influence on the CO_2 distribution in regions close to the continental shelves of Brazil (ITO; GARCIA; TAVANO, 2016; ITO; SCHNEIDER; THOMAS, 2005; LARUELLE et al., 2010), such as the Amazon River in the northern region. The southern branch of South Equatorial Current (sSEC) is the main current that flows to the south of Brazilian coast to become the Brazil Current (BC), and is the western current band of the subtropical gyre (STRAMMA; IKEDA; PETERSON, 1990).

Using the REVIZEE Program dataset (from March 1995 to September 2001), in the northern and north-eastern exclusive economic zones of Brazil, Araujo *et al*. (2019) found that north-eastern Brazil from 4 to 12°S was a source of CO_2 to the atmosphere of 0.3 ± 1.7 mmol $m^{-2} day^{-1}$. They also observed a positive trend in the partial pressure of CO_2 (pCO_2) of $+1.10 \pm 0.2$ µatm $year^{-1}$ during the period of 1987–2010. Thermodynamic processes explained most of the spatial and temporal variability (ARAUJO et al., 2019).

Carvalho *et al*. (2017) studied seawater and atmosphere pCO_2 through oceanographic cruises, in October 2012 (3−5°S) and in September 2014 (1−4°S), off the northeastern coast of Brazil. The results showed the fugacity of seawater CO_2 (fCO_{2sw}) ranging between 400.9 ± 7.3 µatm in October 2012 and 391.1 ± 6.3 µatm in September 2014. In the atmosphere, the fugacity of CO_2 (fCO_{2atm}) was 375.8 ± 2.0 µatm in October 2012 and 368.9 ± 2.2 µatm in September 2014.

Liutti *et al*. (2021) studied the seasonal sea-surface CO_2 fugacity in the south-western South Atlantic Ocean between 20 and 35°S, close to Brazilian coast. Considering the whole study region, there was an increase in fCO_{2sw} between August and February, with the highest values in January and February, followed by a decrease until August. The results of this study showed that the spatial pattern of the sea-surface fCO_2 distribution followed the seasonal variability of sea-surface temperature (LIUTTI et al., 2021).

Here, we use CO_2 observations collected by volunteer ships to analyze the CO_2 flux between 3 and 14°S, to determine the spatial variability of the fCO_{2sw} and of the sea–air CO_2 fluxes in the area between 3 and 14°S. These results will contribute to increase the knowledge about the carbon cycle in the southwestern tropical Atlantic, close to the Brazilian coast.

4.1.2. Materials and Methods

4.1.2.1. Study Area

The study focused on the region covered by the volunteer observing ships from 3°S to 14°S (Fig. 1).

In the region close to the Brazilian north-east, the dynamic of SWTA marine current is mainly led by the South Equatorial Current (SEC) (DOSSA et al., 2021; STRAMMA; SCHOTT, 1999). As can be seen in Fig. 2*a*, the SEC has tree branches, the sSEC, the central branch (cSEC) and the northern branch (nSEC). The sSEC and cSEC are the major surface currents found between 3 and 14°S (Fig. 2*b*). They are affected by the seasonal variability of the winds.

The sSEC flows to the west and is fed by the Benguela Current (Fig. 2*a*). It transports salty and warm waters. Previous studies have suggested that the sSEC bifurcates between 10 and 20°S (RODRIGUES; ROTHSTEIN; WIMBUSH, 2007; STRAMMA; IKEDA; PETERSON, 1990; STRAMMA; SCHOTT, 1999), and shows a variable transport around the year (RODRIGUES; ROTHSTEIN; WIMBUSH, 2007). When reaching the Brazilian coast (Fig. 2*b*), the sSEC is divided into two branches. The branch flowing north is the North Brazilian Undercurrent (NBUC) (LUMPKIN; GARZOLI, 2005) that joins the cSEC near 3−5°S to form the North Brazilian Current (NBC) (DOSSA et al., 2021).

South of 8°S, the surface water is subject to intense evaporation and is characterized by a salinity maximum water (SMW), exceeding 36.6, and located between 8 and 25°S (WIENDER;

ARHAN; MERCIER, 2000). These surface waters are transported by the sSEC, and have average salinities between 36.6 and 37.0 (ARAUJO et al., 2011; WIENDER; ARHAN; MERCIER, 2000).

The main surface-water mass between 3 and 14°S is the tropical surface water (TSW), which is warm, with temperatures of ~27°C, and salty with salinity of ~36 (STRAMMA; ENGLAND, 1999; STRAMMA; SCHOTT, 1999). Between 3 and 14°S, the means of sea-surface temperature (SST) and sea-surface salinity (SSS) are 27.65 ± 0.9°C and 36.5 ± 0.4.

Fig. 1 – Map of the Southwestern Tropical Atlantic with all cruises tracks with underway CO_2 measurements.

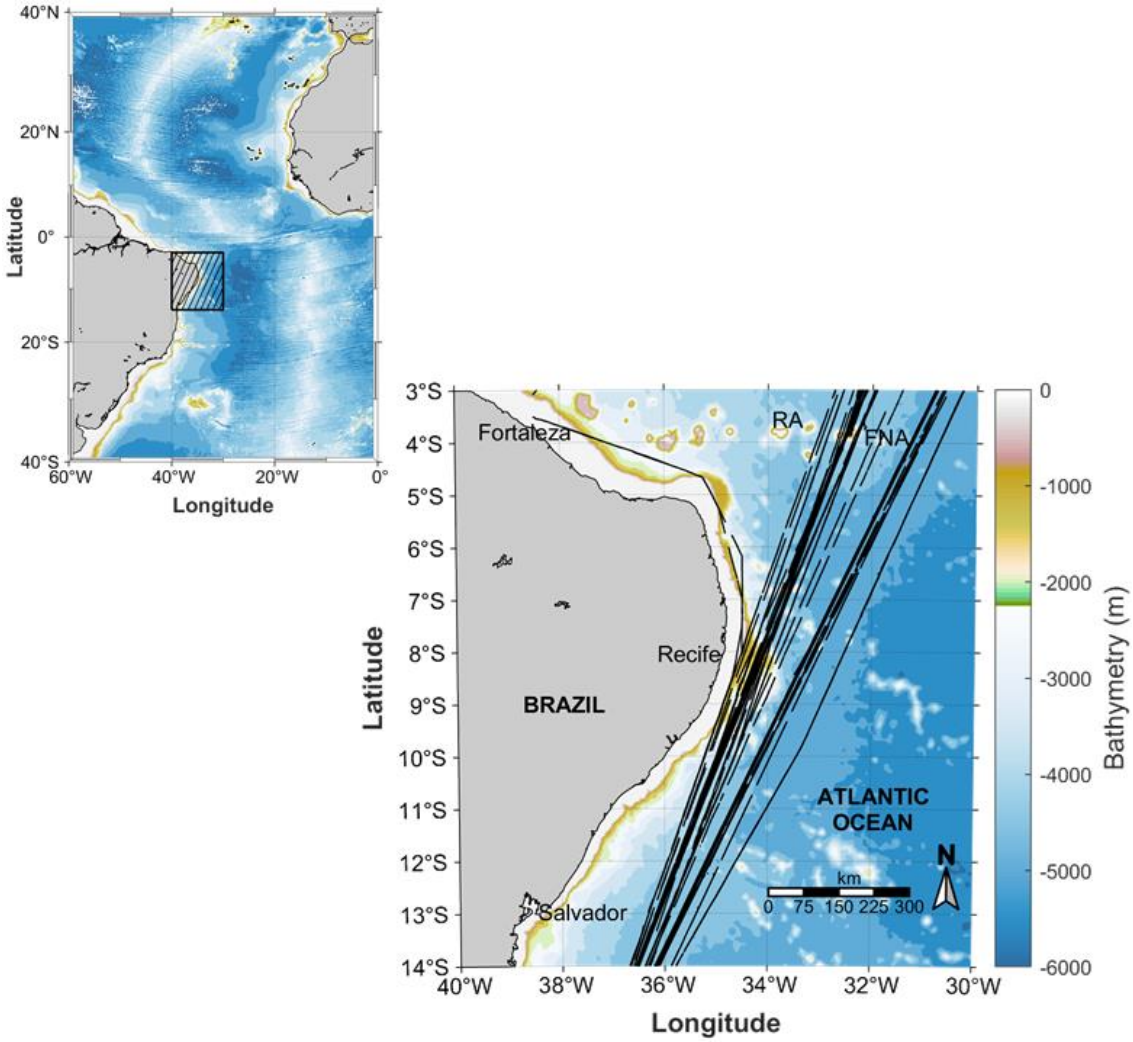

Source: The author (2021).

4.1.2.2. Data

As part of the European project CARBOCHANGE, the French group equipped a volunteer observing ship sailing from France to Brazil (Fig. 1) with an onboard, underway pCO_2

system 8050 from General Oceanics, in which the seawater enters the equilibrator through a spiral nozzle.

This line is part of the Integrated Carbon Observation System (ICOS) European research infrastructure. The pCO_2 system has been described by Pierrot *et al*. (2009). It measures fCO_2 in seawater and in the atmosphere by non-dispersive infrared detection by using a Licor 7000 analyzer with a continuous flux at a rate of 1.5–2.1 L min^{-1} (PIERROT et al., 2009). The analyzer is calibrated using three non-zero CO_2 standard gases manufactured by Air Liquide in France and calibrated at the calibration laboratory of ICOS. The processing of the data has been described in detail by Pierrot *et al*. (2009). The data are publicly available in Surface Ocean CO_2 Atlas (SOCAT). The accuracy of fCO_2 system is within ±2 μatm. Atmospheric measurements are made every 4 h.

The measurements started in 2008. When the ship changed route, the pCO_2 measuring system was installed on a different ship to maintain the same track from 2008 up to now. Four ships contributed to the CO_2 dataset (Fig. 3).

The ship was also equipped with a Seabird thermosalinometer (SBE 21) to measure temperatures and salinities while underway (ALORY et al., 2015). The precision was 0.05 for salinity. The temperature sensors gave an accuracy of 0.01°C. In total, 79 cruises were realized over 12 years (2008–2020), providing 64,028 fCO_{2sw} measurements (Fig. 3, Table 1).

For the analysis of biological processes, the monthly average of chlorophyll-*a* (Chl-*a*) was obtained by satellite images produced from Moderate Resolution Imaging Spectroradiometer (MODIS) (see https://modis.gsfc.nasa. gov/data/dataprod/chlor_a.php) for the same sampling period as for fCO_2 (2008–2020).

To examine the ocean circulation, the ocean surface-current analyses–real time (OSCAR) current data from 2008 to 2020 were used. Monthly zonal (u) and meridional (v) components of the surface currents were produced at 1/3° resolution (EARTH SPACE RESEARCH 2009).

Fig. 2 – a) Schematic representation of surface (solid line) and subsurface (dashed line) currents along the Tropical Atlantic between 30°N – 30°S and 60°W – 15°E, with the box showing for the study area (adapted from Stramma; Schott, 1999); b) Schematic representation of mean currents and edgy generation between 3º S – 14º S and 40º W – 30 º W (Northeast Brazilian coast). Surface currents in solid line and subsurface currents in dashed line (Adapted from Dossa et al., 2021)

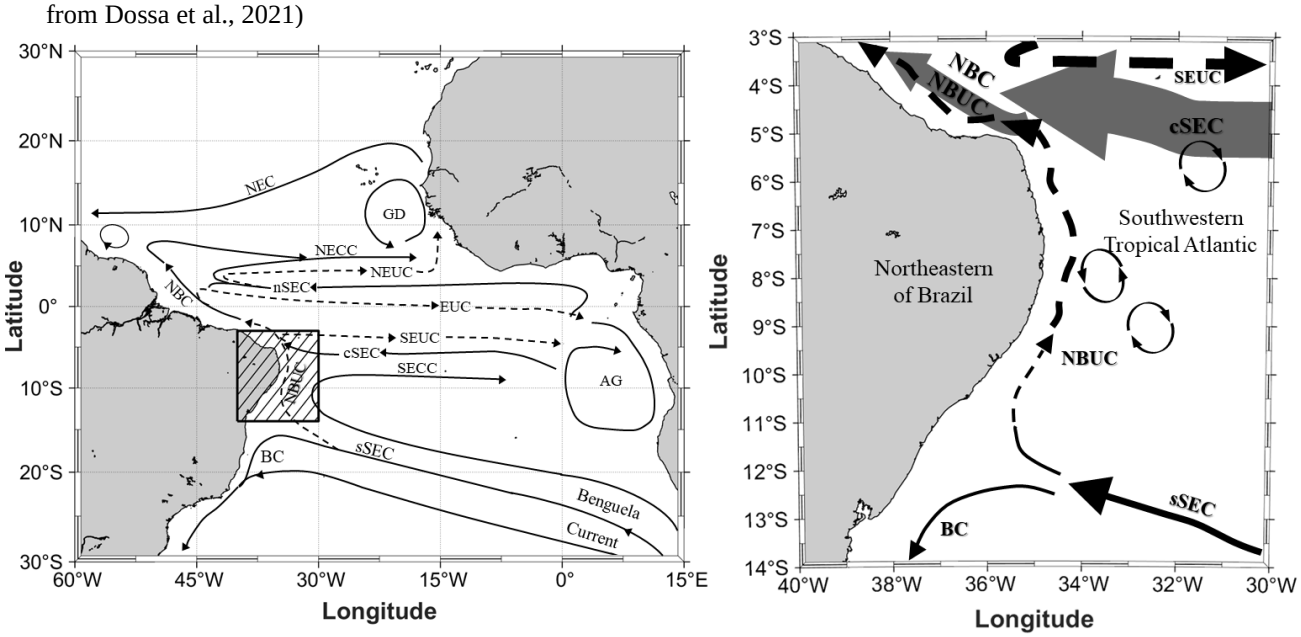

Source: The author (2021).

Fig. 3 - Data collected from 2008 to 2020 by 4 merchant ships: Monte Olivia, Rio Blanco, Santa Cruz and Cap San Lorenzo along the France-Brazil line

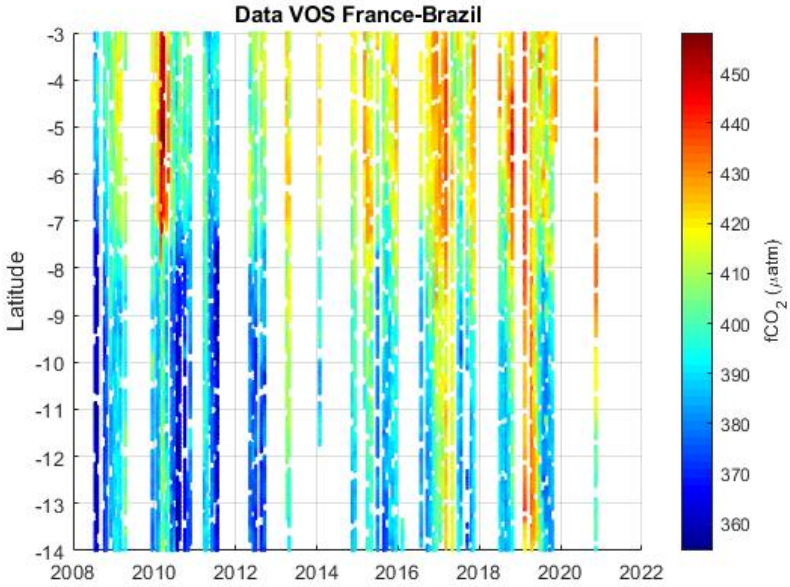

Source: The author (2023).

4.1.2.3. Calculations

The air–sea flux of CO2 (mmol m^{-2} day^{-1}) was calculated as follows:

$$fCO_2 = kS\,(fCO_{2sw} - fCO_{2atm}) \quad (1)$$

where *k* is the gas-transfer velocity by Sweeney et al. (2007) calculated from the European Centre for Medium-Range Weather Forecasts (ECMWF) wind field, *S* is the solubility of CO_2 in seawater, calculated using the formula of Weiss (1974). A positive flux of CO_2 means a source of CO_2 to the atmosphere and a negative flux means a sink of CO_2 to the atmosphere.

The Shapiro-Wilk test was applied to examine the normality of the dataset. The parametric t-test was used for normal distributions, otherwise the non-parametric Mann-Whitney test was used.

Table 1 - Summary of Data Collected on Cruises in the Southwestern Tropical Atlantic. The merchant ship is identified for each voyage: MO – Monte Olivia Ship; RB – Rio Blanco Ship; SC – Santa Cruz Ship; and SL – Cap San Lorenzo.

Year	Number of cruises (N=79)	Data points collected (N=64,028)	Months											
			Jan	**Feb**	**Mar**	**Apr**	**May**	**Jun**	**Jul**	**Aug**	**Sep**	**Oct**	**Nov**	**Dec**
2008	6	3,517							MO	MO		MO	MO	MO
2009	6	4,052	MO	MO	MO	MO								RB
2010	14	9,590	RB	RB	RB	RB	RB	RB	RB	RB	RB	RB	RB	
2011	6	5,190			RB	RB	RB	RB	RB					
2012	4	3,202					SC	SC		SC				
2013	2	1,457				SC								
2014	3	2,494	SC										SL	SL
2015	9	7,825			SL	SL	SL	SL		SL	SL	SL	SL	SL
2016	6	4,666							SL		SL	SL	SL	SL
2017	8	6,194	SL	SL	SL		SL	SL	SL		SL	SL	SL	
2018	5	4,152						SL	SL	SL	SL	SL		
2019	9	7770		SL		SL	SL	SL	SL	SL	SL	SL	SL	
2020	1	802											SL	

4.1.3. Results and Discussion

4.1.3.1. Environmental Setting of the Region Between 3 and 14ºS

From 3 to 14°S, the volunteer ships cross two branches of the SEC. The quarterly climatology of the current data from 2008 to 2020 in SWTA (Fig. 4) shows a strong current, observed between 3 and 8°S in the north-western Atlantic region and flowing westward to the north-eastern Brazilian coast throughout the year. This flow is the cSEC that comes from the African coast (DOSSA et al., 2021; STRAMMA; SCHOTT, 1999). The cSEC intensifies during winter and spring (Fig. 4*c*, *d*).

South of 8°S, there is a complex system of eddies and currents that change direction frequently (Fig. 4). This contrasts with the region north of 8°S, where the surface current has a stronger zonal component. South of 8°S, the region is affected by the sSEC. This system includes the bifurcation of the sSEC, with part of the current flowing southward (AMORIM et al., 2013; DOSSA et al., 2021; STRAMMA; IKEDA; PETERSON, 1990; STRAMMA; SCHOTT, 1999). This southward flow forms the Brazil Current that flows along the Brazilian coast (Fig. 1) near 14°S(LUKO et al., 2021).

The surface salinity is affected by the ITCZ, which influences the evaporation–precipitation balance of the tropical Atlantic. The ITCZ migrates seasonally according to the strength of the trade winds. From January to May (austral summer and autumn), the ITCZ moves southward, reaching the southern hemisphere near 5°S (BERRY; REEDER, 2014; HOUNSOU-GBO et al., 2015; NOBRE; SRUKLA, 1996; RODRIGUES; ROTHSTEIN; WIMBUSH, 2007). During austral summer, there is more rainfall near the equator and over the northern part of north-eastern Brazil, owing to the most southward position of the ITCZ. In the second semester of the year, its position is north of the equator because of the greater strength of the south-eastern trade winds(HOUNSOU-GBO et al., 2015; NOBRE; SRUKLA, 1996). Consequently, the ITCZ affects principally the region between 3 and 8°S during the first semester of the year.

There is no major river discharge that could supply nutrients and lead to biological activity; thus, the coastal region between 3 and 14°S is considered oligotrophic (CIOTTI; GARCIA; JORGE, 2010). The primary productivity is restricted to the narrow and shallow Brazilian continental shelf, in coastal river plume waters, and around the islands, for example, the Saint Peter and Saint Paul Archipelago and the Fernando de Noronha Archipelago (DE QUEIROZ et al., 2015; GASPAR et al., 2018; NORIEGA et al., 2015; SILVA et al., 2019).

The Chl-*a* concentrations are generally very low in the surface layers of the tropical Atlantic, especially on the western border of the Atlantic Ocean (CLARK; REES; JOINT, 2008; MAFALDA JR et al., 2009). The low nutrient concentration causes a limitation in the productivity over much of the surface of the low-latitude ocean (MOORE et al., 2013).

Fig. 4– Climatological (2008-2020) maps of surface marine currents data for a) austral Summer (December-January-February), b) Autumn (March-April-May), c) Winter (June-July-August), and d) Spring (September-October-November), near to Brazilian coast between la latitudes 3º S and 14º S

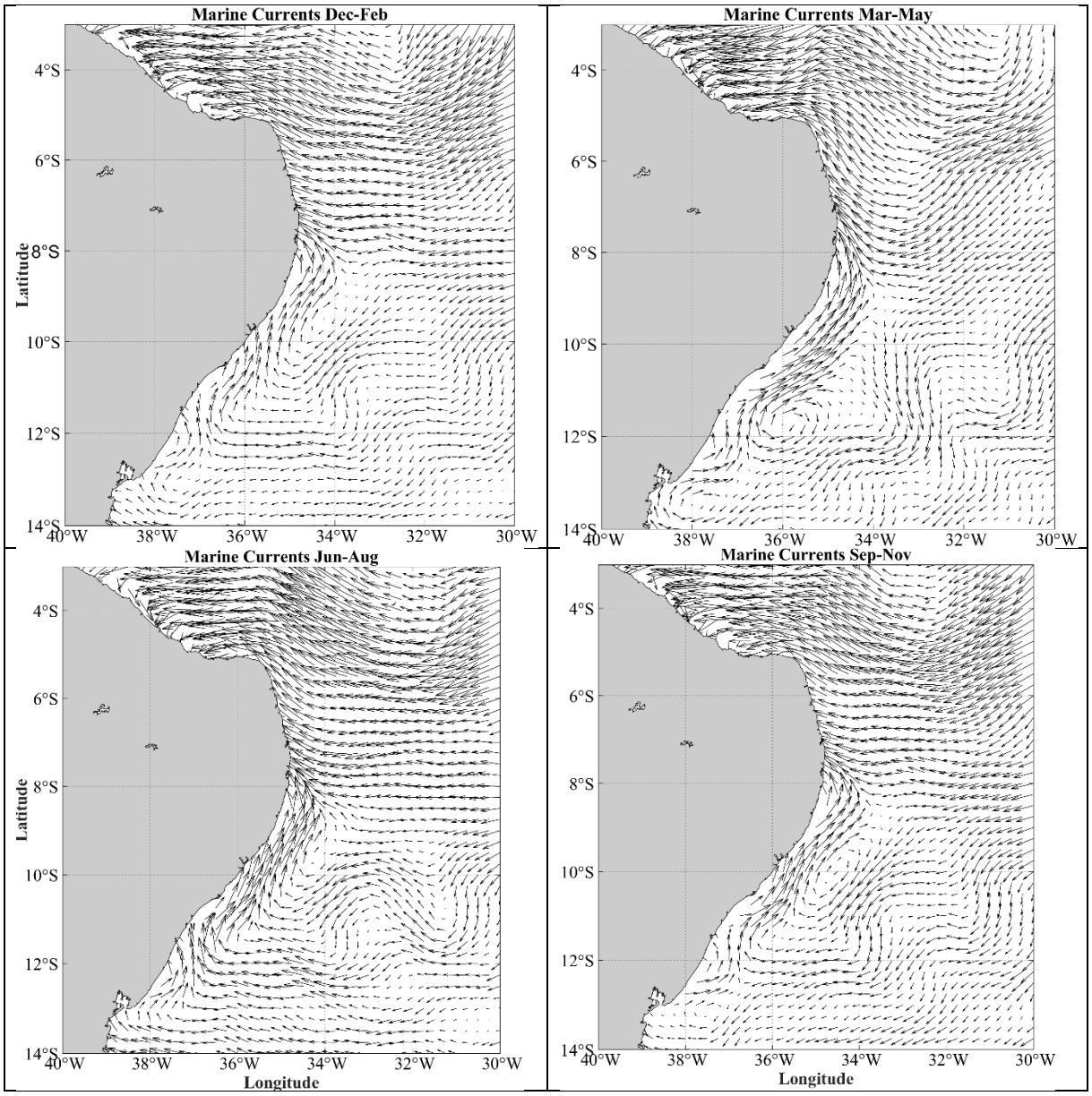

Source: The author (2022).

The relationship between the biological activities and fCO_2 is commonly analyzed through of Chl-*a* (CARVALHO et al., 2017; FORD et al., 2022; ITO; SCHNEIDER; THOMAS, 2005; KITIDIS et al., 2017; LIUTTI et al., 2021; OLSEN et al., 2008; RÖDENBECK et al., 2015). The high concentrations of nutrients stimulate blooms of phytoplankton that reduce the fCO_2 because of the sequestration of inorganic carbon from seawater, changing the CO2 flux at the air–sea interface (SIMPSON; ZIRINO, 1980; TORRES; AMPUERO, 2009).

Previous studies by Padin *et al*. (2010) and Kitidis *et al*. (2017) measured the Chl-*a* concentrations in the South Equatorial Current region. The Chl-*a* concentration in both studies

was low and always <0.2 mg m^{-3} (KITIDIS et al., 2017; PADIN et al., 2010). This also confirms that biological activity is not a dominant process in this region.

The quarterly climatology of Chl-*a* from 2008 to 2020 made through satellite images has confirmed the low concentrations in the region (Fig. 5). The Chl-*a* concentration averages 0.11 ± 0.07 mg m^{-3}.

Fig. 5 – Quarterly climatology of Chlorophyll-a from 2008 to 2020

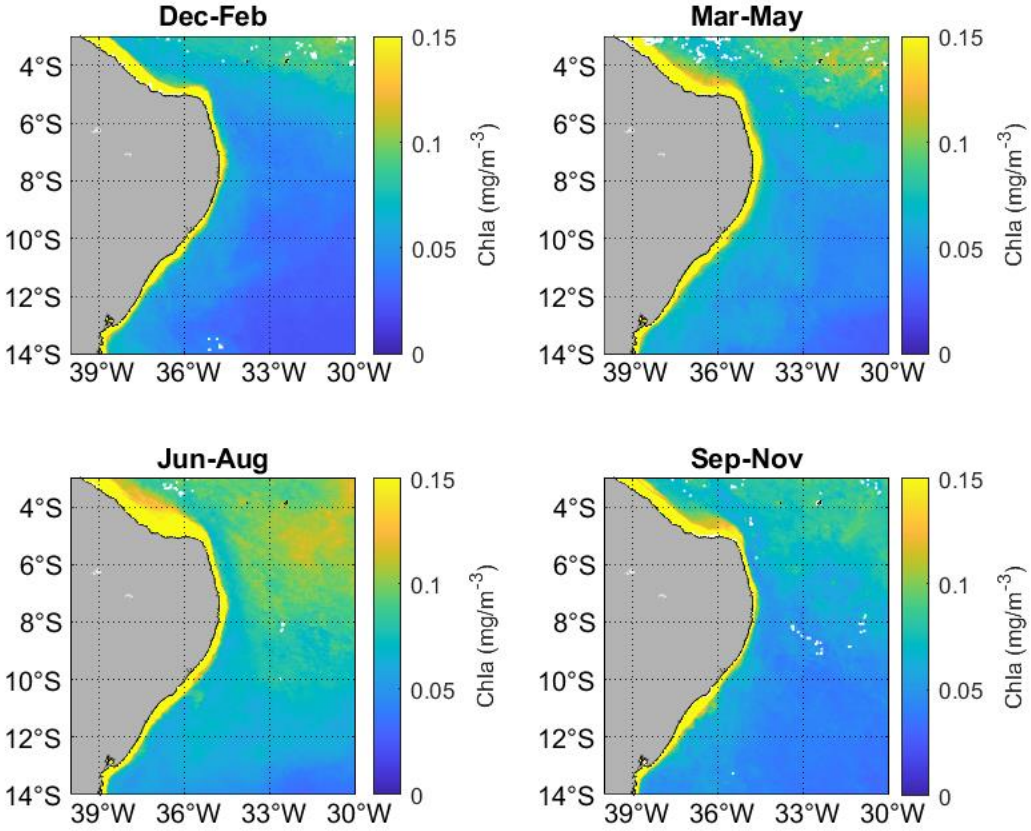

Source: The author (2021).

Fig. 6 – Monthly distribution of fCO_2 from 3ºS to 14ºS in the Southwestern Tropical Atlantic, from 2008 to 2020

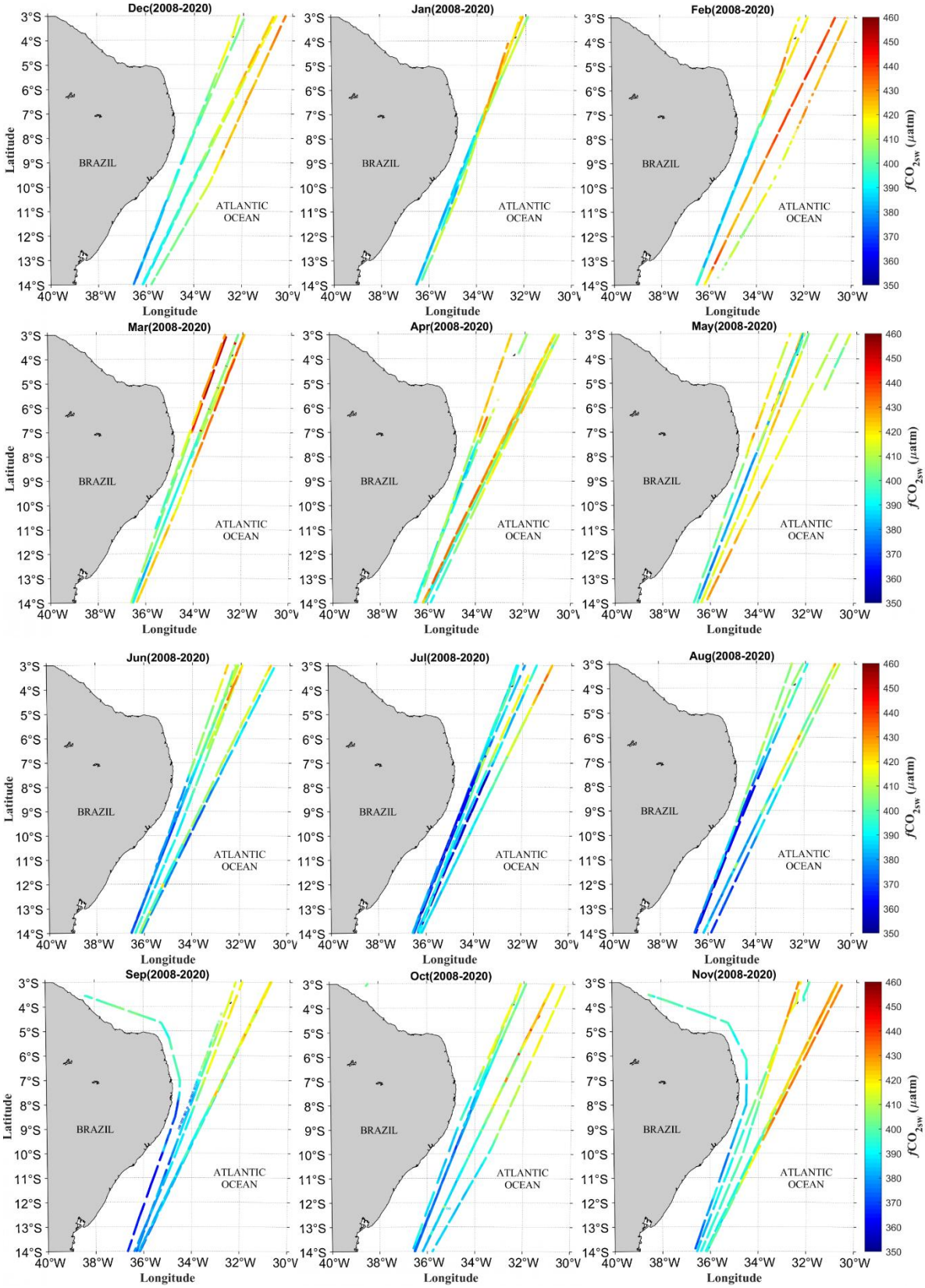

Source: The author (2020).

Although the Chl-*a* concentrations are slightly higher in the northern part of the region (Fig. 5), the concentrations remain very low. Despite these low concentrations, a certain seasonal pattern in the distribution of Chl-*a* was observed, where the Chl-*a* concentrations were relatively higher in the months from June to August than in months from December to February, winter and summer respectively. The Chl-*a* distribution follows the seasonal pattern of the distribution of fCO_2 (Fig. 6), and it may be another influence of the CO_2 concentration in the study region, but the physical conditions have a strong influence on CO_2 (KITIDIS et al., 2017).

4.1.3.2. Variability of fCO_2 between 3ºS and 14ºS

The Fig. 6 shows the monthly distribution of surface fCO_2 collected by volunteer ships between 3 and 14°S from 2008 to 2020. For each month, fCO_2 is higher north of 8°S than south of it. Seasonal variations are superimposed on this north–south gradient of fCO_2, with higher fCO_2 values being observed in February–May and lower values in June–October.

The values of onboard and underway fCO_{2sw} measurements show a significant latitudinal gradient associated with seasonality of ITCZ, mainly in the region between 3 and 8°S, and dynamics of SWTA marine currents (LEFÈVRE et al., 2014; LEFÉVRE; DIVERRÉS; GALLOIS, 2010).

Similar cruises were undertaken from 2000 to 2008 by Padin *et al*. (2010) within the Spanish FICARAM project that took advantage of ship tracks between Spain and the Antarctic in boreal spring (March–April) and boreal autumn (October–November). During these cruises, the difference in fCO_2 between the ocean and the atmosphere was 30 ± 11 µatm in March–April and 24 ± 11 µatm in October–November, for the 2000–2008 period, in the South Equatorial Current region defined between 1°N and 15°S (PADIN et al., 2010). Similar values were observed from 3 to 14°S for the 2008–2020 period with a difference in fCO_2 of 37 ± 15 µatm in March– April and 19 ± 15 µatm in October–November. Temperature and salinity were also in agreement with the values reported by Padin *et al*. (2010) in March–April and October–November, being within the range of variability measured along the ship track. A source of CO_2 occurs at these two seasons.

Cruises from the UK Atlantic Meridional Transect (AMT) program over the period of 1995–2013 also showed CO_2 over-saturation in boreal spring and autumn in the region 2°N–15°S (KITIDIS et al., 2017).

With many cruises every month, the France–Brazil line has highlighted the lower fCO_2 values observed south of 8°S than north of 8°S (Fig. 6).

4.1.3.3. North-South Gradient

Because of the difference in data in the area around 8°S, in this section, we divided the region into a northern subregion of 3−8°S (NS) and a southern subregion of 8−14°S (SS). In both of them, the SST exhibited the same seasonal cycle and similar values, with higher temperatures during austral summer and autumn, January to April, and lower temperatures during austral winter and spring, June to November (Fig. 7*a*). In the NS, the mean annual SST ranged from 26.7 to 29.0°C, with an average of 27.8 ± 0.8°C. In the SS, it ranged from 26.4 to 28.9°C, with an average of 27.5 ± 0.9°C. Despite the SST values in SS being slightly lower than in the NS, there was no significant difference in SST (Mann–Whitney test, $P > 0.05$).

Fig. 7 – Monthly Variability of a) SST, b) Sea Surface Salinity, c) Fugacity of CO_2 in seawater and d) CO_2 Flux in the northern region (blue line) and the southern region (red line), averaged over 2008 – 2020

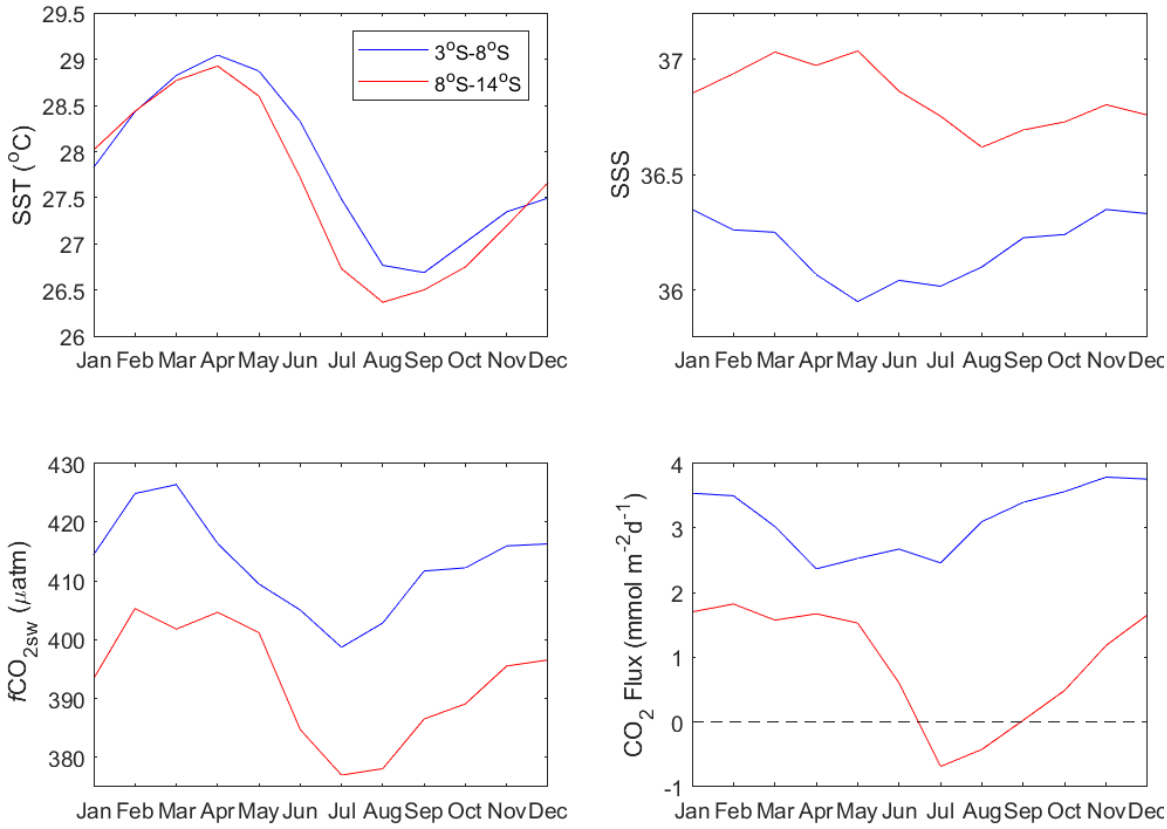

Source: The author (2020).

The SSS shows a clear difference between the northern and southern regions (Fig. 7*b*), with a mean of 36.2 ± 0.1 in the north and a mean of 36.8 ± 0.1 in the south.

In the NS, fCO_{2sw} is maximum in March (426 μatm) and minimum in July (399 μatm). In March, the ITCZ is south of equator and SSS decreases. As fCO_2 decreases with SST, the SSS decrease contributes further to lower fCO_2.

From 2008 to 2020, fCO_{2sw} varies from 378 to 450 μatm in the northern subregion and from 360 to 433 μatm in the southern region. Despite this variability, the differences among the monthly fCO_{2sw} values in the NS and SS were statistically significant (Student's *t*-test; $P < 0.05$). The latitudinal distribution of the CO_2 flux from 3 to 8°S showed CO_2 outgassing (Fig. 7*d*), with monthly values ranging from 2.37 mmol m^{-2} day^{-1} in April to 3.78 mmol m^{-2} day^{-1} in November. It is a strong source CO_2 to the atmosphere throughout the year with a mean of 3.14 ± 0.52 mmol m^{-2} day^{-1}. The CO_2 flux in the southern region was much lower, averaging 0.93 ± 0.90 mmol m^{-2} day^{-1}, with even a sink of CO_2 occurring from July and August. It is explained by the lowest fCO_{2sw} measured at this time of the year in this region.

As high salinity and high SST lead to high fCO_{2sw}, the SST and SSS cannot explain the differences between the northern and southern regions. In addition, the Chl-*a* concentrations were too low to play a significant role. This suggests that the CO_2 content of the water mass was the main factor responsible for the difference in fCO_{2sw} between the two subregions. The SSS gradient is explained by the two main surface currents, the cSEC and the sSEC. From 7°30′ to 25°S, the sSEC transports high salinity waters that can reach a salinty of 37–37.20 (WIENDER; ARHAN; MERCIER, 2000). Near the surface (0–100 m), the sSEC is a broad current between 8 and 20°S near the coast of Brazil (RODRIGUES; ROTHSTEIN; WIMBUSH, 2007).

The cSEC has low salinities, ~36 in this area (WIENDER; ARHAN; MERCIER, 2000). In addition to the low salinity of the cSEC, the salinity decreases further by the proximity to the ITCZ during the first semester, when the ITCZ is at its southern-most position. A salinity minimum is observed in May in the northern region, consistent with the southern-most position of the ITCZ (Fig. 7*b*). In the south, the monthly variability of SSS shows high values during austral summer and autumn, followed by a decrease until August (austral winter). Although rainfall causes chemical dilution and decreases fCO_2 (ASHTON et al., 2016; TURK et al., 2010), this impact on the fCO_2 distribution is not strong enough to obtain similar values as in the southern region.

The north–south gradient observed on the fCO_{2sw} distribution can be explained by the origin of the water masses. The cSEC transports water from the eastern tropical Atlantic near the Angola gyre, whereas the sSEC transports water from further south near the Benguela current (Fig. 2*a*). Observations of fCO_{2sw} at a mooring location of 6°S, 10°W show values higher than 400 µatm from 2006 to 2013, except in June–August (LEFÈVRE et al., 2016) and a similar fCO_2 seasonal cycle as the one observed in the northern region. As the surface water warms up during the transport towards the South American coast, the fCO_{2sw} increases with SST (ANDRIÉ et al., 1986). This is consistent with the fCO_{2sw} measured in the northern region at 3–8°S close to the Brazilian coast.

Using these cruises and other data from the SOCAT database, Monteiro *et al*. (2022) studied the region between 5°S and 15°N. They defined the region under the NBC domain (NBC–NECC) as a weak source of CO_2 to the atmosphere. However, their domain includes the Amazon mouth, which explains the large variability of the mean salinity in this region, with a value of 35.87 ± 1.26 (MONTEIRO et al., 2022). Our region at 3−8°S does not include the Amazon influence; thus, surface salinity is higher and less variable with a mean of 36.2 ± 0.1. This explains why we find a stronger source of CO_2 throughout the year.

The gridded pCO_2 data and the climatological mean pCO_2 product of Landschützer *et al*. (2020) highlighted the lower *p*CO2 values observed further south than in the cSEC where high values have been observed from the Angola gyre and Gulf of Guinea to the Brazilian coast (LANDSCHÜTZER et al., 2020). There is further evidence of lower fCO_2 in the sSEC from a cruise between Cape Town (South Africa) to Arraial do Cabo (Brazil) in July 2015. Along this transect, Orselli *et al*. (2019) reported CO_2 under-saturation with respect to the atmosphere. It is consistent with the sink we observed in July–August between 8 and 14°S. Surface waters transported by the sSEC have a lower CO_2 concentration than those of the cSEC, which explains the north–south gradient observed here. The division between these two water masses occurs near 8°S when the surface currents reach the Brazilian coast.

4.1.4. Conclusion

Using the onboard and underway fCO_{2sw} dataset collected by volunteer observing ships in the SWTA from 3 to 14°S, we identified a north–south difference of fCO_{2sw}, SSS and the air–sea flux of CO_2 at about 8°S. In the northern region, at 3−8°S, the CO_2 flux is higher than

in the latitudes of 8−14°S. Both regions have low Chl-*a* concentrations and biological activity does not play a significant role in explaining the CO_2 variations. The contrast between NS and SS is explained by the origin of the water masses. In the northern region, there is a predominance of the central branch of the South Equatorial Current (cSEC), that is fed by the recirculation from the NECC/Guinea Current and the equatorial upwelling in the Gulf of Guinea, transporting CO_2-rich surface waters, warm with low salinities. Between 3 and 8°S, a source of CO_2 was observed throughout the year, with values ranging from 2.37 mmol m^{-2} day^{-1} in April to 3.78 mmol m^{-2} day^{-1} in November. The southern region, at 8−14°S, includes surface waters transported by the southern branch of the South Equatorial Current (sSEC). This current transports salty and warm waters of the Benguela Current.

The SS is a weaker source of CO_2 for the atmosphere, except in July and August, when it is a small sink of CO_2 of ~−0.55 mmol m^{-2} day^{-1}. The north–south gradient occurs every month, from January to December, with monthly values of SSS, fCO_2 and CO_2 flux significantly lower between 8 and 14°S than from 3 to 8°S. In both regions, the SST follows a seasonal cycle with minimum temperatures in austral winter/spring and higher temperatures in austral autumn. Continued monitoring of fCO_2 using autonomous measurements on ships of opportunity would allow determining the trend of the CO_2 fluxes.

4.1.5. References

ALBUQUERQUE, C. et al. Seasonal variability of carbonate chemistry and its controls in a subtropical estuary. **Estuarine, Coastal and Shelf Science**, v. 276, n. October 2021, 2022.

ALORY, G. et al. The French contribution to the voluntary observing ships network of sea surface salinity. **Deep Sea Research Part I: Oceanographic Research Papers**, v. 105, p. 1–18, 2015.

AMORIM, F. N. et al. The seasonal circulation of the Eastern Brazilian shelf between 10°S and 16°S: A modelling approach. **Continental Shelf Research**, v. 65, p. 121–140, 2013.

ANA, A. N. D. Á. E. S. B. Conjuntura dos recursos hídricos 2023. 2024.

ANDRIÉ, C. et al. CO 2 fluxes in the tropical Atlantic during FOCAL cruises . **Journal of Geophysical Research**, v. 91, n. C10, p. 11741, 1986.

ARAUJO, M. et al. Salinity-induced mixed and barrier layers in the southwestern tropical

Atlantic Ocean off the northeast of Brazil. **Ocean Science**, v. 7, n. 1, p. 63–73, 2011.

ARAUJO, M. et al. On the variability in the CO_2 system and water productivity in the western tropical Atlantic off North and Northeast Brazil. **Journal of Marine Systems**, v. 189, n. September 2018, p. 62–77, 2019.

ASHTON, I. G. et al. A sensitivity analysis of the impact of rain on regional and global sea-air fluxes of CO2. **PLoS ONE**, v. 11, n. 9, p. 1–18, 2016.

ASSUNÇÃO, R. V. et al. 3D characterisation of the thermohaline structure in the southwestern tropical Atlantic derived from functional data analysis of in situ profiles. **Progress in Oceanography**, v. 187, 1 ago. 2020.

BERRY, G.; REEDER, M. J. Objective identification of the intertropical convergence Zone: Climatology and trends from the ERA-Interim. **Journal of Climate**, v. 27, n. 5, p. 1894–1909, 2014.

BONOU, F. K. et al. Distribution of CO_2 parameters in the Western Tropical Atlantic Ocean. **Dynamics of Atmospheres and Oceans**, v. 73, p. 47–60, 2016.

CARVALHO, A. C. O. et al. Air-sea CO2 fluxes for the Brazilian northeast continental shelf in a climatic transition region. **Journal of Marine Systems**, v. 173, p. 70–80, 2017.

CHEN, C. T. A. et al. Air-sea exchanges of coin the world's coastal seas. **Biogeosciences**, v. 10, n. 10, p. 6509–6544, 2013.

CIOTTI, Á. M.; GARCIA, C. A. E.; JORGE, D. S. F. **Temporal and meridional variability of Satellite-estimates of surface chlorophyll concentration over the Brazilian continental shelfPan-American Journal of Aquatic Sciences**. [s.l: s.n.]. Disponível em: <http://oceancolor.gsfc.nasa.gov>.

CLARK, D. R.; REES, A. P.; JOINT, I. Ammonium regeneration and nitrification rates in the oligotrophic Atlantic Ocean: Implications for new production estimates. **Limnology and Oceanography**, v. 53, n. 1, p. 52–62, 2008.

COTOVICZ, L. C.; CHIELLE, R.; MARINS, R. V. Air-sea CO2 flux in an equatorial continental shelf dominated by coral reefs (Southwestern Atlantic Ocean). **Continental Shelf Research**, v. 204, n. June, 2020.

DAI, A.; TRENBERTH, K. E. Estimates of freshwater discharge from continents: Latitudinal

and seasonal variations. **Journal of Hydrometeorology**, v. 3, n. 6, p. 660–687, 2002.

DE QUEIROZ, A. R. et al. Vertical and horizontal distribution of phytoplankton around an oceanic archipelago of the Equatorial Atlantic. **Marine Biodiversity Records**, v. 8, 8 abr. 2015.

DOSSA, A. N. et al. Near-surface western boundary circulation off Northeast Brazil. **Progress in Oceanography**, v. 190, n. January 2020, 2021.

FORD, D. J. et al. Derivation of seawater pCO2 from net community production identifies the South Atlantic Ocean as a CO2 source. **Biogeosciences**, v. 19, n. 1, p. 93–115, 2022.

GASPAR, F. L. et al. Alkalinity, inorganic carbon and CO2 flux variability during extreme rainfall years (2010-2011) in two polluted tropical estuaries ne Brazil. **Brazilian Journal of Oceanography**, v. 66, n. 1, p. 115–130, 1 jan. 2018.

GIFFARD, P. et al. Contribution of the amazon river discharge to regional sea level in the tropical Atlantic Ocean. **Water (Switzerland)**, v. 11, n. 11, p. 1–16, 2019.

HOUNSOU-GBO, G. A. et al. Tropical Atlantic contributions to strong rainfall variability along the northeast Brazilian coast. **Advances in Meteorology**, v. 2015, 2015.

IBÁNHEZ, J. S. P. et al. Seasonal and interannual variability of sea-air CO_2 fluxes in the tropical Atlantic affected by the Amazon River plume. **Global Biogeochemical Cycles**, v. 29, n. 10, p. 1640–1655, out. 2015.

IBÁNHEZ, J. S. P.; ARAUJO, M.; LEFÈVRE, N. The overlooked tropical oceanic CO2 sink. **Geophysical Research Letters**, v. 43, n. 8, p. 3804–3812, 2016.

IBÁNHEZ, J. S. P.; FLORES, M.; LEFÈVRE, N. Collapse of the tropical and subtropical North Atlantic CO2 sink in boreal spring of 2010. **Scientific Reports**, v. 7, n. January, p. 1–9, 2017.

IBÁNHEZ, J. S. P.; FLORES MONTES, M.; LEFÈVRE, N. Evidence for enhanced primary production driving significant CO2 drawdown associated with the Atlantic ITCZ. **Science of The Total Environment**, v. 838, n. January, p. 156592, 2022.

ITO, R. G.; GARCIA, C. A. E.; TAVANO, V. M. Net sea-air CO2 fluxes and modelled pCO2 in the southwestern subtropical Atlantic continental shelf during spring 2010 and summer 2011. **Continental Shelf Research**, v. 119, p. 68–84, 2016.

ITO, R. G.; SCHNEIDER, B.; THOMAS, H. Distribution of surface fCO2 and air-sea fluxes in the Southwestern subtropical Atlantic and adjacent continental shelf. **Journal of Marine**

Systems, v. 56, n. 3–4, p. 227–242, 2005.

KERR, R. et al. The Western South Atlantic Ocean in a High-CO2 World: Current Measurement Capabilities and Perspectives. **Environmental Management**, v. 57, n. 3, p. 740–752, 2016.

KITIDIS, V. et al. Surface ocean carbon dioxide during the Atlantic Meridional Transect (1995–2013); evidence of ocean acidification. **Progress in Oceanography**, v. 158, p. 65–75, 2017.

LANDSCHÜTZER, P. et al. A uniform pCO2 climatology combining open and coastal oceans. **Earth System Science Data Discussions**, p. 1–30, 2020.

LARUELLE, G. G. et al. Evaluation of sinks and sources of CO2 in the global coastal ocean using a spatially-explicit typology of estuaries and continental shelves. **Geophysical Research Letters**, v. 37, n. 15, p. 1–6, 2010.

LARUELLE, G. G. et al. Regionalized global budget of the CO 2 exchange at the air-water interface in continental shelf seas. **Global Biogeochemical Cycles**, v. 28, n. 11, p. 1199–1214, nov. 2014.

LEFÈVRE, N. et al. Impact of physical processes on the seasonal distribution of the fugacity of CO2 in the western tropical Atlantic. **Journal of Geophysical Research: Oceans**, v. 119, n. 2, p. 646–663, 2014.

LEFÈVRE, N. et al. Variability and trends of carbon parameters at a time series in the eastern tropical Atlantic. **Tellus, Series B: Chemical and Physical Meteorology**, v. 68, n. 1, 2016.

LEFÈVRE, N. et al. Net heterotrophy in the Amazon continental shelf changes rapidly to a sink of CO_2 in the outer Amazon plume. **Frontiers in Marine Science**, v. 4, n. SEP, p. 1–16, 2017.

LEFÈVRE, N. et al. Amazon River propagation evidenced by a CO2 decrease at 8°N, 38°W in September 2013. **Journal of Marine Systems**, v. 211, 1 nov. 2020.

LEFÉVRE, N.; DIVERRÉS, D.; GALLOIS, F. Origin of CO_2 undersaturation in the western tropical Atlantic. **Tellus, Series B: Chemical and Physical Meteorology**, v. 62, n. 5, p. 595–607, 2010.

LIUTTI, C. C. et al. Sea surface CO2 fugacity in the southwestern South Atlantic Ocean: An evaluation based on satellite-derived images. **Marine Chemistry**, v. 236, n. August, p. 104020,

2021.

LUKO, C. D. et al. Revisiting the Atlantic South Equatorial Current. **Journal of Geophysical Research: Oceans**, v. 126, n. 7, p. 1–25, 2021.

LUMPKIN, R.; GARZOLI, S. L. Near-surface circulation in the Tropical Atlantic Ocean. **Deep-Sea Research Part I: Oceanographic Research Papers**, v. 52, n. 3, p. 495–518, mar. 2005.

MAFALDA JR, P. O. et al. Oceanografia Biológica: Biomassa Fitoplanctônica na ZEE da Região Nordeste do Nordeste do Brasil. In: FÁBIO HISSA VIEIRA HAZIN (Ed.). . **Coleção Programa REVIZEE SCORE NORDESTE**. Fortaleza: Martins & Cordeiro Ltda, 2009. p. 11–26.

MOLINIER, M. et al. Les regimes hydrologiques de l'Amazone et de ses affluents. **IAHS-AISH Publication**, n. 238, p. 209–222, 1996.

MONTEIRO, T. et al. Contrasting Sea-Air CO 2 Exchanges in the Western Tropical Atlantic Ocean. **Global Biogeochemical Cycles**, v. 36, n. 8, 15 ago. 2022.

MOORE, C. M. et al. Processes and patterns of oceanic nutrient limitation. **Nature Geoscience**, v. 6, n. 9, p. 701–710, 2013.

MOUSSA, H. et al. Satellite-derived CO2 fugacity in surface seawater of the tropical Atlantic Ocean using a feedforward neural network. **International Journal of Remote Sensing**, v. 37, n. 3, p. 580–598, 1 fev. 2016.

NOBRE, P.; SRUKLA, J. Variations of Sea Surface Temperature, Wind Stress, and Rainfall over the Tropical Atlantic and South America. **Journal of Climate**, v. 9, n. 10, p. 2464–2479, out. 1996.

NORIEGA, C. et al. Spatial and temporal variability of CO2 fluxes in tropical estuarine systems near areas of high population density in Brazil. **Regional Environmental Change**, v. 15, n. 4, p. 619–630, 1 abr. 2015.

OLIVEIRA, R. R. et al. First measurements of the ocean-atmosphere CO2 fluxes at the Cabo Frio upwelling system region, Southwestern Atlantic Ocean. **Continental Shelf Research**, v. 181, n. April, p. 135–142, 2019.

OLSEN, A. et al. Biogeosciences 2008 5 535-547.pdf. p. 535–547, 2008.

ORSELLI, I. B. M. et al. The sea-air CO2 net fluxes in the South Atlantic Ocean and the role played by Agulhas eddies. **Progress in Oceanography**, v. 170, p. 40–52, 1 jan. 2019.

PADIN, X. A. et al. Air-Sea CO2 fluxes in the atlantic as measured during boreal spring and autumn. **Biogeosciences**, v. 7, n. 5, p. 1587–1606, 2010.

PAILLER, K.; BOURLÈS, B.; GOURIOU, Y. The barrier layer in the western tropical Atlantic ocean. **Geophysical Research Letters**, v. 26, n. 14, p. 2069–2072, 15 jul. 1999.

PASSAIA, O. A. et al. Impact of large reservoirs on simulated discharges of brazilian rivers. **Revista Brasileira de Recursos Hidricos**, v. 25, n. Imd, p. 1–9, 2020.

PIERROT, D. et al. Recommendations for autonomous underway pCO_2 measuring systems and data-reduction routines. **Deep-Sea Research Part II: Topical Studies in Oceanography**, v. 56, n. 8–10, p. 512–522, 2009.

RÖDENBECK, C. et al. Data-based estimates of the ocean carbon sink variability - First results of the Surface Ocean pCO2 Mapping intercomparison (SOCOM). **Biogeosciences**, v. 12, n. 23, p. 7251–7278, 2015.

RODRIGUES, R. R.; ROTHSTEIN, L. M.; WIMBUSH, M. Seasonal variability of the South Equatorial Current bifurcation in the Atlantic Ocean: A numerical study. **Journal of Physical Oceanography**, v. 37, n. 1, p. 16–30, jan. 2007.

ROOBAERT, A. et al. The Spatiotemporal Dynamics of the Sources and Sinks of CO_2 in the Global Coastal Ocean. **Global Biogeochemical Cycles**, v. 33, n. 12, p. 1693–1714, 16 dez. 2019.

SILVA, B. J. et al. Carbon chemistry variability around a tropical archipelago. **Marine and Freshwater Research**, v. 70, n. 6, p. 767–780, 2019.

SIMPSON, J. J.; ZIRINO, A. Biological control of pH in the Peruvian coastal upwelling area. **Deep Sea Research Part A. Oceanographic Research Papers**, v. 27, n. 9, p. 733–743, set. 1980.

STRAMMA, L.; ENGLAND, M. On the water masses and mean circulation of the South Atlantic Ocean. **Journal of Geophysical Research: Oceans**, v. 104, n. C9, p. 20863–20883, 15 set. 1999.

STRAMMA, L.; IKEDA, Y.; PETERSON, R. G. Geostrophic transport in the Brazil current

region north of 20°S. **Deep Sea Research Part A, Oceanographic Research Papers**, v. 37, n. 12, p. 1875–1886, 1990.

STRAMMA, L.; SCHOTT, F. **The mean flow field of the tropical Atlantic OceanDeep-Sea Research II**. [s.l: s.n.].

TAKAHASHI, T. et al. Global sea–air CO_2 flux based on climatological surface ocean pCO_2, and seasonal biological and temperature effects. **Deep Sea Research Part II: Topical Studies in Oceanography**, v. 49, n. 9–10, p. 1601–1622, jan. 2002.

TAKAHASHI, T. et al. Climatological mean and decadal change in surface ocean pCO_2, and net sea-air CO_2 flux over the global oceans. **Deep-Sea Research Part II: Topical Studies in Oceanography**, v. 56, n. 8–10, p. 554–577, 2009.

TORRES, R.; AMPUERO, P. Strong CO2 outgassing from high nutrient low chlorophyll coastal waters off central Chile (30°S): The role of dissolved iron. **Estuarine, Coastal and Shelf Science**, v. 83, n. 2, p. 126–132, 2009.

TURK, D. et al. Rain impacts on CO2 exchange in the western equatorial Pacific Ocean. **Geophysical Research Letters**, v. 37, n. 23, p. 1–6, 2010.

WIENDER, N.; ARHAN, M.; MERCIER, H. Circulation at the western boundary of the south and equatorial atlantic: Exchanges with the ocean interior. **Journal of Marine Research**, v. 58, n. 6, p. 1007–1039, 2000.

4.2. ARTIGO 2 – AIR-SEA CO_2 FLUX THROUGHOUT 2008 AND 2020 IN THE SOUTHWEST TROPICAL ATLANTIC OCEAN ADJACENT TO THE NORTHEAST OF BRAZIL (3ºS TO 14ºS)

4.2.1. Introduction

It has been estimated that about ~25% of total anthropogenic CO_2 emissions are absorbed through the ocean surface (FRIEDLINGSTEIN et al., 2022). However, the Tropical Atlantic Ocean is considered the second oceanic source of CO_2 to the atmosphere, after the Tropical Pacific (TAKAHASHI et al., 2009). This characteristic can be explained by the CO_2-rich waters from equatorial upwelling in the Gulf of Guinea that are transported by recirculation from the NECC/Guinea Current, with warm waters and low salinities, through the South Equatorial Current (SEC) (GUIMARÃES; MONTES; LEFÈVRE, 2024; STRAMMA; SCHOTT, 1999; TAKAHASHI et al., 2009). The ocean dynamics of the surface current system, coupled with precipitation, also can add complexity into the CO_2 distribution in the Southwestern Tropical Atlantic Ocean (SWTA) (IBÁNHEZ et al., 2015; JOHNS et al., 2021).

Furthermore, the sea surface CO_2 fugacity (fCO_{2sw}), its temporal variability, and spatial distribution have not yet been comprehensively investigated in SWTA. Both the local continental shelf, river discharge, biological activity, and the region's open ocean dominance must be analyzed.

4.2.1.1. Trophic State of the Southwestern Tropical Atlantic Ocean Adjacent to Northeastern Brazil

The coastal region of Northeastern Brazil (NEB, 3ºS to 14ºS), which encompasses the SWTA, constitutes approximately 24% of its coastal territory. Geographically, it is characterized as a passive continental shelf, as it receives relatively little continental runoff and meets directly with the main current of this region, the Surface Equatorial Current (SEC, KNOPPERS; EKAU; FIGUEIREDO, 1999). Between 3ºS and 14ºS, the major surface currents are two branches of the SEC, the central branch (cSEC) and the southern branch (sSEC). South of 14°S near the surface, the sSEC reaches the Brazilian continental margin and bifurcates. This bifurcation has seasonal variability, reaching a southernmost position in July (~ 17°S) and northernmost position in November, around 13°S (RODRIGUES; ROTHSTEIN; WIMBUSH, 2007). Northward, the sSEC contributes to the formation of the superficial portion of the

complex North Brazilian Undercurrent/ North Brazilian Current (NBUC/NBC) system (DOSSA et al., 2021; LUMPKIN; GARZOLI, 2005; VELEDA et al., 2011). Southward, the sSEC forms the Brazil Current (BC) (STRAMMA; IKEDA; PETERSON, 1990).

The cumulative annual runoff of freshwater for the NEB is around 3345 m^3 s^{-1}, being the main annual discharge by São Francisco river with 2729 m^3 s^{-1} (CARVALHO OLIVEIRA et al., 2018). However, despite the substantial volume of freshwater, the inflow of freshwater along the coast is insufficient to maintain a detectable fraction of freshwater along the coast due to tropical surface waters (TSW) and this discharge does not advance beyond the Brazilian continental shelf. Consequently, most materials and essential nutrients into adjacent marine primary productivity from river inputs exhibit a tendency to be restricted to the narrow and shallow Brazilian continental shelf, in coastal rivers plume waters, and around the islands, for example, St. Peter and St. Paul Archipelago and the Fernando de Noronha Archipelago (DE QUEIROZ et al., 2015; GASPAR et al., 2018; NORIEGA et al., 2015; SILVA et al., 2019).

These characteristics of riverine supply to lead the biological activity in the NEB corroborate the classification of the SWTA region as oligotrophic (CIOTTI; GARCIA; JORGE, 2010). The low nutrient concentration causes a limitation in productivity over much of the low-latitude surface ocean (MOORE et al., 2013). The surface layers on the western border of the SWTA have had low Chlorophyll-*a* (Chl*a*) concentrations (CLARK; REES; JOINT, 2008; GUIMARÃES; MONTES; LEFÈVRE, 2024; KITIDIS et al., 2017; MAFALDA JR et al., 2009; PADIN et al., 2010).

Therefore, the processes that affect the fCO_{2sw} in the NEB are mainly physical-chemical processes, such as variations in temperature, salinity, winds, and rainfall over the years (GUIMARÃES; MONTES; LEFÈVRE, 2024).

Certain studies next to the NEB coast has been classified the area as a source of CO_2 for the atmosphere, with seasonal variations (ARAUJO et al., 2019; CARVALHO et al., 2017; GUIMARÃES; MONTES; LEFÈVRE, 2024; LEFÈVRE et al., 1998, 2014). This characterization arises from multiple factors, including the fact that it has waters of Tropical Atlantic adjacent of NEB are oligotrophic (CIOTTI; GARCIA; JORGE, 2010; CLARK; REES; JOINT, 2008; GUIMARÃES; MONTES; LEFÈVRE, 2024; KITIDIS et al., 2017; MAFALDA JR et al., 2009; PADIN et al., 2010).

Additionally, the coastal region is influenced mainly the physical-chemical conditions prevailing established and different atmospheric forcing (MÜNNICH; NEELIN, 2005). In the northern NEB, above approximately 5°S, the rainy season can be observed from February to May, associated with the Intertropical Convergence Zone (ITCZ), which reaches its southernmost position during March-April (DONOHOE et al., 2013; HASTENRATH, 2012; HOUNSOU-GBO et al., 2015). In the eastern NEB, the rainfall regime occurs between the months of April and July, and is strongly modulated by Easterly Waves Disturbances (EWD) (GOMES et al., 2015; HOUNSOU-GBO et al., 2015). These EWDs are atmospheric disturbances that propagate westward across tropical Atlantic, carrying significant amounts of moisture to dry areas as they move. (GOMES et al., 2015).

Previous studies have also defined that in the westernmost region of the tropical South Atlantic there is a South Atlantic Warm Pool (SAWP), which is characterized by a source of heat and moisture, with well-defined seasonal patterns in terms of time and space, creating atmospheric instability of weather systems for the NEB and adjacent ocean (SILVA et al., 2021). These oceanic warm pools are regions with temperatures above 28.5°C. This is an area of low annual thermal variability, but presents interannual anomalies. There is also an intensification of atmospheric systems that cause rainfall on the east coast of the NEB (SILVA et al., 2018).

The Pacific *El Niño* teleconnection and the Atlantic *Niño* are two phenomena that exert a substantial influence over sea surface temperatures (SST) and sea surface salinity (SSS), are the external cause of the rainfall variability in NEB until to a recorded maximum of 5°S latitude (HASTENRATH, 2012; KOSEKI et al., 2023). During Atlantic *Niño* are observed strong CO_2 anomalies in Western Atlantic, there the CO_2 outgassing is suppressed, induced by higher precipitation during this phenomenon (KOSEKI et al., 2023).

All these physical-chemical conditions exhibit seasonal fluctuations that shape the carbon dynamics of the NEB region. In addition, the great intensity of the winds (BONOU et al., 2016; IBÁNHEZ; ARAUJO; LEFÈVRE, 2016; KOSEKI et al., 2023; LEFÈVRE et al., 2014, 2020)..

In this work, we used the regular underway CO_2 measurements made along the shipping line from France to Brazil to document the CO_2 distribution from 2008 to 2020. The area studied is between 3ºS and 30°W, 14ºS and 37°W, the ocean adjacent to the Northeast of Brazil.

4.2.2. Methods and Data

An automated pCO_2 system, using infrared detection, described by Pierrot et al. (2009), has been installed on the volunteer ships sailing from France to Brazil. Here, we focus on the fCO_2 data recorded between 3ºS and 14ºS, illustrated by dashed lines in Fig. 1. seawater and atmospheric fCO_2 measurements started from July 2008 to November 2020 (Table 1.

The volunteer ships have been equipped with a Seabird thermosalinograph SBE 21 recording SST and SSS.

The air-sea flux of CO_2 (mmol m^{-2} d^{-1}) is calculated using:

$$FCO_2 = kS\ (fCO_{2sw} - fCO_{2atm})$$

where k is the gas transfer velocity by Sweeney et al. (2007) calculated with the European Centre for Medium-Range Weather Forecasts (ECMWF) wind field, S is the solubility of CO_2 in seawater calculated using the formula by Weiss (1974). A positive flux of CO_2 means a source of CO_2 to the atmosphere, and a negative flux means a sink of CO_2 to the atmosphere.

To analyze Sea Surface Temperature (SST) and compare it with data collected by the thermosalinograph, the monthly average of SST was obtained by satellite images produced from MODIS/Aqua Water Reservoir Monthly L3 Global V061. All data were downloaded for the same sampling period as fCO_2 (2008-2020). SST anomalies and monthly precipitation were computed for this period and for the two sub-regions divided by Guimarães et al. 2024.

The daily wind speed was obtained by *Windsat* data produced by Remote Sensing Systems and sponsored by the NASA Earth Science MEaSUREs DISCOVER Project and the NASA Earth Science Physical Oceanography Program. RSS WindSat data are available at www.remss.com.

To analyze the precipitation, the Global Precipitation Climatology Project (GPCP) monthly data sets were used. The GPCP data were available from 2008 to 2020.

Figure 1 - Map of the Southwestern Tropical Atlantic with all cruise tracks with underway CO_2 measurements and schematic representation of mean currents and edgy generation between 3° S – 14° S and 40° W – 30° W (Northeast Brazilian coast). Surface currents in in solid line and subsurface currents in dashed line (Adapted from Guimarães et al., 2024).

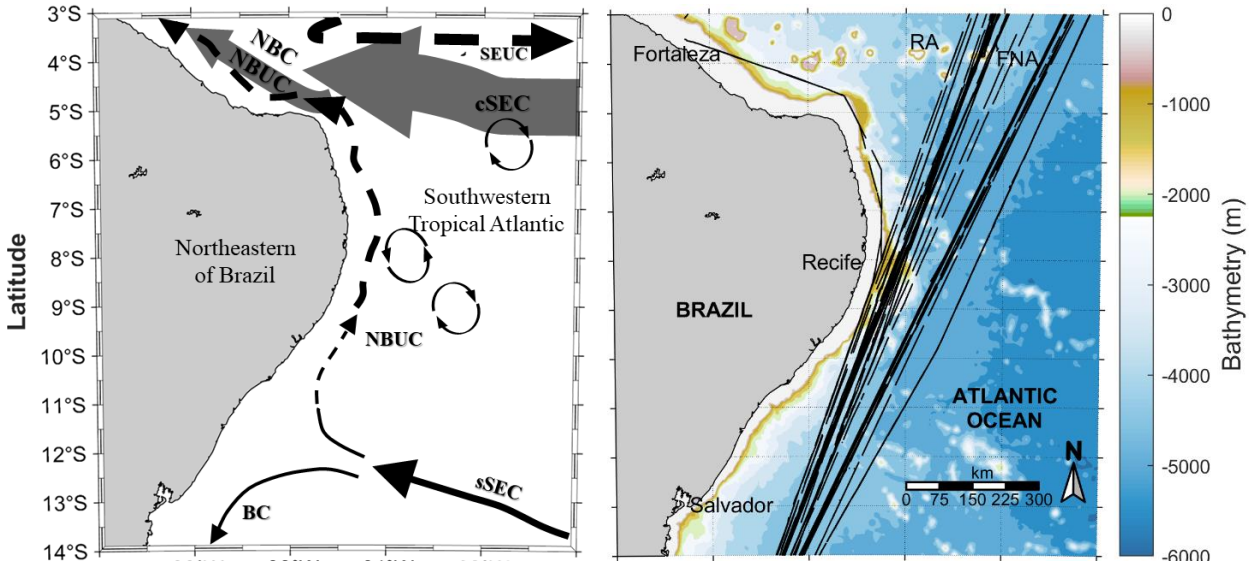

Source: The author (2024).

Table 1 - Summary of Data Collected on Cruises in the Southwestern Tropical Atlantic. The merchant ship is identified for each voyage: MO – Monte Olivia Ship; RB – Rio Blanco Ship; SC – Santa Cruz Ship; and SL – Cap San Lorenzo.

Year	Number of cruises (N=79)	Data points collected (N=64,028)	Months											
			Jan	Feb	Mar	Apr	May	Jun	Jul	Aug	Sep	Oct	Nov	Dec
2008	6	3,517							MO	MO		MO	MO	MO
2009	6	4,052	MO	MO	MO	MO								RB
2010	14	9,590	RB	RB	RB	RB	RB	RB	RB	RB	RB	RB	RB	
2011	6	5,190			RB	RB	RB	RB	RB					
2012	4	3,202					SC	SC		SC				
2013	2	1,457				SC								
2014	3	2,494	SC										SL	SL
2015	9	7,825			SL	SL	SL	SL		SL	SL	SL	SL	SL
2016	6	4,666							SL		SL	SL	SL	SL
2017	8	6,194	SL	SL	SL		SL	SL	SL		SL	SL	SL	
2018	5	4,152						SL	SL	SL	SL	SL		
2019	9	7770		SL		SL	SL	SL	SL	SL	SL	SL	SL	
2020	1	802											SL	

Normality of the data was assessed using the Lilliefors test, an adaptation of the Kolmogorov-Smirnov test. The results indicated that none of the datasets followed a normal distribution, as the p-values for all tests were less than 0.0001 (p(normal) = 0.0001). After that, the Kruskal-Wallis test was applied, in order to perform the variance analysis between periods with CO_2 flux for the both subregions. The annual trend analysis of data was performed using

linear regressions. Mann-Kendall test was used to verify the temporal variations significance (α = 0,05). The Spearman correlation was performed to assess the relationship between the collected CO_2 flux with SST and SSS.

4.2.3. Results and Discussion

4.2.3.1. Time Evolution of fCO_2 in Complex System of Currents

The time evolution of seawater fCO_2 and atmosphere fCO_2 at 3°S-14°S exhibits an increase from 2008 to 2020 (Figure 2). The volunteer ships cross complex systems of currents along its track from 3ºS to 14ºS (Figure 1). Close to the NEB, the main current is the South Equatorial Current (SEC). The sSEC and the cSEC are the major surface currents found in this area (AMORIM et al., 2013; PEREIRA et al., 2014; STRAMMA; ENGLAND, 1999). They are affected by the seasonal variability of the winds.

According to Guimarães et al. (2024), there is a difference in pCO_2 data in the area around 8ºS, and they divide the SWTA adjacent NEB into a northern subregion 3ºS-8ºS (NS) and a southern subregion 8ºS-14ºS (SS). The Kruskal-Wallis test showed significant differences for all measured parameters ($p < 0.001$) among subregions. This division was observed due to the main system of current to the region, the SEC and its branches sSEC and cSEC by Guimaraes et al. (2024). Therefore, the monthly evolution of fCO_{2sw} has been represented by both subregions.

From 2008 to 2020, fCO_{2sw} varied from 355.0 to 458.0 (411.0 ± 15.6) µatm in the NS, presenting a significant time trend (Kendall's tau = 0.352; $p < 0.001$). The temporal trend was also significant (Kendall's tau = 0.351; $p < 0.001$) in SS, ranging and from 360 to 433 (391.0 ± 16.3) µatm. For fCO_{2atm}, a significant trend also was showed (Kendall's tau = 0.820; $p < 0.001$) in the NS, ranging from 364 to 397 (379.0 ± 9.0) µatm. To the SS, there was also a significant trend (Kendall's tau = 0.812; $p < 0.001$), with the fCO_{2atm} varying between 366 and 396 (380.0 ± 9.2) µatm.

Figure 2 - The time evolution of seawater fCO_2 (a) and atmosphere fCO_2 (b) measured by merchant ships at 3°S-14°S from 2008 to 2020.

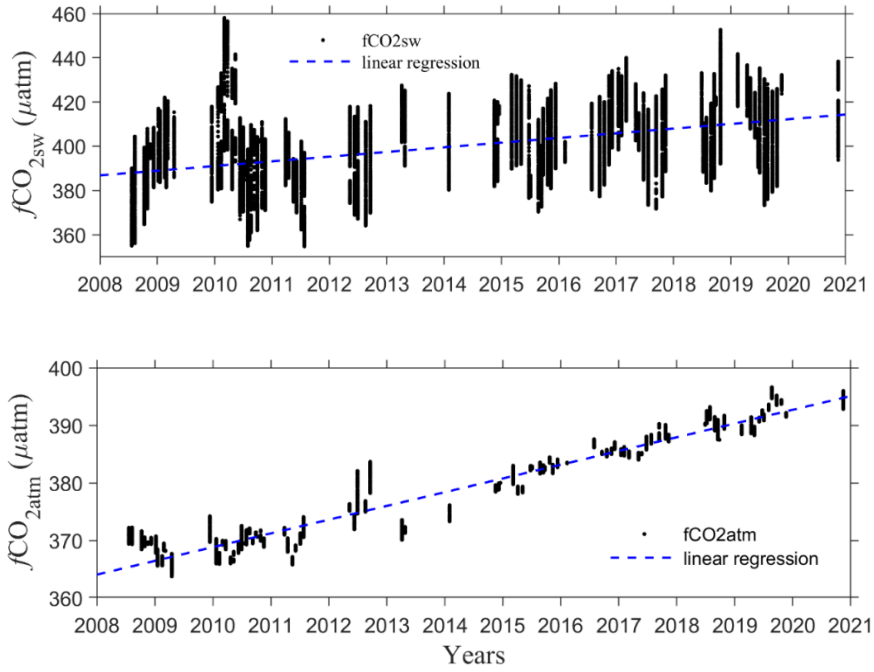

In both regions, the seasonal fCO_{2sw} variability (Figure 3) is mainly explained by the temperature variations and its seasonal cycle (Figure 4), with minimum values in austral winter (July – August) and maximum values in austral summer-autumn (March — April).

In the NS (Figure 3a), there is a seasonal variability. Considering seasonal variability, it was observed a significant difference ($p < 0.001$) in fCO_{2sw} values in both subregions. Specifically, an anomaly in fCO_{2sw} was observed in March 2010, where the fCO_{2sw} distribution exhibited higher values in 2010 compared to 2009, 2011, 2015, and 2017 (Figure 3). During the same period, the highest SST values were recorded relative to other years (Figure 4a), which can help to understand this rise in CO_2.

Figure 3 - Monthly Distribution of fCO_{2sw} for each year, from 2008 to 2020, divided into northern sub-region (3ºS – 8ºS) and southern sub-region (8ºS – 14ºS). The monthly average was calculated for each day collected in the month of the year and each dotted line color represents a collected year. Red line represents the monthly variability

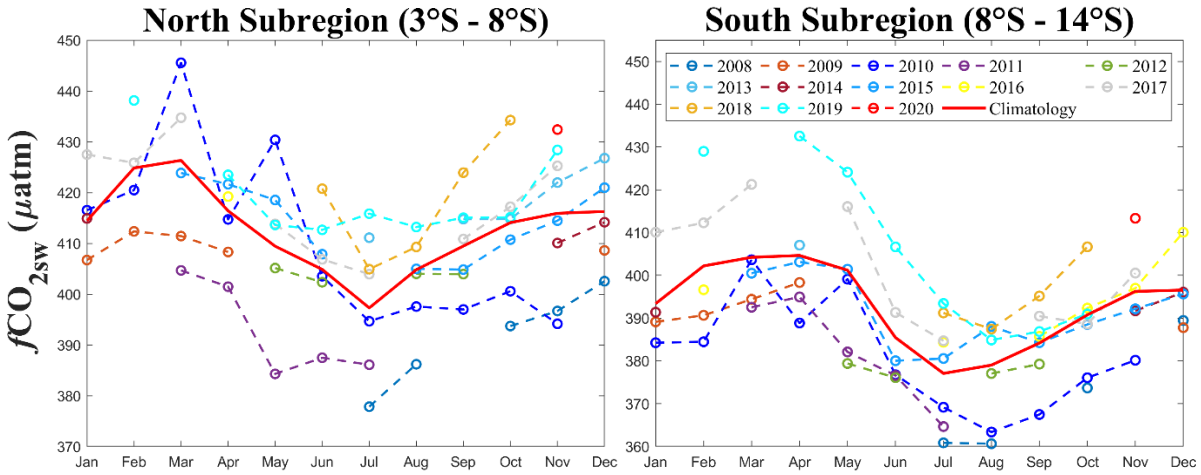

Source: The author (2024).

In SS sub-region, seasonal variability is also present. However, the fCO_{2sw} anomaly observed in March 2010 in the NS is not present here. Instead, it is possible to observe elevated fCO_{2sw} values between February and June in 2019 when compared to other years (Figure 3b, SM1, Supplementary Material). The average temperature of the months of 2010 for NS is higher than the average temperature of the same months of other years, disregarding the months of February and April 2019. The highest SST values were recorded for the same period (Feb-Jun) in 2019 in relation to the other years (Figure 4b). The SSS values during the same period in 2019 were similar to those of other years, suggesting that SSS could not explain this anomaly in the fCO_{2sw} values for that year. Therefore, the high SST values provide a better explanation for the increase in fCO_{2sw}.

South of 8ºS, the water is influenced by sSEC. The variability of fCO_{2sw} in the SS sub-region shows a minimum value in August of around 360 µatm and a maximum value in April of around 430 µatm (Figure 3b), which corresponds to the seasonal variations of the SST.

Figure 4 - Monthly Mean of Sea Surface Temperature (SST) measured by volunteer ships from 2008 to 2020 divided in northern sub-region (3ºS – 8ºS) and southern sub-region (8ºS – 14ºS). The monthly average was calculated for each day collected in the month of the year and each dotted line color represents a collected year

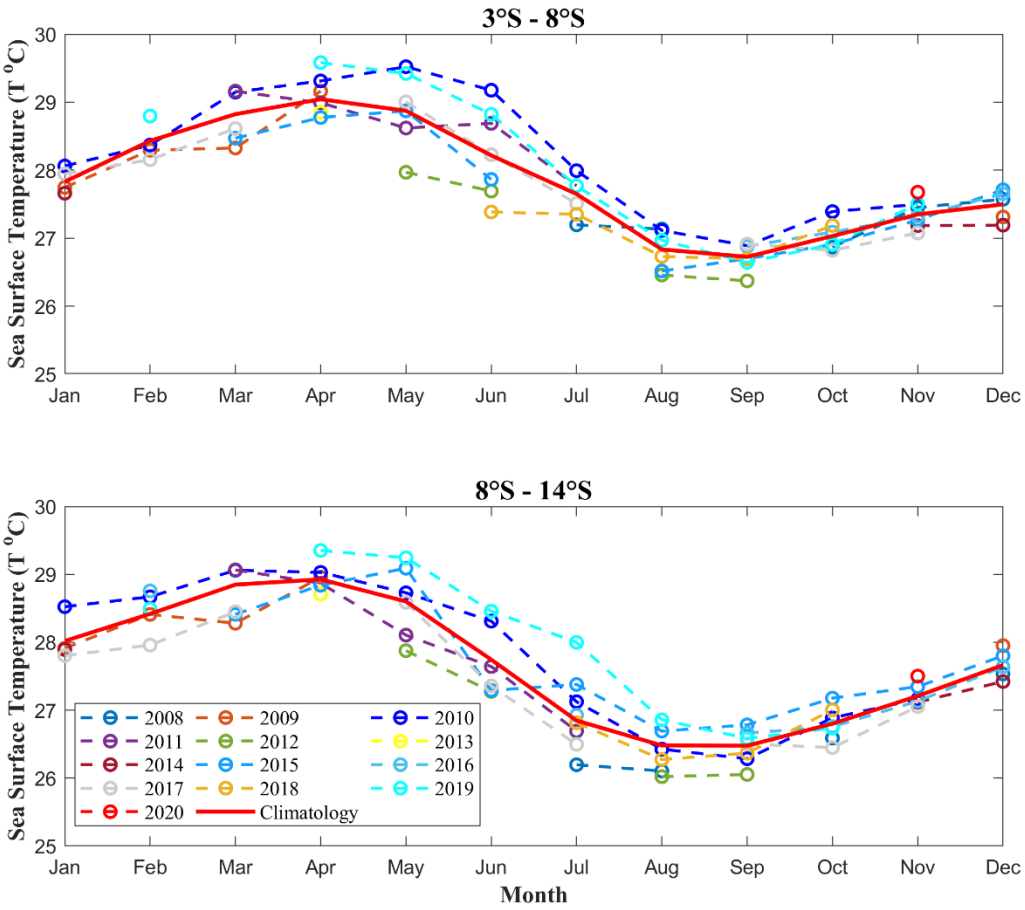

Source: The author (2024).

4.2.3.2. Latitudinal Distributions of fCO_{2sw}

The fCO_{2sw} varies between 375 and 442 µatm from December to February, between 374 and 458 µatm from March to May, between 355 and 435 from June to August, and between 361 and 453 µatm from September to November. Higher fCO_2 values are measured from 3 to 8°S, whereas lower fCO_2 values are measured from 8 to 14°S (SM1, Supplementary Material).

The sSEC flow varies seasonally, but at approximately 8°S, where the sSEC bifurcates its waters contribute to form Brazil Current (BC) to the south and the North Brazil Current (NBC) to the north (PEREIRA et al., 2014). Analyzing the fCO_2 data above 8°S, it was possible to notice that all values are above 380 µatm. This high CO_2 observed above 8°S can be explained by equatorial upwelling in the Gulf of Guinea, which transports CO_2-rich surface waters, warm with low salinities (GUIMARÃES; MONTES; LEFÈVRE, 2024; TAKAHASHI et al., 2009).

Using CO_2 observations of the merchant ships *Monte Olivia* and *Rio Blanco* (from 2008 to 2011) along the France-Brazil line, Lefèvre et al. (2013) discussed the anomalous warming of 2010 and its impact on the CO_2 flux. They observed high fCO_{2sw} values in early 2010, between approximately 8°S and 8°N, during the boreal spring (March) and concluded that a northward shift of the ITCZ position and a reduction of precipitation in 2010 were associated with the higher fCO_2 observed in this year, where the 2009 *El Niño* contributed to this pattern. Lefèvre et al. (2013) identified an anomalous position of the ITCZ after the 2009 *El Niño* in the Pacific Ocean, that remained further north in March 2010, reducing rainfall in the Tropical Atlantic, which is mainly responsible for the increase in sea surface salinity (AWO et al., 2018; IBÁNHEZ; FLORES; LEFÈVRE, 2017; LEFÈVRE et al., 2013).

Extending the observations by Lefèvre et al. (2013) with the data used in this study, from 2008 to 2020, we compare the year-to-year variability between 3ºS and 8ºS for the same period to complement the data described by Lefèvre et. al (2013). The fCO_{2sw} distribution shows higher values in March 2010 into NS than in other years for the same month, with values reaching 460 µatm (Figure 5). It can be noticed that there is a strong fCO_{2sw} anomaly, particularly pronounced between 3°S and approximately 8°S, followed by an abrupt drop in its values around 8ºS, obtaining values close to 400 µatm. In May 2010, the elevated levels of fCO_{2sw} persisted with values close to 450 µatm. However, in May 2011, it was less than 390 µatm, and in the same month in 2012, 2015, and 2019, the fCO_{2sw} showed values below 420 µatm. From June 2010, there is a normalization of fCO_{2sw} values, closely with in other years. The previously notable CO_2 anomaly dissipates and is no longer visible.

Figure 5 - Distribution of the fCO_{2sw} as a function of latitude along the March of each year with data. 2009, 2010, 2011, 2015 and 2017

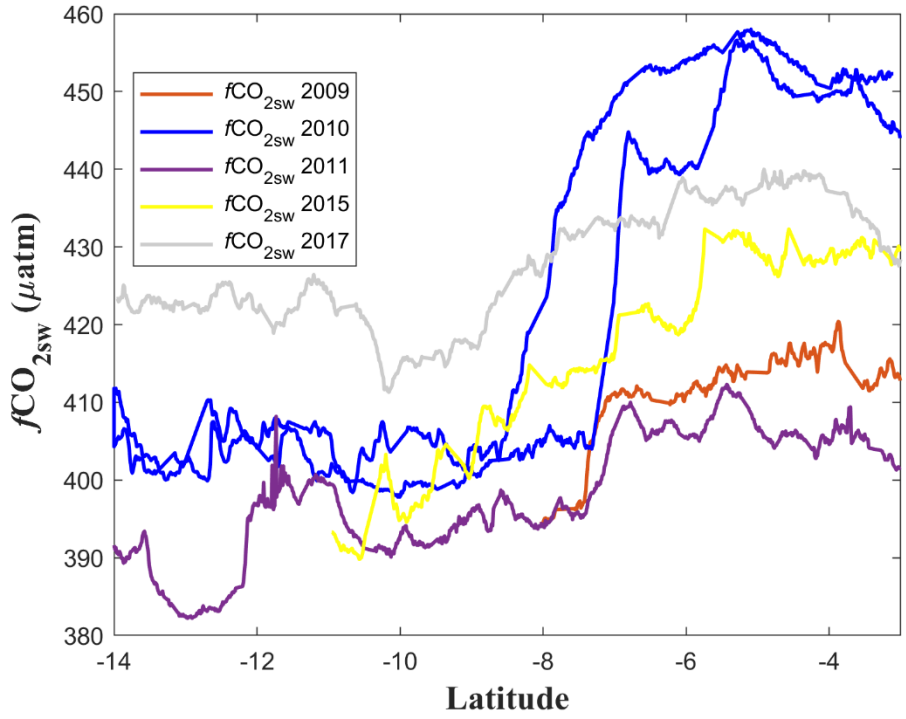

Source: The author (2024).

In the southern region (8°S to 14°S), the fCO_{2sw} in 2010 was similar to the fCO_{2sw} recorded in other years (Figure 1). However, it was observed that for the month of April 2019, there were higher values than in other years starting from 8º S. While in the years in which the month of April was analyzed (2009, 2010, 2011, 2013, 2015), the fCO_{2sw} values were between 380 and 410 µatm, for April 2019, it was close to 440 µatm, as can be seen in Figure 3.

4.2.3.3. Latitudinal Distributions of SST, SSS and Wind Speed

Our data showed that the highest SSTs occur over the years in the first months of the year (Figure 4). There is no significant difference in SST from one year to another and from subregions, with the exception of SST satellite data for the year 2011 (Figure 6), where its highest SST did not reach 28º C for both sub-regions.

According Boening et al. (2012), in 2010/2011, after *El Niño* condition 2009/2010, there was a *La Niña* that was the strongest ENSO cold event in the past 80 years. The studies by Silva et al. (2018) also showed that in June 2010 the SWTA region was influenced by heavy rainfall and the SAWP, in turn, recorded anomalous values of + 1°C, significantly influencing the

instability of meteorological systems. It was also observed in this study that warmer atmospheric conditions cause the oceanic environment to remain warmer, maintaining unstable conditions over the SAWP. Thus, SST anomalies and their interactions can be explain the difference of the pattern of satellite images of SST in Figure 6, which also affected precipitation patterns on the world (BOENING et al., 2012; SILVA et al., 2018)

Using a combination of SST data measured *in situ* by ships from 2008 to 2020, and satellite images of SST, for the same time interval (Figure 6), it was possible to characterize the annual patterns of SST for the study area. There was a similarity in the data, further corroborating the robustness of the data collected. The difference of SST data *in situ* and satellite SST is directly related to the wind speed and net air-sea heat flux (EMERY, 2015). However, is notably that the seasonal variability is stronger than the interannual variability.

Utilizing the dataset, the amplitude of the seasonal cycle of SST was calculated and was approximately 2.32º C to the NS subregion and 2.45º C to the SS subregion. According to Guimarães et al. (2024), in the NS sub-region, the mean annual SST ranges vary from 26.7 to 29.0º C, and in the SS sub-region, it ranges from 26.4 to 28.9º C. There is no significant difference in SST from 3ºS to 14ºS (SM2, Supplementary Material).

For the data series collected in situ and satellite images; changes can be observed in the SST satellite image data from 2011, where the SST was below 28° C, a lower annual temperature peak than in other years. The 2019 SST was the annual temperature peak for the data series collected in situ and satellite images, and it was close to 30° C, a record for the data series.

An SST anomaly was observed from 2010 to 2011 in both subregions (Figure 7). A strong *La Niña* condition in 2010/2011, after a strong *El Niño* condition (2009/2010), and the instability of meteorological systems influenced by SAWP temperature, may explain this SST anomaly for that year, as it affected weather patterns worldwide (BOENING et al., 2012; SILVA et al., 2018, 2021). This analysis of SST satellite images follows the dataset collected by volunteer ships for both subregions.

Figure 6 - Combination of SST data measured in situ by ships (blue points) and satellite images of SST (red line), from 2008 to 2020 divided in northern sub-region (3ºS – 8ºS) and southern sub-region (8ºS – 14ºS)

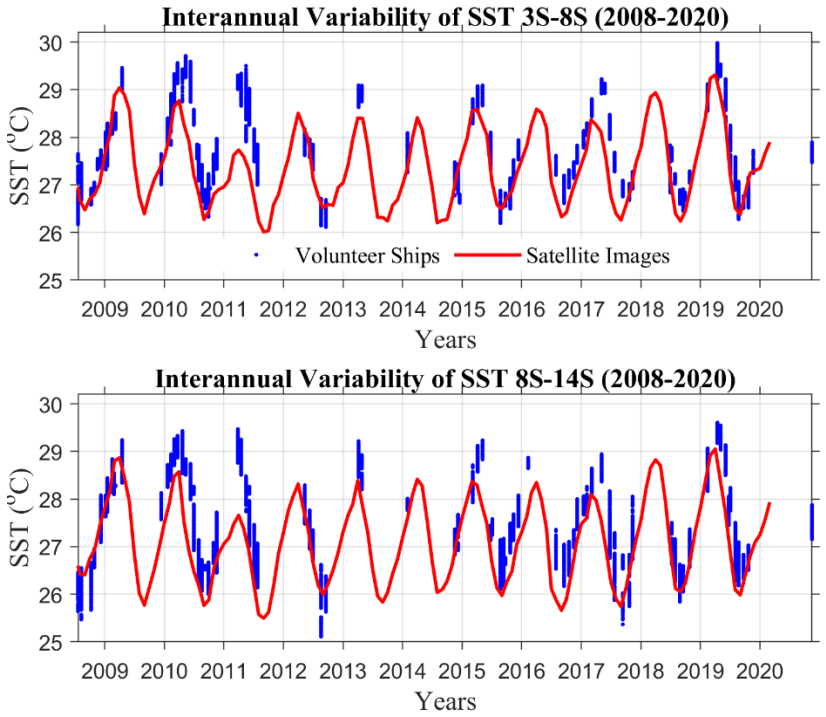

Source: The author (2024).

Figure 7 - SST anomaly by satellite image data from 2008 to 2020

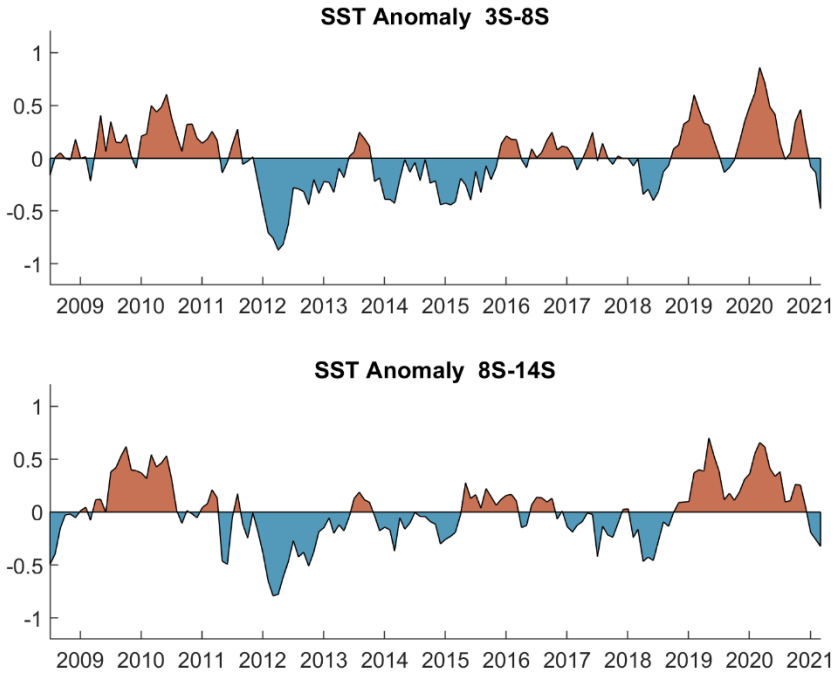

Source: The author (2024).

About the distribution of SSS, Guimaraes et al. (2024) showed that there was a clear difference between the NS and SS sub-regions with a mean of 36.2 ± 0.1 in the north and a mean of 36.8 ± 0.1 in the south (GUIMARÃES; MONTES; LEFÈVRE, 2024).

The distribution of SSS exhibits important differences between sub-regions (SM3, Supplementary Material). As can be seen in Figure 9 and SM3, most of each year's monthly average of data collected for NS sub-region is below 36.5. As for SS sub-region, the monthly average collected for each year is above 36.5. Between 3º and 8º S, from January to May, the salinity decreased all the years except 2010; in this same period, there were no low salinity values (Figure 9). This decrease in salinity, followed the highest SST, can be explained by precipitation under the presence of the ITCZ until 5°S (AWO et al., 2018; LEFÈVRE et al., 2013), which is generally located further south of the equator at this time of year (MOURA; VITORINO, 2012), the presence of Atlantic *Niño* that causes an increase of precipitation in western basin of Tropical Atlantic (KOSEKI et al., 2023), and the NEB precipitations well correlated with the positive SST anomalies (MOURA et al., 2009).

About the daily wind speed at 10 m presents a regularity pattern, but with a visible seasonal pattern (Figure 8). It means in the NS of 7.55 ± 1.24 m s^{-1} and SS 7.34 ± 1.28 m s^{-1} over 2008-2019. It is observed that lowest wind speeds are in the first semester of each year and the highest wind speed in the second semester.

Figure 8 - The daily wind speed at 10 m by *WindSAT* from 2008 to 2020 at North subregion (3°S – 8°S) and South subregion (8°S – 14°S).

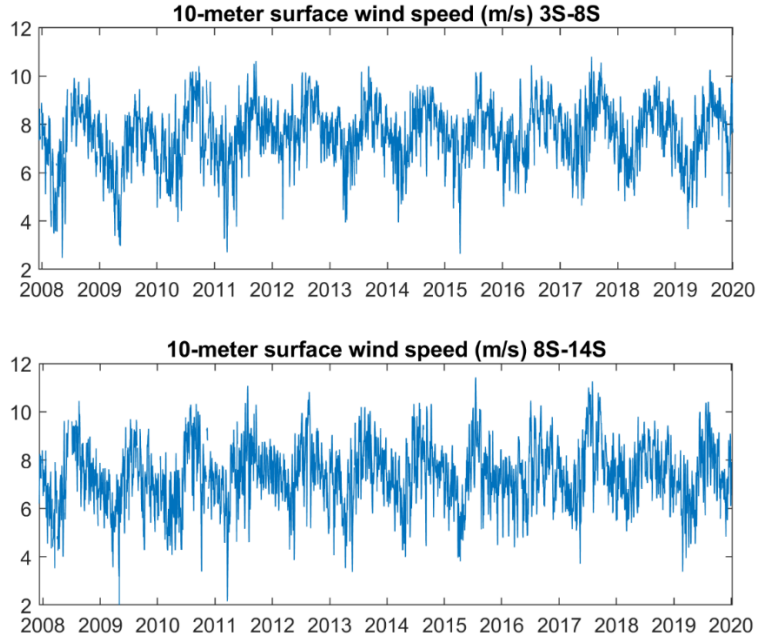

Source: The author (2024).

4.2.3.4. Impact on the Air-Sea Flux of CO_2

Guimarães et al. (2024) showed that the latitudinal distribution of the CO_2 flux in the NS as a strong source CO_2 to the atmosphere through-out the year with a mean 3.14 ± 0.52 mmol m^{-2} day^{-1}. In the SS, the CO_2 flux averaging 0.93 ± 0.90 mmol m^{-2} day^{-1} with even a weak sink of CO_2 occurring July (-0.47 mmol m^{-2} day^{-1}) and August (-0.51 mmol m^{-2} day^{-1}) (GUIMARÃES; MONTES; LEFÈVRE, 2024).

Table 2 provides the mean values of the air-sea CO_2 flux in the region from 3°S to 8°S (NS) and from 8°S to 14°S (SS). The data encompass a temporal range from 2008 to 2020, with some lack of data. In NS, the Spearman correlation between the CO_2 flux with SST and SSS was -0.232 and 0.317, respectively. Both with a $p < 0.001$, indicating a statistically significant negative association to SST and positive to SSS. It was observed that the average CO_2 flux values in the NS were higher to February (4.42 mmol m^{-2} d^{-1}), March (4.31 mmol m^{-2} d^{-1}), April (3.65 mmol m^{-2} d^{-1}) and May (3.79 mmol m^{-2} d^{-1}) in 2010, if compared to other years within the same period. There is a strong contrast when compared to the flux values measured in the following year, 2011. In this year, the mean CO_2 flux from February to May were substantially lower, with values 1.50, 2.10, 1.51 and 1.87 mmol $^{-2}$ d^{-1}, respectively.

These values showed a positive CO_2 anomalies in 2010 and 2011 caused for climatic events. Previously, in 2009 and 2010, there was *El Niño* event in Pacific Ocean that displaced to north of normal position the Atlantic ITCZ (BOENING et al., 2012; LEFÈVRE et al., 2013). This anormal position of ITCZ contributes to a lower rainfall in northward of NEB and increasing the drought of this region with high SST. Another climatic event is the warm pool in June 2010 with the warming of SST with anomalies temperatures above 1°C and extreme rainfall events (SILVA et al., 2018, 2021).

The 2009/2010 *El Nino* event was followed by a *La Niña* event in 2010/2011 (BOENING et al., 2012). This transition between these climatic events had an impact on the position of the ITCZ, SST, SSS, wind speed and in the rainfall regime.

According the Oceanic Niño Index (ONI), a measure of *El Niño*-Southern Oscillation, the years 2015-2016 were period marked by an *El Niño* event. Unfortunately, there iso a lack of data of pCO_2 that were not collected for this period. Therefore, there is no way to discuss anomalies for these years.

. In SS, the Spearman correlation between the CO_2 flux with SST and SSS was 0.697 and 0.041, respectively. Both with a $p < 0.001$, indicating a statistically a strong significant positive association to SST and weak positive to SSS. It was observed that SS values are below NS, with average values below of 2.75 mmol $^{-2}$ d $^{-1}$ (May 2017), becoming negative for part of the year, between July and September, with negative maximum of -1.57 mmol $^{-2}$ d $^{-1}$, in July 2008.

Table 2 - Mean CO_2 Flux (mmol m^{-2} d^{-1}) between Northern Subregion (3°S – 8°S) and Southern Subregion (8°S – 14°S) from 2008 to 2020.

						3º - 8º S						
Year	**Months**											
	Jan	**Feb**	**Mar**	**Apr**	**May**	**Jun**	**Jul**	**Aug**	**Sep**	**Oct**	**Nov**	**Dec**
2008							1.08	2.18		2.96	3.30	3.03
2009	3.03	3.40	2.59	1.62								3.42
2010	3.60	4.42	4.31	3.65	3.79	3.44	2.95	4.27	3.21	2.92	3.35	
2011			1.50	2.10	1.51	1.87	1.88					
2012					3.03	3.15		4.03	3.04			
2013				2.60								
2014	4.03										3.42	3.73
2015			2.87	2.50	3.32	2.48		3.40	2.59	3.27	3.06	3.63
2016							3.48		3.75	4.04	4.45	4.48
2017	3.86	3.37	3.19		2.19	2.30	2.28		3.73	3.82	4.24	
2018						3.95	2.16	2.58	4.65	4.69		
2019		2.92		1.84	2.13	2.46	2.67	2.24	2.65	2.38	3.73	
2020											4.51	

						8° - 14° S						
Year	**Months**											
	Jan	**Feb**	**Mar**	**Apr**	**May**	**Jun**	**Jul**	**Aug**	**Sep**	**Oct**	**Nov**	**Dec**
2008							-1.57	-1.17		0.01		1.72
2009	1.81	1.53	1.44	1.42								1.16
2010	1.38	1.17	1.93	1.27	1.28	0.82	-0.33	-1.05	-0.33	0.41	1.07	
2011			1.10	2.18	1.54	0.70	-0.85					
2012					0.25	-0.04		0.25	-0.06			
2013				1.92								
2014	1.40										1.27	1.68
2015			1.32	1.04	1.40	-0.29	-0.23	0.63	0.19	0.38	0.88	1.11
2016		0.83					-0.29		0.08	0.86	1.11	2.51
2017	2.03	2.00	2.09		2.75	0.50	-0.54		0.32	-0.06	1.17	
2018							-0.05	-0.27	0.58	1.41		
2019		2.24		2.11	1.74	1.83	0.27	-1.06	-0.76	-0.27		
2020											1.88	

2.1.1.1.Impact of SST and SSS on the Interannual Distribution of Fugacity of CO_2

In the Tropical Atlantic, the variability of fCO_2 is affected by temperature and salinity changes (LEFÈVRE et al., 2014). A strong CO_2 undersaturation in Western Tropical Atlantic has been observed in the regions influenced by large freshwater input from the Amazon River, where there is also a high dynamic of precipitation associated with the southernmost presence of the ITCZ in the austral summer-autumn (IBÁNHEZ et al., 2015; LEFÈVRE et al., 2013, 2017; LEFÉVRE; DIVERRÉS; GALLOIS, 2010; MONTEIRO et al., 2022; MU et al., 2021).

However, the western region of the tropical Atlantic analyzed in this study does not cover the Amazon region, and it is influenced by the ITCZ in the NS sub-region until 5º S. South of 5°S the eastern of NEB is influenced by the SAWP, which comes from Africa, providing rainfall in the opposite period to the ITCZ, between March and August being considered a strong CO_2 oversaturation that is fed by the recirculation of the NECC/Guinea Current and the equatorial upwelling in the Gulf of Guinea, carrying warm, CO_2-rich surface waters with low salinities. The SS is a weaker source of CO_2, except during within July and August, being a small sink of CO_2. This subregion is fed by salty and warm waters of the Benguela Current transported by the sSEC (GUIMARÃES; MONTES; LEFÈVRE, 2024; LANDSCHÜTZER et al., 2020).

As shown in Figure 9, the distribution of SSS between February and May of 2010 stands out with important differences compared with other years, and the distribution of SSS between February and May of 2010 stands out with important differences compared with other years in the NS sub-region. The distribution of CO_2 Flux shows higher values from February to May in this same year than other years for the same season, influenced by strong fCO_{2sw} anomaly in this region. In addition, the monthly variability of SST for each year doesn’t show an increase in temperature in surface water that can identify its influence on the 2010 anomaly. Thus, the increase in SSS, due to the anomalous position of the ITCZ, which increases in the January-May period, may explain the high values of fCO_{2sw} observed for March 2010. So, the SSS is the main factor associated with the CO_2 anomalies until May 2010.

Figure 9 - Monthly Mean of Sea Surface Salinity (SSS) measured by volunteer ships from 2008 to 2020 divided into northern sub-region (3ºS – 8ºS) and southern sub-region (8ºS – 14ºS)

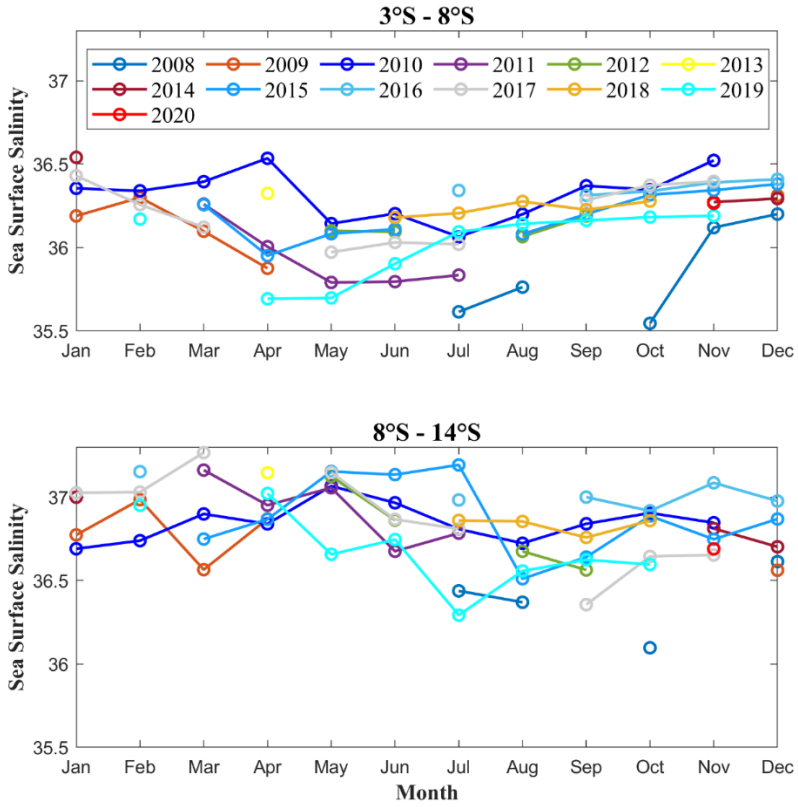

Source: The author (2024).

2.1.1.2. Precipitation in the Study Area

Precipitation in the Atlantic Ocean adjacent in the NEB is influenced by a combination of global and regional climate factors, which can vary throughout the year and influence rainfall distribution. In our study we have already mentioned the main factors that influence this regional precipitation and how they can influence the variation in the CO_2 flux.(AMORIM; CHAVES; SILVA, 2014; BOENING et al., 2012; KOSEKI et al., 2023; SILVA et al., 2018; SOUZA; CAVALCANTI, 2009).

With the GPCP precipitation data, it was possible to analyze the seasonal variation of rainfall for the entire study area, also separating it into NS and SS from 2008 to 2020 (Figure 10).

For NS, there is an increase in this amount of rainfall in the first months of each year. Except for the year 2010, when there is an anomaly that can be explained by the El Niño condition of the following year (GUIMARÃES; MONTES; LEFÈVRE, 2024; LEFÈVRE et

al., 2013). And in 2011, there was a peak in rainfall due to the 2011 La Niña condition, which was followed by the El Niño of the previous year (BOENING et al., 2012).

Figure 10 - The precipitation anomaly and daily precipitation by GPCP from 2008 to 2020 at North subregion (3°S – 8°S) and South subregion (8°S – 14°S).

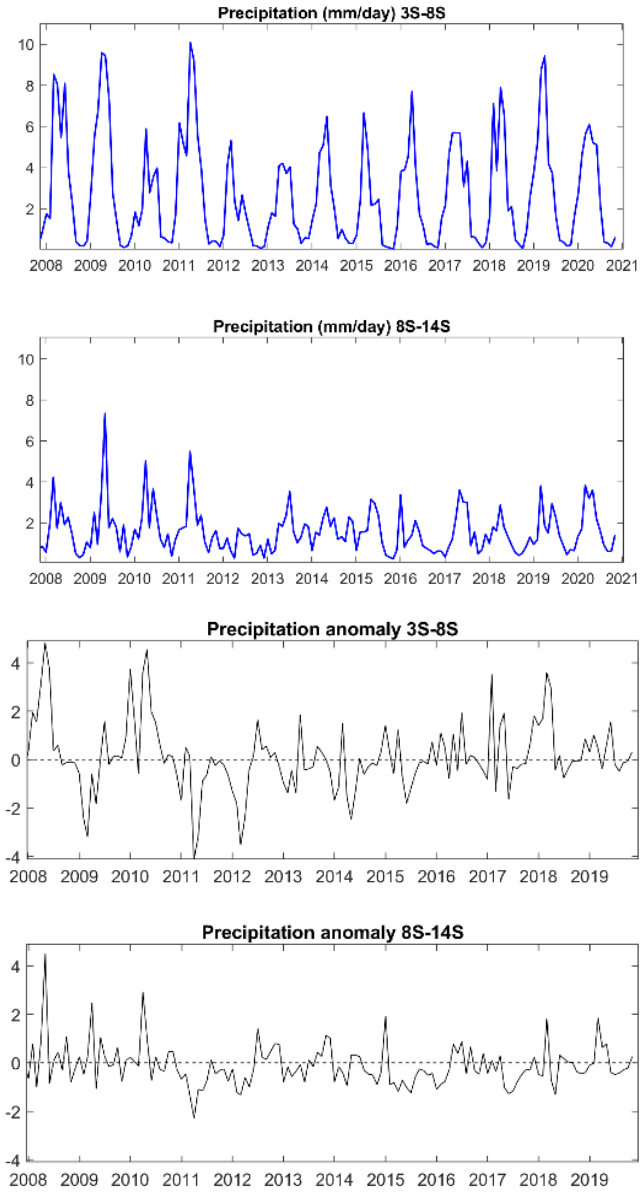

The precipitation patterns observed in the SS are closely linked to the SAWP. This connection is essential to understanding the occurrence of extreme precipitation events, particularly in the eastern portion of the NEB. In this area, heat and humidity serve as the primary mechanisms responsible for generating the necessary water vapor that fuels extreme rainfall events (SILVA et al., 2018).

In June 2010, the eastern NEB was influenced by intense rainfall and increased SST during this period, with positive anomalies exceeding 1°C (SILVA et al., 2021). In contrast, the situation changed drastically in early 2012. During this time, a severe drought affected the whole NEB, reducing notably the rainfall. Silva et al. (2021) highlight that this period coincided with negative SST anomalies in the SAWP, reaching values as low as -0.5°C.

The contrasting SST anomalies in 2010 and 2012 underscore the significant influence that the SAWP has on the regional climate, particularly below the latitude of 5°S. As seen in Figure 10, the area south 8°S is particularly sensitive to the variations and instabilities with the SAWP and associated meteorological systems.

2.1.2. Conclusion

The CO_2 data collected by merchant ships shows us the distribution of this CO_2 during 12 years (2008-2020) of data collection, within of 3°S and 14°S adjacent NEB. This is yet another study that shows the influence of the Pacific *El Niño/La Niña* teleconnection on the Tropical Atlantic Ocean.

It was possible to notice an anomaly in the distribution of CO_2 in some years due to the *El Niño* and *La Niña* phenomena that influence the position of the ITCZ in certain periods of the year and it influence the rainfall regime and the variability of SST and SSS. In 2010, a northward shift of the ITCZ position was associated with a reduction of precipitation. Therefore, there was an increase of air-sea CO_2 flux observed in austral summer and autumn between 3°S and 8°S.

The lack of data in some uncollected months raises doubts about the distribution of CO_2, but continuous monitoring of CO_2 not only in this area but in coastal areas can help in documenting and investigating the variability of CO_2 flux.

2.1.3. Supplementary Material

SM 1 - Distribution of the fCO_{2sw} as a function of latitude along the different months of the years 2008, 2009 (red), 2010 (blue), 2011, 2012, 2013, 2014, 2015 (cyan), 2016 (magenta), 2017 (green), 2018 (yellow), 2019 (black) and 2020 for months from January to December

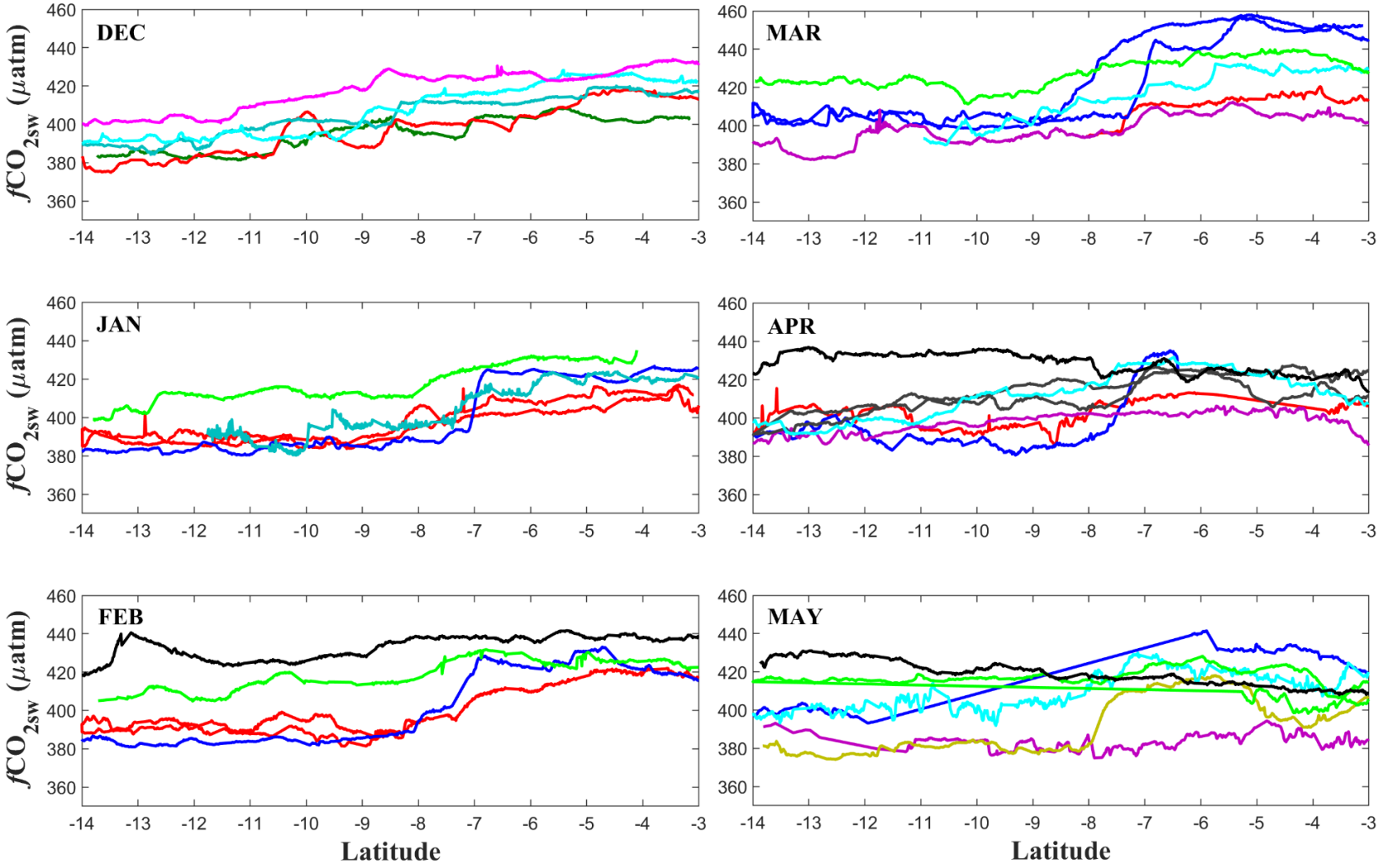

SM1 (continuation) – Distribution of the fCO_2 as a function of latitude along the different months of the years 2008, 2009 (red), 2010 (blue), 2011, 2012, 2013, 2014, 2015 (cyan), 2016 (magenta), 2017 (green), 2018 (yellow), 2019 (black) and 2020 for months from January to December

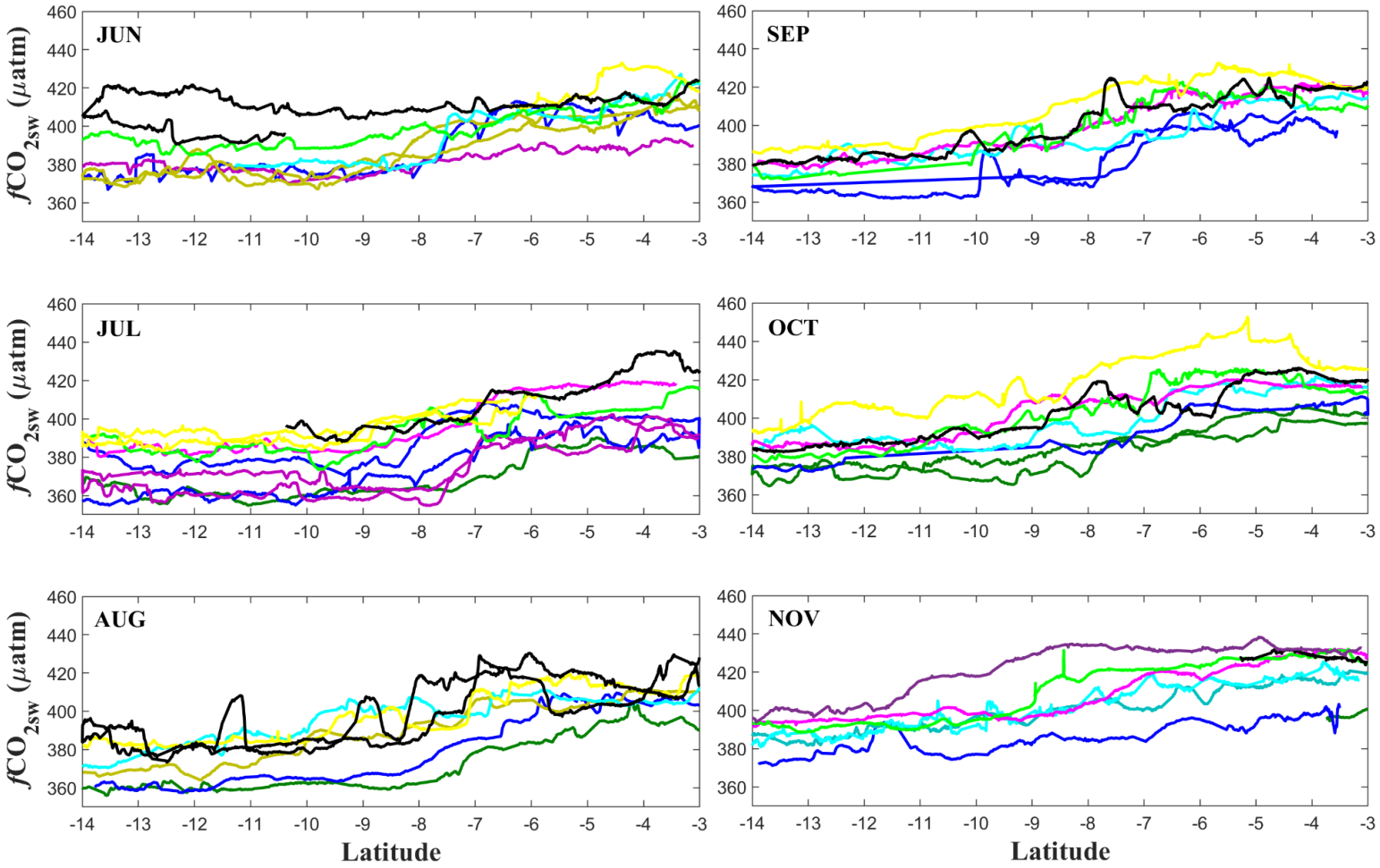

SM 2 - Distribution of the Sea Surface Temperature as a function of latitude along the different months of the years 2008, 2009 (red), 2010 (blue), 2011, 2012, 2013, 2014, 2015 (cyan), 2016 (magenta), 2017 (green), 2018 (yellow), 2019 (black) and 2020 for months from January to December

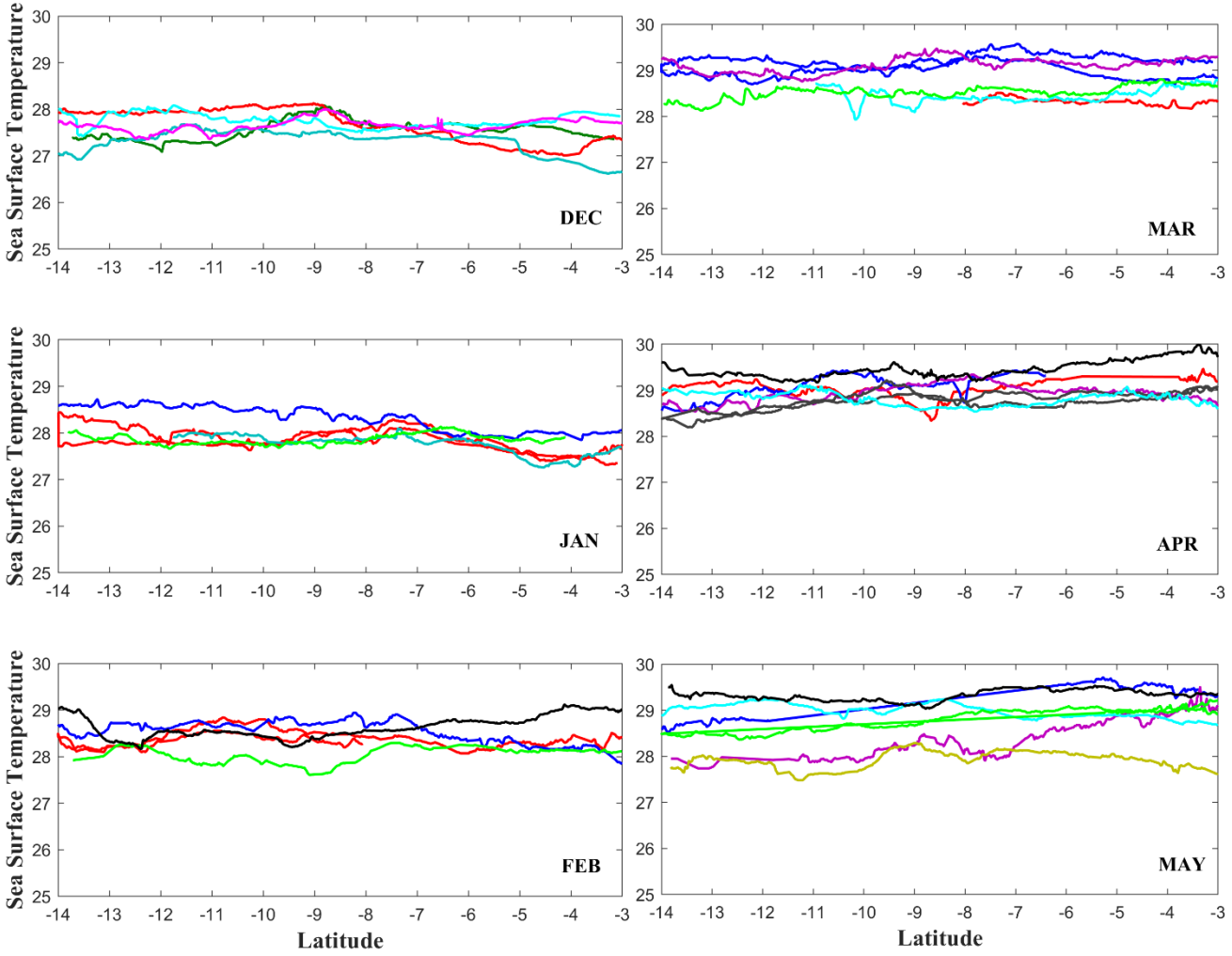

SM2 (continuation) - Distribution of the Sea Surface Temperature as a function of latitude along the different months of the years 2008, 2009 (red), 2010 (blue), 2011, 2012, 2013, 2014, 2015 (cyan), 2016 (magenta), 2017 (green), 2018 (yellow), 2019 (black) and 2020 for months from January to December.

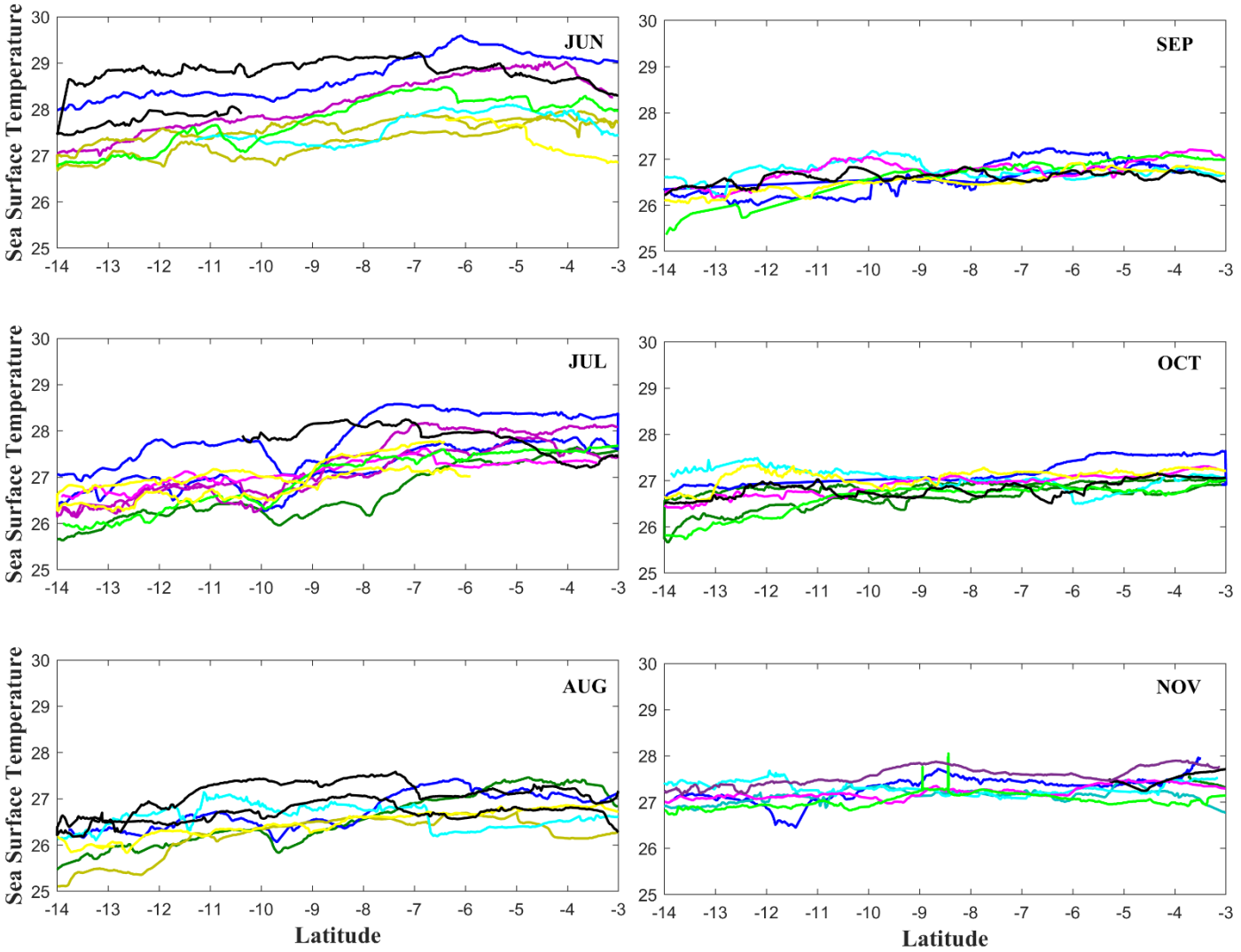

SM 3 - Distribution of the Sea Surface Salinity as a function of latitude along the different months of the years 2008, 2009 (red), 2010 (blue), 2011, 2012, 2013, 2014, 2015 (cyan), 2016 (magenta), 2017 (green), 2018 (yellow), 2019 (black) and 2020 for months from January to December.

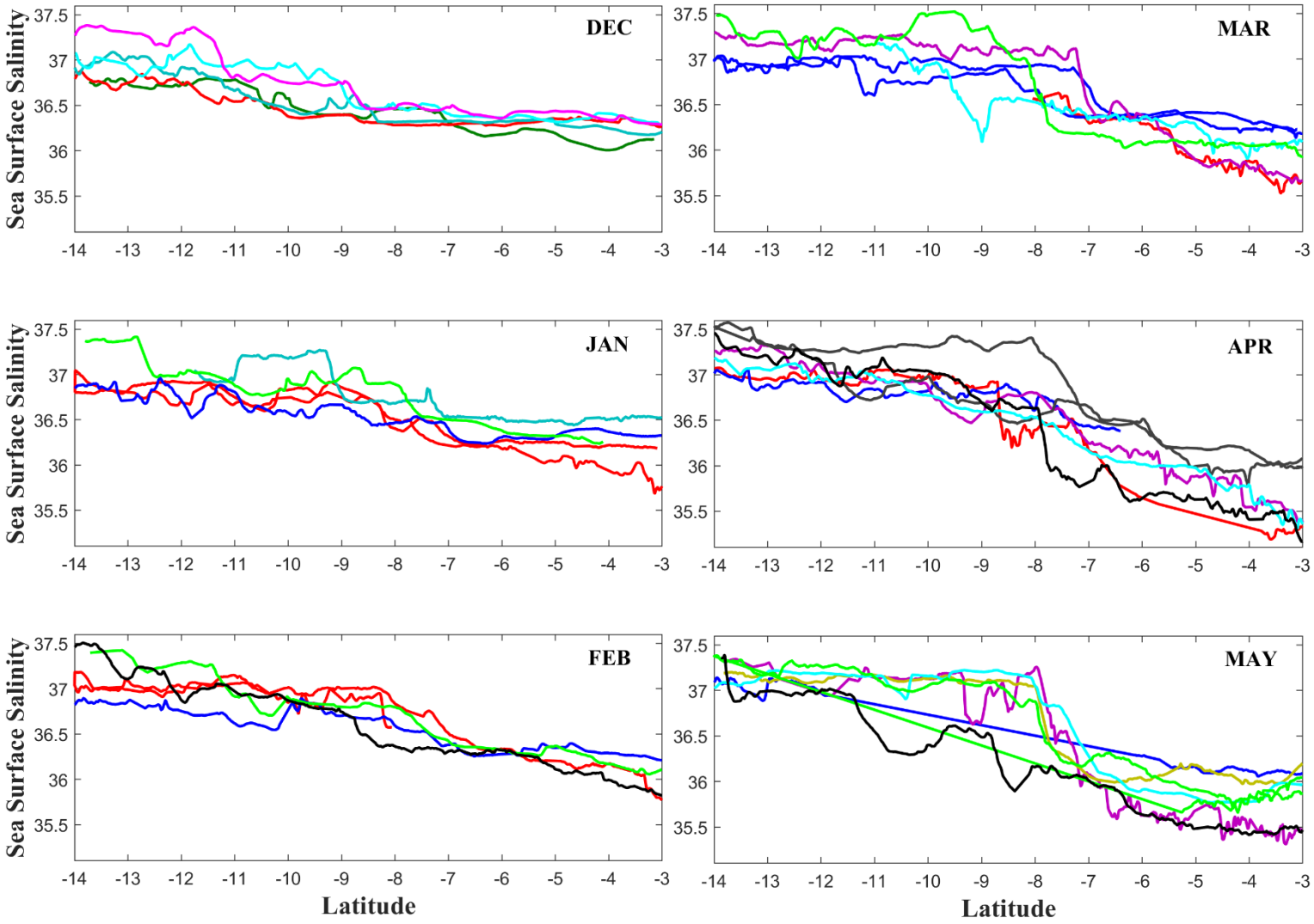

SM3 (continuation) - Distribution of the Sea Surface Salinity as a function of latitude along the different months of the years 2008, 2009 (red), 2010 (blue), 2011, 2012, 2013, 2014, 2015 (cyan), 2016 (magenta), 2017 (green), 2018 (yellow), 2019 (black) and 2020 for months from January to December

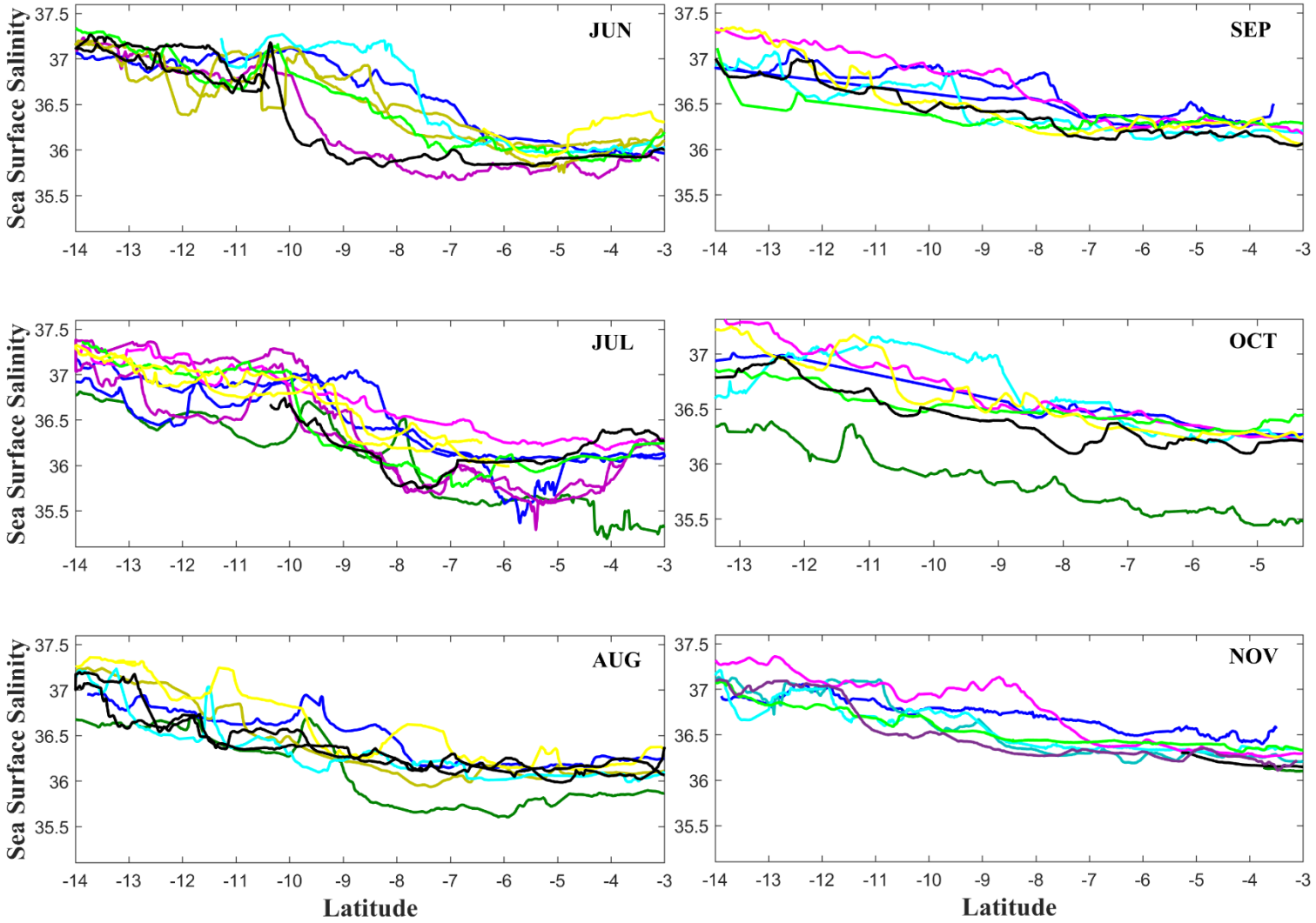

2.1.4. References

AMORIM, A. C. B.; CHAVES, R. R.; SILVA, C. M. S. E. Influence of the Tropical Atlantic Ocean's Sea Surface Temperature in the Eastern Northeast Brazil Precipitation. **Atmospheric and Climate Sciences**, v. 04, n. 05, p. 874–883, 2014.

AMORIM, F. N. et al. The seasonal circulation of the Eastern Brazilian shelf between 10°S and 16°S: A modelling approach. **Continental Shelf Research**, v. 65, p. 121–140, 2013.

ARAUJO, M. et al. On the variability in the CO_2 system and water productivity in the western tropical Atlantic off North and Northeast Brazil. **Journal of Marine Systems**, v. 189, n. September 2018, p. 62–77, 2019.

AWO, F. M. et al. Sea Surface Salinity Signature of the Tropical Atlantic Interannual Climatic Modes. **Journal of Geophysical Research: Oceans**, v. 123, n. 10, p. 7420–7437, 2018.

BOENING, C. et al. The 2011 La Niña: So strong, the oceans fell. **Geophysical Research Letters**, v. 39, n. 19, 16 out. 2012.

BONOU, F. K. et al. Distribution of CO_2 parameters in the Western Tropical Atlantic Ocean. **Dynamics of Atmospheres and Oceans**, v. 73, p. 47–60, 2016.

CARVALHO, A. C. O. et al. Air-sea CO2 fluxes for the Brazilian northeast continental shelf in a climatic transition region. **Journal of Marine Systems**, v. 173, p. 70–80, 2017.

CARVALHO OLIVEIRA, J. et al. A climatology of the annual cycle of river discharges into the Brazilian continental shelves: from seasonal to interannual variability. **Environmental Earth Sciences**, v. 77, n. 5, p. 192, 2 mar. 2018.

CIOTTI, Á. M.; GARCIA, C. A. E.; JORGE, D. S. F. **Temporal and meridional variability of Satellite-estimates of surface chlorophyll concentration over the Brazilian continental shelfPan-American Journal of Aquatic Sciences**. [s.l: s.n.]. Disponível em: <http://oceancolor.gsfc.nasa.gov>.

CLARK, D. R.; REES, A. P.; JOINT, I. Ammonium regeneration and nitrification rates in the oligotrophic Atlantic Ocean: Implications for new production estimates. **Limnology and Oceanography**, v. 53, n. 1, p. 52–62, 2008.

DE QUEIROZ, A. R. et al. Vertical and horizontal distribution of phytoplankton around an oceanic archipelago of the Equatorial Atlantic. **Marine Biodiversity Records**, v. 8, 8 abr. 2015.

DONOHOE, A. et al. The relationship between ITCZ location and cross-equatorial atmospheric heat transport: From the seasonal cycle to the last glacial maximum. **Journal of Climate**, v. 26, n. 11, p. 3597–3618, jun. 2013.

DOSSA, A. N. et al. Near-surface western boundary circulation off Northeast Brazil. **Progress in Oceanography**, v. 190, n. January 2020, 2021.

EMERY, W. J. **Air Sea Interactions: Sea Surface Temperature**. Second Edi ed. [s.l.] Elsevier, 2015. v. 1

FRIEDLINGSTEIN, P. et al. Global Carbon Budget 2022. **Earth System Science Data**, v. 14, n. 11, p. 4811–4900, 2022.

GASPAR, F. L. et al. Alkalinity, inorganic carbon and CO2 flux variability during extreme rainfall years (2010-2011) in two polluted tropical estuaries ne Brazil. **Brazilian Journal of Oceanography**, v. 66, n. 1, p. 115–130, 1 jan. 2018.

GOMES, H. B. et al. Easterly wave disturbances over Northeast Brazil: An observational analysis. **Advances in Meteorology**, v. 2015, 2015.

GUIMARÃES, L. M.; MONTES, M. J. F.; LEFÈVRE, N. Regional differences in the air–sea CO2 flux between 3 and 14°S in the south-western tropical Atlantic. **Marine and Freshwater Research**, v. 75, n. 7, 9 maio 2024.

HASTENRATH, S. Exploring the climate problems of Brazil's Nordeste: A review. **Climatic Change**, v. 112, n. 2, p. 243–251, 2012.

HOUNSOU-GBO, G. A. et al. Tropical Atlantic contributions to strong rainfall variability along the northeast Brazilian coast. **Advances in Meteorology**, v. 2015, 2015.

IBÁNHEZ, J. S. P. et al. Seasonal and interannual variability of sea-air CO_2 fluxes in the tropical Atlantic affected by the Amazon River plume. **Global Biogeochemical Cycles**, v. 29, n. 10, p. 1640–1655, out. 2015.

IBÁNHEZ, J. S. P.; ARAUJO, M.; LEFÈVRE, N. The overlooked tropical oceanic CO2 sink. **Geophysical Research Letters**, v. 43, n. 8, p. 3804–3812, 2016.

IBÁNHEZ, J. S. P.; FLORES, M.; LEFÈVRE, N. Collapse of the tropical and subtropical North Atlantic CO2 sink in boreal spring of 2010. **Scientific Reports**, v. 7, n. January, p. 1–9, 2017.

JOHNS, W. et al. **Tropical Atlantic Observing System (TAOS)**. [s.l: s.n.]. Disponível em:

<https://www.researchgate.net/publication/351617393>.

KITIDIS, V. et al. Surface ocean carbon dioxide during the Atlantic Meridional Transect (1995–2013); evidence of ocean acidification. **Progress in Oceanography**, v. 158, p. 65–75, 2017.

KNOPPERS, B.; EKAU, W.; FIGUEIREDO, A. G. The coast and shelf of east and northeast Brazil and material transport. **Geo-Marine Letters**, v. 19, n. 3, p. 171–178, 1999.

KOSEKI, S. et al. Disentangling the impact of Atlantic Niño on sea-air CO2 flux. **Nature Communications**, v. 14, n. 1, p. 3649, 20 jun. 2023.

LANDSCHÜTZER, P. et al. A uniform pCO2 climatology combining open and coastal oceans. **Earth System Science Data Discussions**, p. 1–30, 2020.

LEFÈVRE, N. et al. Variability of pCO2 in the tropical Atlantic in 1995. **Journal of Geophysical Research**, v. 103, n. C3, p. 5623–5634, 15 mar. 1998.

LEFÈVRE, N. et al. Increased CO2 outgassing in February-May 2010 in the tropical Atlantic following the 2009 Pacific El Niño. **Journal of Geophysical Research: Oceans**, v. 118, n. 4, p. 1645–1657, 1 abr. 2013.

LEFÈVRE, N. et al. Impact of physical processes on the seasonal distribution of the fugacity of CO2 in the western tropical Atlantic. **Journal of Geophysical Research: Oceans**, v. 119, n. 2, p. 646–663, 2014.

LEFÈVRE, N. et al. Net heterotrophy in the Amazon continental shelf changes rapidly to a sink of CO_2 in the outer Amazon plume. **Frontiers in Marine Science**, v. 4, n. SEP, p. 1–16, 2017.

LEFÈVRE, N. et al. Amazon River propagation evidenced by a CO2 decrease at 8°N, 38°W in September 2013. **Journal of Marine Systems**, v. 211, 1 nov. 2020.

LEFÉVRE, N.; DIVERRÉS, D.; GALLOIS, F. Origin of CO_2 undersaturation in the western tropical Atlantic. **Tellus, Series B: Chemical and Physical Meteorology**, v. 62, n. 5, p. 595–607, 2010.

LUMPKIN, R.; GARZOLI, S. L. Near-surface circulation in the Tropical Atlantic Ocean. **Deep-Sea Research Part I: Oceanographic Research Papers**, v. 52, n. 3, p. 495–518, mar. 2005.

MAFALDA JR, P. O. et al. Oceanografia Biológica: Biomassa Fitoplanctônica na ZEE da

Região Nordeste do Nordeste do Brasil. In: FÁBIO HISSA VIEIRA HAZIN (Ed.). . **Coleção Programa REVIZEE SCORE NORDESTE**. Fortaleza: Martins & Cordeiro Ltda, 2009. p. 11–26.

MONTEIRO, T. et al. Contrasting Sea-Air CO 2 Exchanges in the Western Tropical Atlantic Ocean. **Global Biogeochemical Cycles**, v. 36, n. 8, 15 ago. 2022.

MOORE, C. M. et al. Processes and patterns of oceanic nutrient limitation. **Nature Geoscience**, v. 6, n. 9, p. 701–710, 2013.

MOURA, G. B. DE A. et al. Relação entre a precipitação do leste do Nordeste do Brasil e a temperatura dos oceanos. **Revista Brasileira de Engenharia Agrícola e Ambiental**, v. 13, n. 4, p. 462–469, 2009.

MOURA, M. DO N.; VITORINO, M. I. Variabilidade Da Precipitação Em Tempo E Espaço Associada À Zona De Convergência Intertropical Maurício Do Nascimento Moura E Maria Isabel Vitorino. **Revista Brasileira de Meteorologia**, v. 27, n. 4, p. 475–483, 2012.

MU, L. et al. Temporal Variability of Air-Sea CO 2 flux in the Western Tropical North Atlantic Influenced by the Amazon River Plume. **Global Biogeochemical Cycles**, v. 35, n. 6, 10 jun. 2021.

MÜNNICH, M.; NEELIN, J. D. Seasonal influence of ENSO on the Atlantic ITCZ and equatorial South America. **Geophysical Research Letters**, v. 32, n. 21, p. 1–4, 2005.

NORIEGA, C. et al. Spatial and temporal variability of CO2 fluxes in tropical estuarine systems near areas of high population density in Brazil. **Regional Environmental Change**, v. 15, n. 4, p. 619–630, 1 abr. 2015.

PADIN, X. A. et al. Air-Sea CO2 fluxes in the atlantic as measured during boreal spring and autumn. **Biogeosciences**, v. 7, n. 5, p. 1587–1606, 2010.

PEREIRA, J. et al. The bifurcation of the western boundary current system of the South Atlantic Ocean. **Revista Brasileira de Geofisica**, v. 32, n. 2, p. 241–257, 2014.

RODRIGUES, R. R.; ROTHSTEIN, L. M.; WIMBUSH, M. Seasonal variability of the South Equatorial Current bifurcation in the Atlantic Ocean: A numerical study. **Journal of Physical Oceanography**, v. 37, n. 1, p. 16–30, jan. 2007.

SILVA, B. J. et al. Carbon chemistry variability around a tropical archipelago. **Marine and**

Freshwater Research, v. 70, n. 6, p. 767–780, 2019.

SILVA, T. L. DO V. et al. Ocean-atmosphere feedback during extreme rainfall events in eastern Northeast Brazil. **Journal of Applied Meteorology and Climatology**, v. 57, n. 5, p. 1211–1229, 2018.

SILVA, T. L. DO V. et al. Assessing the Tropical South Atlantic atmosphere thermodynamics under distinct Sea Surface Temperature patterns. **Research Square**, p. 0–25, 2021.

SOUZA, P.; CAVALCANTI, I. F. A. Atmospheric centres of action associated with the Atlantic ITCZ position. **International Journal of Climatology**, v. 29, n. 14, p. 2091–2105, 30 nov. 2009.

STRAMMA, L.; ENGLAND, M. On the water masses and mean circulation of the South Atlantic Ocean. **Journal of Geophysical Research: Oceans**, v. 104, n. C9, p. 20863–20883, 15 set. 1999.

STRAMMA, L.; IKEDA, Y.; PETERSON, R. G. Geostrophic transport in the Brazil current region north of 20°S. **Deep Sea Research Part A, Oceanographic Research Papers**, v. 37, n. 12, p. 1875–1886, 1990.

STRAMMA, L.; SCHOTT, F. **The mean flow field of the tropical Atlantic OceanDeep-Sea Research II**. [s.l: s.n.].

TAKAHASHI, T. et al. Climatological mean and decadal change in surface ocean pCO_2, and net sea-air CO_2 flux over the global oceans. **Deep-Sea Research Part II: Topical Studies in Oceanography**, v. 56, n. 8–10, p. 554–577, 2009.

VELEDA, D. et al. Seasonal and interannual variability of the southern south Equatorial Current bifurcation and meridional transport along the eastern brazilian edge. **Tropical Oceanography**, v. 39, n. 1, p. 27–59, 1 jun. 2011.

5. CONSIDERAÇÕES FINAIS

Este estudo apresentou a distribuição da fugacidade do CO_2 da água do mar (fCO_{2sw}), da fugacidade do CO_2 atmosférico (fCO_{2atm}) e do fluxo de CO_2 próximo à costa do Nordeste do Brasil, entre 3°S e 14°S. Foram utilizadas observações coletadas por navios mercantes equipados com um sistema autônomo de pCO_2. Esta análise preenche uma lacuna importante nos estudos e melhora as séries temporais de observações de CO_2 em todo o mundo, especificamente no Atlântico Tropical Sudoeste (SWTA) adjacente ao Brasil.

No primeiro artigo, foi possível observar uma significativa diferença na região, mostrando um contraste entre uma parte norte (NS), 3°S – 8° S, onde o fluxo de CO_2 e a fCO_{2sw} são maiores do que na parte sul (SS), 8°S – 14°S. Foi observado que este contraste entre NS e SS deveu-se, principalmente, às diferenças nas correntes superficiais em cada área. A Sub-região Norte é influenciada pelo braço central da Corrente Sul Equatorial (cSEC). Esta corrente é alimentada pela recirculação da NECC/Corrente da Guiné e pela ressurgência equatorial no Golfo da Guiné, explicando os valores mais elevados de fCO_{2sw} comparados à Sub-região Sul. Esta última é influenciada pelo braço sul da Corrente Sul Equatorial (sSEC), que contém a Salinidade Máxima da Água (SMW), superior a 36,6, sugerindo que a fCO_{2sw} e o fluxo de CO_2 são efeito da Salinidade da Superfície do Mar.

A diferença de regiões também foi destacada através da atuação do Atlântico Tropical Sudoeste, onde a NS apresentou ser uma forte fonte de CO_2 para a atmosfera, corroborando para as hipóteses iniciais. Destacou-se também a parte SS sendo considerada uma fonte mais fraca de CO_2 e com período de Julho a Agosto como uma região de fraco sumidouro de CO_2, com valores negativos do seu fluxo.

No segundo artigo, foi possível observar a evolução temporal dos parâmetros de CO_2 em um sistema complexo de correntes marítimas superficiais juntamente as variações anuais da Temperatura da Superfície do Mar (TSM) e da Salinidade da Superfície do Mar (SSM). Foram destacadas as anomalias do CO_2 a partir das mudanças de posição da Zona de Convergência Intertropical, influenciadas pelos fenômenos de *El Niño*, *La Niña* e *Atlantic Niño* na região mais ao norte do Nordeste brasileiro (até 5°S), e o fenômeno de *South Atlantic Warm Pool* (SAWP), como influenciador do oceano Atlântico adjacente ao leste da região Nordeste. Esse artigo também observou o impacto da TSM e SSM na distribuição interanual da fCO_{2sw}.

Através desse estudo, pode-se destacar que há uma tendência ascendente no CO_2 atmosférico e no fluxo de CO_2 de 2008 a 2020, que está ligada ao aumento do CO_2 na água do

mar. Existem variabilidades sub-regionais e sazonais significativas nas distribuições de fCO_{2sw}, fluxo de CO_2 e fCO_{2atm} das águas superficiais no SWTA. Os padrões forneceram a base para identificar processos ligados a latitudes mensuráveis.

Estas informações são importantes para a compreensão da variabilidade tempo-espaço da pCO_2 na região do oceano Atlântico Tropical Sudoeste, adjacente à região Nordeste do Brasil e para o planejamento de futuras investigações de campo próximas às regiões costeiras. Para tanto, são necessários mais cruzeiros pela costa brasileira para identificar lacunas de dados e incertezas sobre fCO_2 e coletar amostras de água para analisar Carbono Inorgânico Dissolvido (DIC) e Alcalinidade Total (TA), a fim de aprimorar os estudos do ciclo do carbono.

REFERÊNCIAS

ANDRES, R. J. et al. A synthesis of carbon dioxide emissions from fossil-fuel combustion. **Biogeosciences**, v. 9, n. 5, p. 1845–1871, 2012.

ARAUJO, M. et al. On the variability in the CO_2 system and water productivity in the western tropical Atlantic off North and Northeast Brazil. **Journal of Marine Systems**, v. 189, n. September 2018, p. 62–77, 2019.

AYAR, P. V. et al. Contrasting projections of the ENSO-driven CO2flux variability in the equatorial Pacific under high-warming scenario. **Earth System Dynamics**, v. 13, n. 3, p. 1097–1118, 2022.

BONAN, G. B. Forests and Climate Change: Forcings, Feedbacks, and the Climate Benefits of Forests. **Science**, v. 320, n. 5882, p. 1444–1449, 13 jun. 2008.

BONOU, F. K. et al. Distribution of CO_2 parameters in the Western Tropical Atlantic Ocean. **Dynamics of Atmospheres and Oceans**, v. 73, p. 47–60, 2016.

BRONSELAER, B. et al. The influence of Southern Ocean winds on the North Atlantic carbon sink. **Global Biogeochemical Cycles**, v. 30, n. 6, p. 844–858, 1 jun. 2016.

CARROLL, J. J.; SLUPSKY, J. D.; MATHER, A. E. **The Solubility of Carbon Dioxide in Water at Low PressureJournal of Physical and Chemical Reference Data**, 1991.

CARVALHO, A. C. O. et al. Air-sea CO2 fluxes for the Brazilian northeast continental shelf in a climatic transition region. **Journal of Marine Systems**, v. 173, p. 70–80, 2017.

COOLEY, S. R. et al. Seasonal variations in the Amazon plume-related atmospheric carbon sink. **Global Biogeochemical Cycles**, v. 21, n. 3, p. 1–15, 2007.

DE JESUS AFFE, H. M. et al. Sea-air CO2 fluxes along the Brazilian continental margin. **Ocean and Coastal Research**, v. 71, n. suppl 2, p. 1–18, 2023.

DICKSON, A. G. The carbon dioxide sustem in seawater: equilibrium chemistry and measurement. In: Guide to best practices for ocean acidification. **Guide to best practices for ocean acidification research and data reporting**, v. 1, p. 17–40, 2010.

ESSIEN, P. et al. Intertropical Convergence Zone as the Possible Source Mechanism for Southward Propagating Medium-Scale Traveling Ionospheric Disturbances over South American Low-Latitude and Equatorial Region. **Atmosphere**, v. 13, n. 11, p. 1–15, 2022.

FINDLAY, H. S.; TURLEY, C. Ocean acidification and climate change. In: **Climate Change**. [s.l.] Elsevier, 2021. p. 251–279.

FRIEDLINGSTEIN, P. et al. Global Carbon Budget 2020. **Earth System Science Data**, v. 12, n. 4, p. 3269–3340, 11 dez. 2020.

FRIEDLINGSTEIN, P. et al. Global Carbon Budget 2022. **Earth System Science Data**, v. 14, n. 11, p. 4811–4900, 2022.

HASTENRATH, S. Exploring the climate problems of Brazil's Nordeste: A review. **Climatic Change**, v. 112, n. 2, p. 243–251, 2012.

IBÁNHEZ, J. S. P. et al. Seasonal and interannual variability of sea-air CO_2 fluxes in the tropical Atlantic affected by the Amazon River plume. **Global Biogeochemical Cycles**, v. 29, n. 10, p. 1640–1655, out. 2015.

IBÁNHEZ, J. S. P.; ARAUJO, M.; LEFÈVRE, N. The overlooked tropical oceanic CO2 sink. **Geophysical Research Letters**, v. 43, n. 8, p. 3804–3812, 2016.

IBÁNHEZ, J. S. P.; FLORES, M.; LEFÈVRE, N. Collapse of the tropical and subtropical North Atlantic CO2 sink in boreal spring of 2010. **Scientific Reports**, v. 7, n. January, p. 1–9, 2017.

IBÁNHEZ, J. S. P.; FLORES MONTES, M.; LEFÈVRE, N. Evidence for enhanced primary production driving significant CO2 drawdown associated with the Atlantic ITCZ. **Science of The Total Environment**, v. 838, n. January, p. 156592, 2022.

KNOPPERS, B.; EKAU, W.; FIGUEIREDO, A. G. The coast and shelf of east and northeast Brazil and material transport. **Geo-Marine Letters**, v. 19, n. 3, p. 171–178, 1999.

KÖRTZINGER, A. A significant CO_2 sink in the tropical Atlantic Ocean associated with the Amazon River plume. **Geophysical Research Letters**, v. 30, n. 24, 2003.

LE QUÉRÉ, C. et al. Global carbon budget 2013. **Earth System Science Data**, v. 6, n. 1, p. 235–263, 17 jun. 2014.

LEDUC, G. et al. ITCZ rather than ENSO signature for abrupt climate changes across the tropical Pacific? **Quaternary Research**, v. 72, n. 1, p. 123–131, 2009.

LEFÈVRE, N. et al. Increased CO2 outgassing in February-May 2010 in the tropical Atlantic following the 2009 Pacific El Niño. **Journal of Geophysical Research: Oceans**, v. 118, n. 4, p. 1645–1657, 1 abr. 2013.

LEFÈVRE, N. et al. Impact of physical processes on the seasonal distribution of the fugacity of CO2 in the western tropical Atlantic. **Journal of Geophysical Research: Oceans**, v. 119, n. 2, p. 646–663, 2014.

LEFÈVRE, N. et al. Net heterotrophy in the Amazon continental shelf changes rapidly to a sink of CO_2 in the outer Amazon plume. **Frontiers in Marine Science**, v. 4, n. SEP, p. 1–16, 2017.

LEFÈVRE, N. et al. Amazon River propagation evidenced by a CO2 decrease at 8°N, 38°W in September 2013. **Journal of Marine Systems**, v. 211, 1 nov. 2020.

LEFÉVRE, N.; DIVERRÉS, D.; GALLOIS, F. Origin of CO_2 undersaturation in the western tropical Atlantic. **Tellus, Series B: Chemical and Physical Meteorology**, v. 62, n. 5, p. 595–607, 2010.

LIBES, S. Introduction to Marine Biogeochemistry. In: INTERGOVERNMENTAL PANEL ON CLIMATE CHANGE (Ed.). . Cambridge: Cambridge University Press, 2009.

MARINOV, I.; SARMIENTO, J. L. The Role of the Oceans in the Global Carbon Cycle: An Overview. In: **The Ocean Carbon Cycle and Climate**. [s.l.] Springer Netherlands, 2004. p. 251–295.

MILLERO, F. J. **The marine inorganic carbon cycleChemical Reviews**American Chemical Society, , 2007.

MONTEIRO, T. et al. Contrasting Sea-Air CO 2 Exchanges in the Western Tropical Atlantic Ocean. **Global Biogeochemical Cycles**, v. 36, n. 8, 15 ago. 2022.

MU, L. et al. Temporal Variability of Air-Sea CO 2 flux in the Western Tropical North Atlantic Influenced by the Amazon River Plume. **Global Biogeochemical Cycles**, v. 35, n. 6, 10 jun. 2021.

MÜNNICH, M.; NEELIN, J. D. Seasonal influence of ENSO on the Atlantic ITCZ and equatorial South America. **Geophysical Research Letters**, v. 32, n. 21, p. 1–4, 2005.

MURPHY, P. P. et al. CARBON DIOXIDE CONCENTRATIONS IN SURFACE WATER AND THE. n. February, 1994.

OLIVEIRA, R. et al. FONTE OU SUMIDOURO? UMA REVISÃO SOBRE OS FLUXOS DE CO2 NA PLATAFORMA CONTINENTAL BRASILEIRA. **Química Nova**, v. 46, n. 6, p. 561–572, 2023.

PADÍN, X. A. et al. Air-sea CO2 fluxes in the Atlantic as measured during the FICARAM cruises. **Biogeosciences Discussions**, v. 6, n. 3, p. 5589–5622, 2009.

PASSAIA, O. A. et al. Impact of large reservoirs on simulated discharges of brazilian rivers. **Revista Brasileira de Recursos Hidricos**, v. 25, n. Imd, p. 1–9, 2020.

PIERROT, D. et al. Recommendations for autonomous underway pCO_2 measuring systems and data-reduction routines. **Deep-Sea Research Part II: Topical Studies in Oceanography**, v. 56, n. 8–10, p. 512–522, 2009.

PIERROT, D.; STEINHOFF, T. Installation of Autonomous Underway pCO_2 Instruments onboard Ships of Opportunity. **NOAA Technical Report**, n. April, p. 31, 2019.

QUÉRÉ, C. et al. Global Carbon Budget 2018. **Earth System Science Data**, v. 10, n. 4, p. 2141–2194, 5 dez. 2018.

RAYNER, P. J.; LAW, R. M.; DARGAVILLE, R. The relationship between tropical CO2 fluxes and the El Niño-Southern Oscillation. **Geophysical Research Letters**, v. 26, n. 4, p. 493–496, 1999.

SABINE, C. L. et al. The oceanic sink for anthropogenic CO2. **Science**, v. 305, n. 5682, p. 367–371, 2004.

SCHNEIDER, T.; BISCHOFF, T.; HAUG, G. H. Migrations and dynamics of the intertropical convergence zone. **Nature**, v. 513, n. 7516, p. 45–53, 2014.

SCHOTT, F. A.; FISCHER, J.; STRAMMA, L. Transports and pathways of the upper-layer circulation in the western tropical Atlantic. **Journal of Physical Oceanography**, v. 28, n. 10, p. 1904–1928, 1998.

SENEVIRATNE, S. I. et al. Changes in Climate Extremes and their Impacts on the Natural Physical Environment. In: **Managing the Risks of Extreme Events and Disasters to Advance Climate Change Adaptation**. [s.l.] Cambridge University Press, 2012. v. 9781107025p. 109–230.

STRAMMA, L. Geostrophic transport of the South Equatorial Current in the Atlantic. **Journal of Marine Research**, v. 49, n. 2, p. 281–294, 2008.

STRAMMA, L.; SCHOTT, F. **The mean flow field of the tropical Atlantic OceanDeep-Sea Research II**. [s.l: s.n.].

TAKAHASHI, T. et al. **SEASONAL VARIATION OF CO2 AND NUTRIENTS IN THE HIGH-LATITUDE SURFACE OCEANS: A COMPARATIVE STUDYGLOBAL BIOGEOCHEMICAL CYCLES**. [s.l: s.n.].

TAKAHASHI, T. et al. Global sea–air CO_2 flux based on climatological surface ocean pCO_2, and seasonal biological and temperature effects. **Deep Sea Research Part II: Topical Studies in Oceanography**, v. 49, n. 9–10, p. 1601–1622, jan. 2002.

TAKAHASHI, T. et al. Climatological mean and decadal change in surface ocean pCO_2, and net sea-air CO_2 flux over the global oceans. **Deep-Sea Research Part II: Topical Studies in Oceanography**, v. 56, n. 8–10, p. 554–577, 2009.

VALSALA, V.; MAKSYUTOV, S. Simulation and assimilation of global ocean pCO2 and air-sea CO2 fluxes using ship observations of surface ocean pCO2 in a simplified biogeochemical offline model. **Tellus, Series B: Chemical and Physical Meteorology**, v. 62, n. 5, p. 821–840, nov. 2010.

WANG, X. et al. Seasonal to decadal variations of sea surface pCO2 and sea-air CO2 flux in the equatorial oceans over 1984-2013: A basin-scale comparison of the Pacific and Atlantic Oceans. **Global Biogeochemical Cycles**, v. 29, n. 5, p. 597–609, 1 maio 2015.

WANNINKHOF, R. et al. Global ocean carbon uptake: Magnitude, variability and trends. **Biogeosciences**, v. 10, n. 3, p. 1983–2000, 2013.

WANNINKHOF, R. et al. Comparison of discrete and underway CO2 measurements: Inferences on the temperature dependence of the fugacity of CO2 in seawater. **Marine Chemistry**, v. 247, n. October, p. 104178, 2022.

WANNINKHOF, R.; THONING, K. Measurement of fugacity of CO_2 in surface water using continuous and discrete sampling methods. **Marine Chemistry**, v. 44, n. 2–4, p. 189–204, dez. 1993.

WEISS, R. F. Carbon dioxide in water and seawater: the solubility of a non-ideal gas. **Marine Chemistry**, v. 2, n. 3, p. 203–215, 1974.

XIE, S. P.; CARTON, J. A. Tropical atlantic variability: Patterns, mechanisms, and impacts. **Geophysical Monograph Series**, v. 147, p. 121–142, 2004.

YAN, Y. Y. Intertropical convergence zone (ITCZ). **Encyclopedia of Earth Sciences Series**, p. 429–432, 2005.

APÊNDICE

CSIRO PUBLISHING

RESEARCH PAPER
https://doi.org/10.1071/MF22276

MARINE & FRESHWATER RESEARCH

Regional differences in the air–sea CO_2 flux between 3 and 14°S in the south-western tropical Atlantic

Lucas Medeiros Guimarães[A,*], Manuel J. Flores Montes[A] and Nathalie Lefèvre[B]

For full list of author affiliations and declarations see end of paper

*Correspondence to:
Lucas Medeiros Guimarães
Department of Oceanography, Federal University of Pernambuco, Arquitetura Avenue, Cidade Universitária, Recife, PE 50740-550, Brazil
Email: lmguimaraes1@gmail.com

Handling Editor:
Yunlin Zhang

Received: 15 January 2023
Accepted: 14 April 2024
Published: 9 May 2024

Cite this: Guimarães LM *et al.* (2024) Regional differences in the air–sea CO_2 flux between 3 and 14°S in the south-western tropical Atlantic. *Marine and Freshwater Research* **75**, MF22276. doi:10.1071/MF22276

ABSTRACT

Context. The fugacity of surface-seawater CO_2 (fCO_{2sw}) and the sea–air CO_2 fluxes in the south-western tropical Atlantic (SWTA) were studied to increase the knowledge about the carbon cycle in this region. **Aims.** This paper aims to describe the distribution of fCO_{2sw} in SWTA. **Methods.** The fCO_{2sw} was measured from 2008 to 2020 by volunteer merchant ships with an onboard system that measures pCO_2 while the vessels were underway. **Key results.** Higher values occurred north of 8°S than in the region south of 8°S. The north is a strong source of CO_2 for the atmosphere, with an annual mean value of 3.14 ± 0.52 mmol m^{-2} day^{-1}. The south is a weaker source of CO_2, with an annual average of 0.93 ± 0.90 mmol m^{-2} day^{-1}. In the months of July and August, a weak sink of CO_2 was observed, with a mean of -0.55 mmol m^{-2} day^{-1}. **Conclusions and implications.** The differences between these two regions are explained by the origin of the surface-water masses encountered along the ship track. The central branch of the South Equatorial Current (SEC) transports surface water, with a higher CO_2 concentration and lower salinity, north of 8°S, whereas the surface waters between 8 and 14°S come from the southern branch of the SEC. The intertropical convergence zone is another physical process influencing the region north of 8°S.

Keywords: CO_2 flux, CO_2 fugacity, Intertropical Convergence Zone, North Brazilian Undercurrent, north-eastern Brazil, sea-surface salinity, sea-surface temperature, South Equatorial Current.

Introduction

The carbon dioxide (CO_2) distribution in the ocean shows a large spatial and temporal variability. Ocean–atmosphere exchanges are very dynamic and controlled by physical, chemical and biological processes (Takahashi *et al.* 2002, 2009).

Efforts have been made to determine the temporal evolution of surface seawater CO_2 and sea–air CO_2 fluxes. Recently, more studies have been conducted on the CO_2 distribution in the western tropical Atlantic (Lefèvre *et al.* 2010, 2014, 2020; Ibánhez *et al.* 2015; Bonou *et al.* 2016; Moussa *et al.* 2016; Carvalho *et al.* 2017; Araujo *et al.* 2019; Monteiro *et al.* 2022). Nevertheless, few studies exist on the seasonal and spatial variability of CO_2 fluxes south of the equator next to Brazilian coast (Lefèvre *et al.* 2010, 2014; Carvalho *et al.* 2017; Cotovicz *et al.* 2020).

The south-western tropical Atlantic (SWTA) region is oligotrophic (Takahashi *et al.* 2009; Lefèvre *et al.* 2010; Silva *et al.* 2019) and characterised by warm surface waters. The coastal ecosystems of north-eastern Brazil have a limited spatial extend to significantly alter the carbon chemistry of the SWTA (Chen *et al.* 2013; De Queiroz *et al.* 2015; Noriega *et al.* 2015; Silva *et al.* 2019).

The intertropical convergence zone (ITCZ) is a physical process that influences the balance of evaporation–precipitation in this region (Pailler *et al.* 1999; Stramma and Schott 1999; Assunção *et al.* 2020). The ITCZ explains the low salinities in the North Equatorial Counter Current (NECC) and affects the fluxes of CO_2 between the ocean and the atmosphere (Ibánhez *et al.* 2022).

Previous coastal-budget studies have shown that there are almost no data on the tropical South Atlantic (Laruelle *et al.* 2014). There is uncertainty over the CO_2 distribution in these